



# **Stratigraphic evolution and characteristics of lobes: a high-resolution study of Fan 3, Tanqua Karoo, South Africa.**

by  
J.M. Neethling

Thesis presented in partial fulfilment of the requirements for the degree of  
Master of Science  
at the University of Stellenbosch



Supervisors  
Dr. H. de V. Wickens  
Dr. D.M. Hodgson

March 2009



*Geology*  
Stellenbosch University

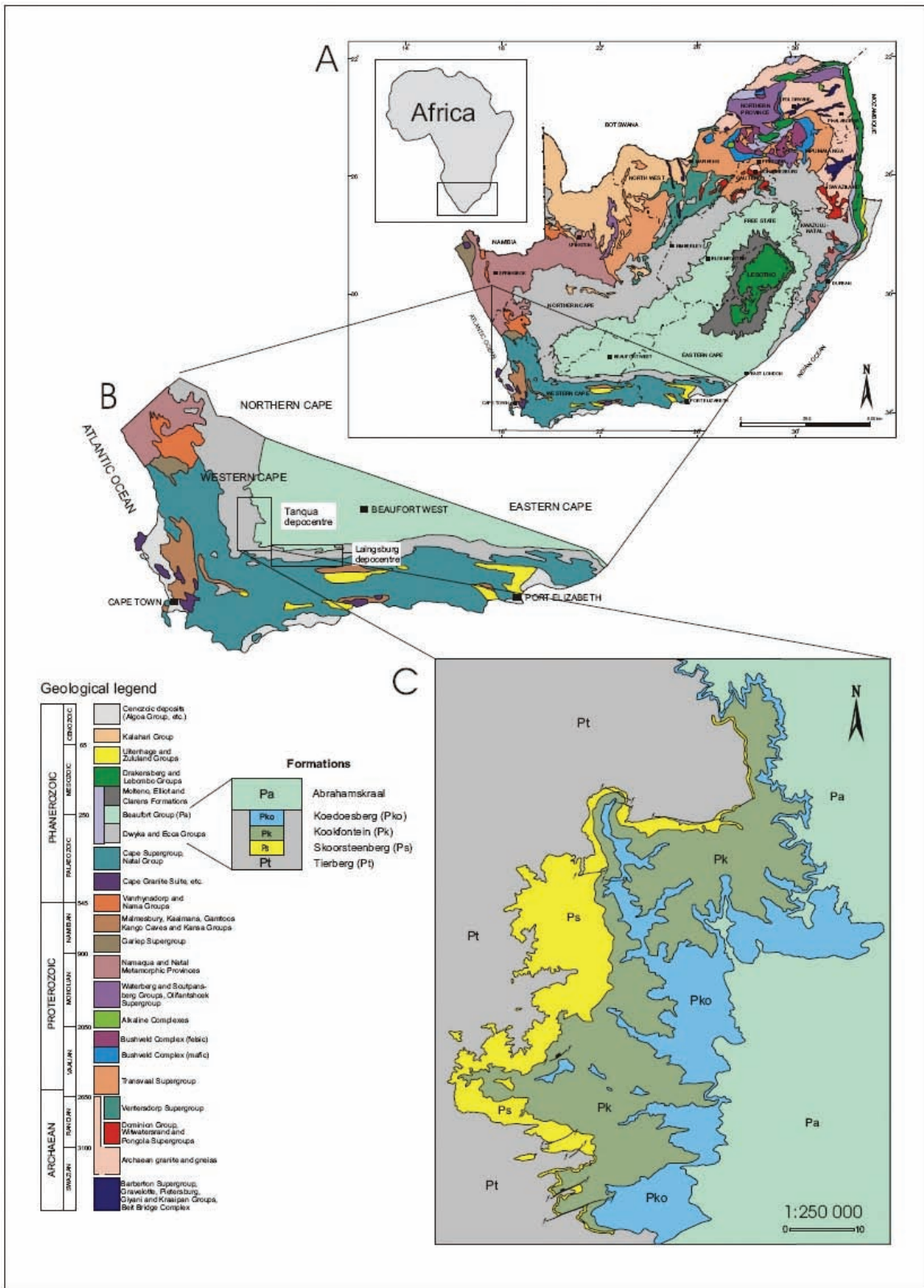


**Figure 1.1** A simplified geological map of South Africa to show the location of the Tanqua sub-basin (Geological map, Council for Geoscience, 2000). The Laingsburg and Tanqua sub-basins can be seen in (B). The yellow area in (C) represents the total outcrop of the Skoorsteenberg Formation in the Tanqua sub-basin.



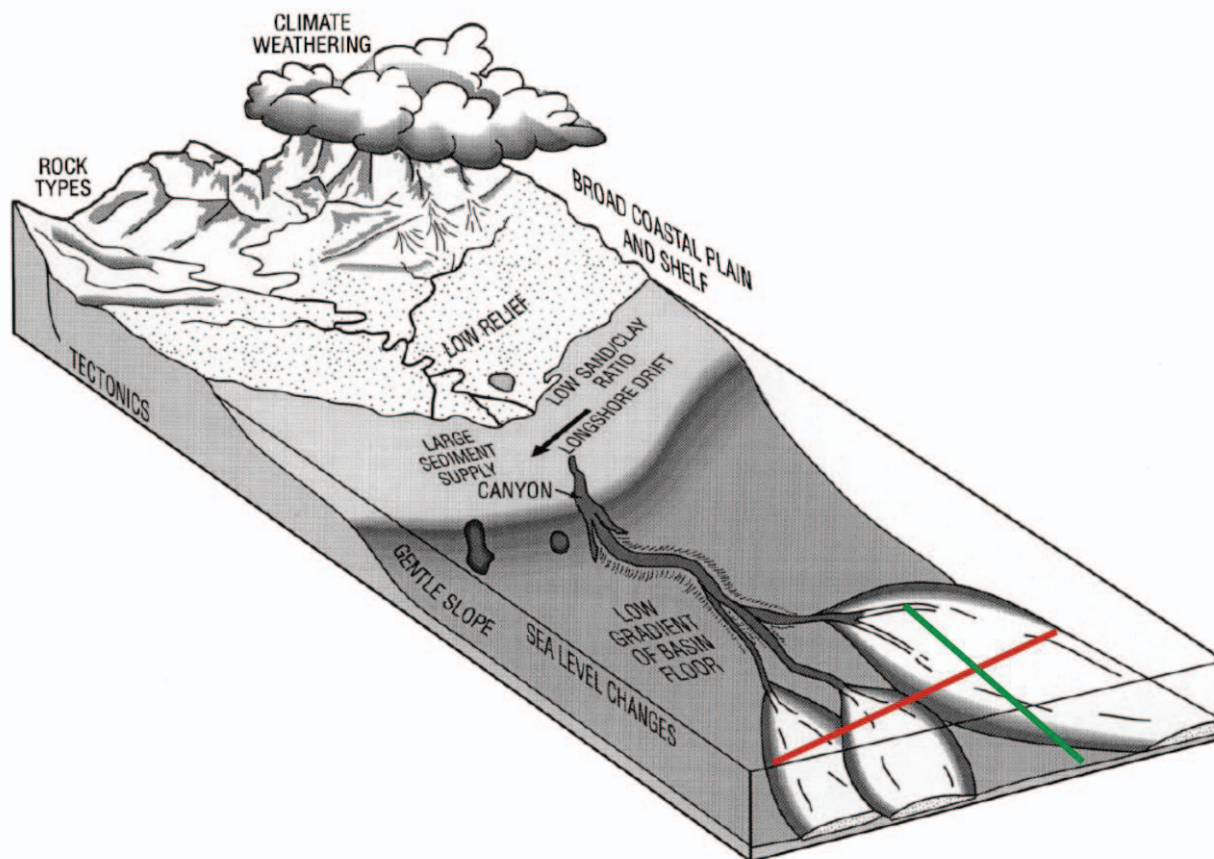


**Figure 1.4** Locations of the south Gemsbok River valley outcrops in relation to a depositional diagram for fine-grained turbidites. The red line represents the oblique strike section of the southern Zoet Meisjies Fontein 75 and Rondavel 34 outcrops, and the red line the dip-sections of the Los Kop 74 and Krans Kraal 83 outcrops. Modified from Bouma (2000).

## 1.5 Methods and Materials

The field area for this study is represented by Figure 1.5. The exposed outcrops represent a 7 kilometre oblique strike-section along the southern Gemsbok River valley, and a 5 kilometre roughly north-south trending dip-section. Several gullies extend westward from this dip-section, providing several shorter up-dip strike-sections.

The outcrops were examined on a centimetre scale by measuring 72 vertical profiles, recording grain-size, bed thicknesses, palaeoflow indicators and other depositional features. Measurements were made using a maximum 1.9 metre retractable Jacob staff and measuring tape. High-resolution digital photographs were also collected of all measured outcrops. Palaeoflow measurements were taken using a Krantz geological compass, with a declination set to 20°.

profiles, using  $x^2 = y^2 + z^2 - 2yz \cos \Theta$  (Figure 1.5), and has proven to be a most accurate method.

The vertical profiles were digitised using DSL, an in-house program used by Liverpool University, CorelDraw X3 and Microsoft Excel 2003 (Chapter 5). The CorelDraw profiles were used to create detailed correlation and facies distribution panels. Correlations between profiles were walked out where possible, and determined from a distance using binoculars (easier to get a good lateral overview). The 2D panels were used to describe the stratigraphy and architecture of Fan 3 south of the Gemsbok River valley (Chapter 3). These descriptions, combined with the data from the Lobe project to the north, were used in the construction of a conceptual depositional model for Fan 3 (Chapter 6).

The data were finally manipulated in Petrel (Chapter 7). Petrel was used to create isopach maps, and to create a 3D facies distribution map of Fan 3 south of the Gemsbok River valley. Petrel used the digital data exported from DSL and Excel.

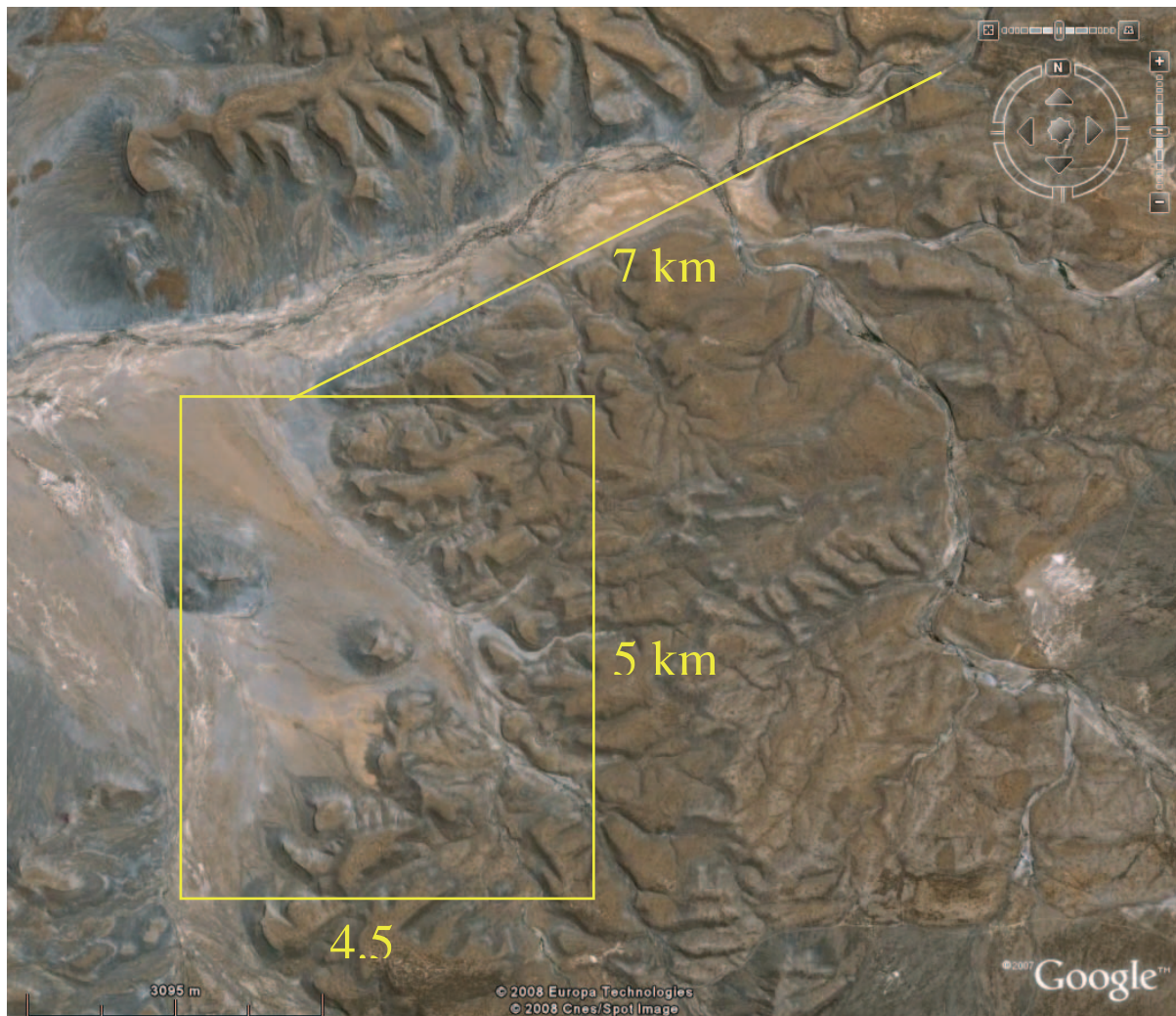


**Figure 1.6** Google Earth (2008) satellite image of the study area, indicating the dimensions and location of the field area.

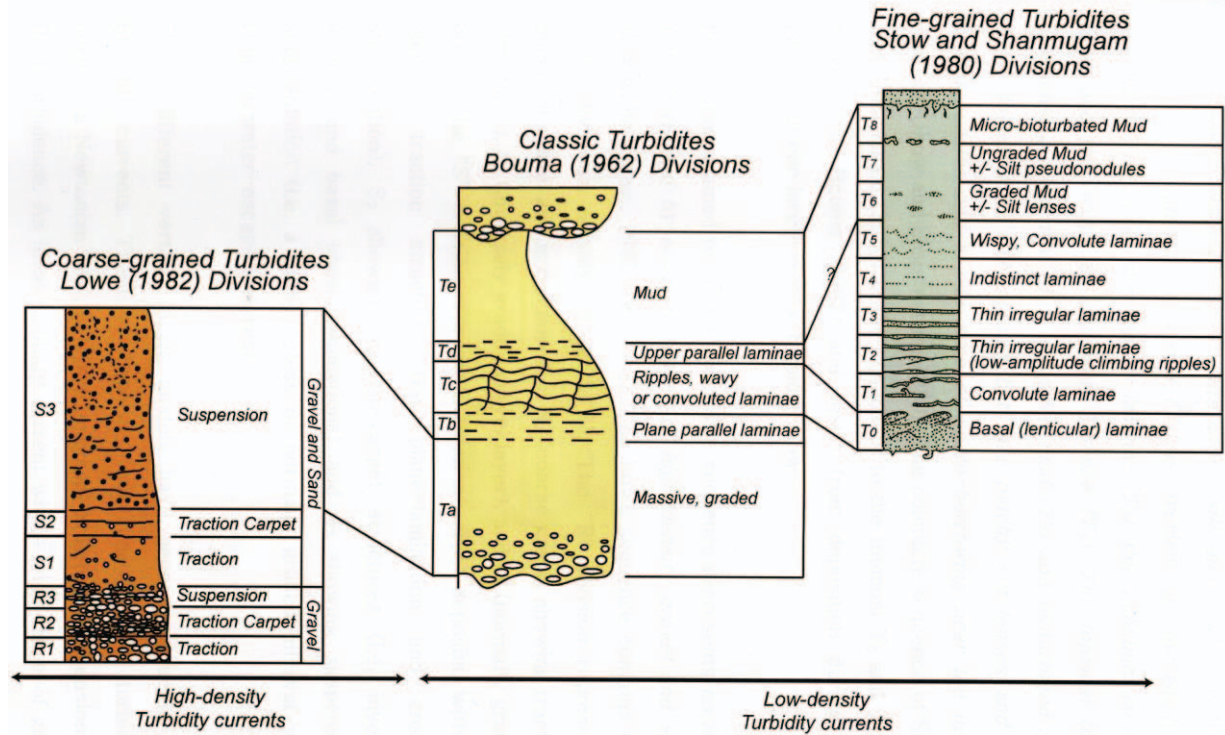


**Figure 2.1** A summary diagram of the Lowe (1982), Bouma (1962) and Stow and Shanmugam (1980) subdivisions for turbidites (from Shanmugam, 2000).

## 2.4 Terminology

A hierarchical subdivision is used in order to compare the different stratigraphic and architectural elements. The mid- to outer part of Fan 3 can be subdivided into several lobes, each of which consists of one or more lobe-elements. A lobe is defined in the Lobe project as a set of lobe-elements, be they amalgamated or bedded, separated from other lobes by significant thin-bedded, fine-grained siltstone breaks that can be traced along strike and dip for several kilometres. The above terms can be compared with a hierarchical classification provided by Mutti and Normark, 1987, to provide a rough estimate of the time constraints involved during the formation of turbidites. For example, their “Turbidite system” compares with “Lobe-complex” in the Lobe project, whereas their “Turbidite stage” compare to “Lobe”.

as apposed to the darker colour of the claystones, as well as the bedding pattern of the siltstones. Siltstones generally display a laminated nature, be it parallel- or ripple-laminated, whereas the laminations of claystones are usually not easy to discern.

*Interpretation:*

The claystones are interpreted as the result of background suspension sedimentation taking place continuously in the basin. The siltstones are interpreted as low-volume, low-density turbidites. The transitional base and top of the fans respectively mark the initiation and decay of the fans (Hodgson *et al.*, 2006). The true stratigraphic base and top of the fan is rarely identified at outcrop, but is clearly seen in well logs (Luthi *et al.*, 2006) and core (Hodgson *et al.*, 2006) from the research boreholes.

### 3.2.2 Lithofacies 2: Parallel- and ripple cross-laminated siltstone

*Description:*

These fine- to very fine-grained siltstone units are mostly finely laminated to micro-cross-

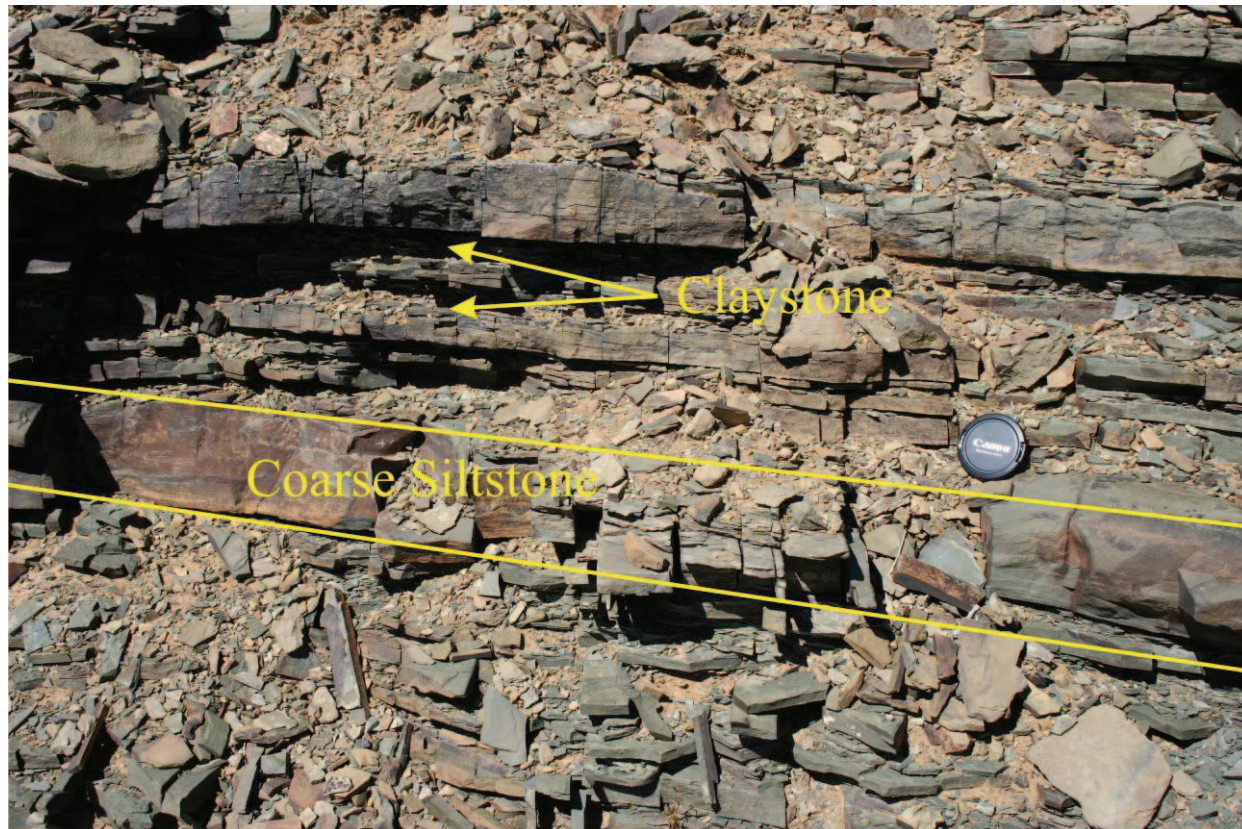


**Figure 3.1** An example of the siltstone to claystone relation close to the base of the succession. This relation is only present at the base and top of Fan 3, as no claystones are present within the fan succession.

laminated, and are commonly interbedded with layers of very fine-grained sandstone or claystone of a few centimetres in thickness (claystone is only present close to the lithological base of the fan; Fig. 3.1). The sandy units (beds) tend to thicken upwards in the succession, whilst the siltstone units thin to millimetre scale units. The reverse holds true for the top of the succession. The siltstone successions generally form the breaks between the individual lobe elements of Fan 3. This lithofacies can also be treated as a lithofacies association: Johnson *et al.* (2001) refer to this grouping of siltstone grading into sandstone as thin-bedded turbidites.

In cases where the siltstones form breaks between the sandstone units (lobes), they form a fairly distinct alternating pattern (Fig. 3.2). They consist of alternating fine- and coarse-grained siltstone units, and individual units vary greatly in thickness, as do the successions. The former varies between a few millimetres to almost 30cm, and the latter can be anything from less than 5cm to almost 2 metres. There is no perceivable pattern along strike as to the exact thickness of



**Figure 3.2** Alternating relationship between coarse- and fine-grained siltstone that is present throughout the study area. This relationship forms the most common breaks between lobes. They are commonly referred to simply as thin-bedded intervals.

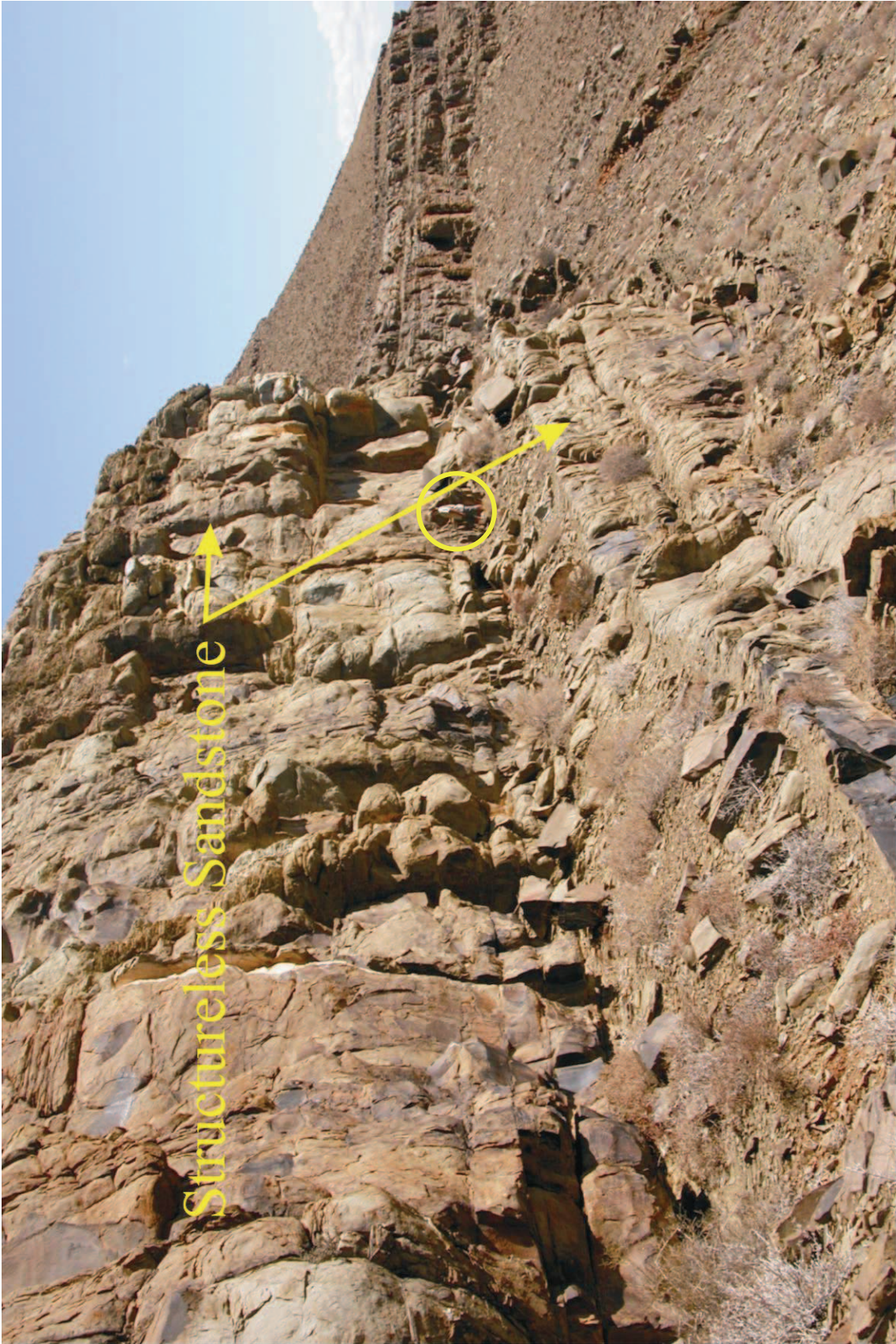


**Figure 3.3** An example of the general appearance of structureless sands in the study area. This particular section is located in one of several highly amalgamated channelised areas, with sandstone cliffs reaching 10 metres or more in thickness. Note person for scale underneath the overhang (circle).

Amalgamation of individual sandstone units is common. The contacts with other lithofacies are generally sharp and planar. Irregularities such as those caused by loading and local scouring are also common. Rip-up clasts of finer, softer lithologies (claystones) are commonly associated

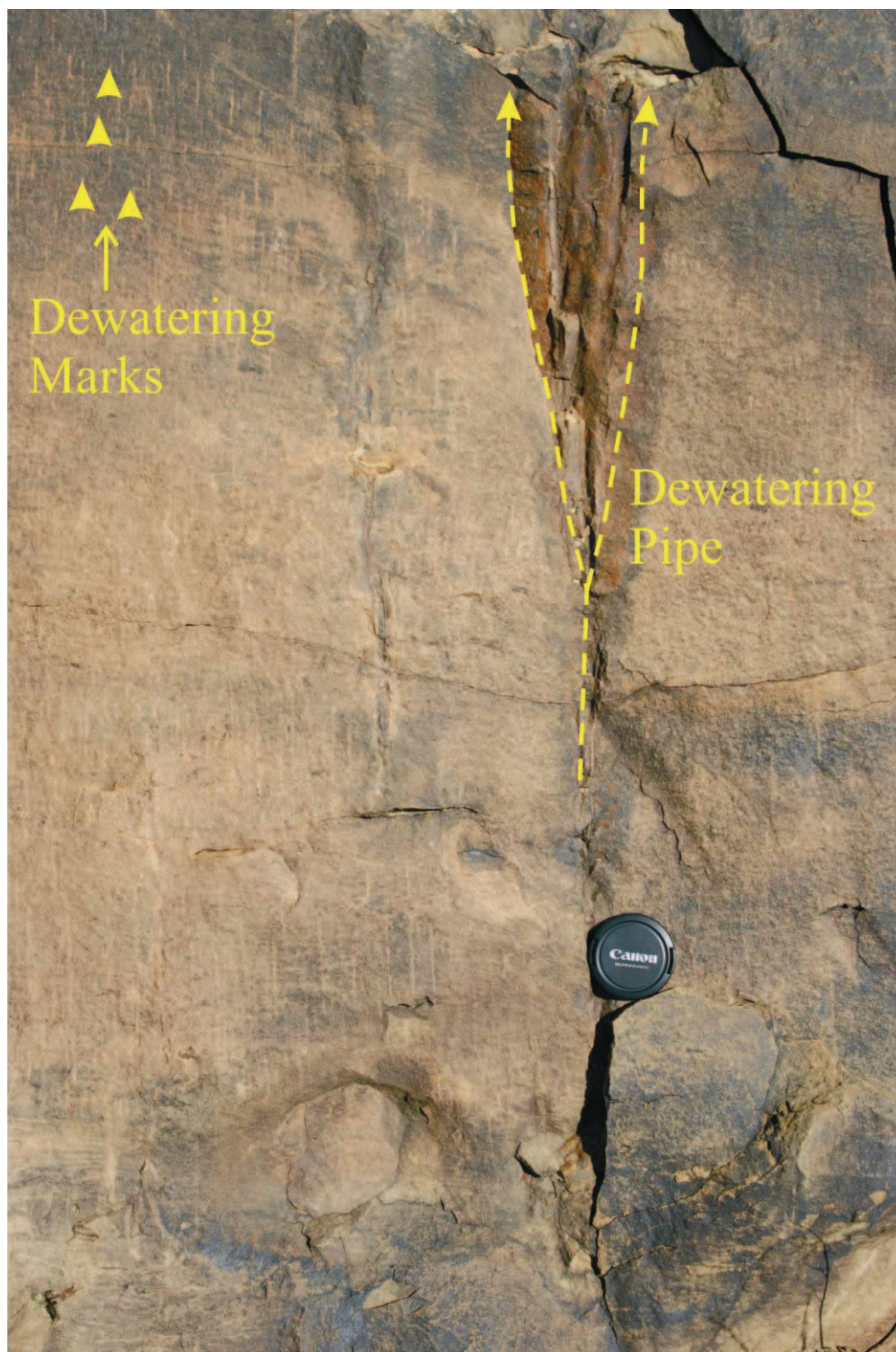


**Figure 3.4** Example of the dewatering features found in structureless sands. Here the smaller linear features are present, as well as a much larger dewatering pipe with significant alteration along its edges.

with the amalgamated surfaces. They are common lower down in the succession, associated with the earlier sandstone units. Clasts are generally angular and elongated. Clast-rich units become more prominent higher in the stratigraphy and closer to the margin of the fan, as lower stratigraphic units slowly pinch out.

Several elongated and/or rounded calcareous concretions of various sizes (up to 1 m in diameter) are also present near to the base of some of the thicker sandstone units (Fig. 3.7).

*Interpretation:*

Structureless sandstones represent the Ta units in the Bouma subdivision. Dewatering features (mostly at the top of the succession in the study area; Fig. 3.4), deformation of the lower contacts (Fig. 3.5), rip-up clasts (Fig 3.6), amalgamation of beds and sole structures can all be used to infer the velocity and density of currents, as well as the transport mechanism active during deposition of the sediment. Clasts are especially common in high-energy channelised environments, whereas sole structures are generally at the base of thicker sandstone units.

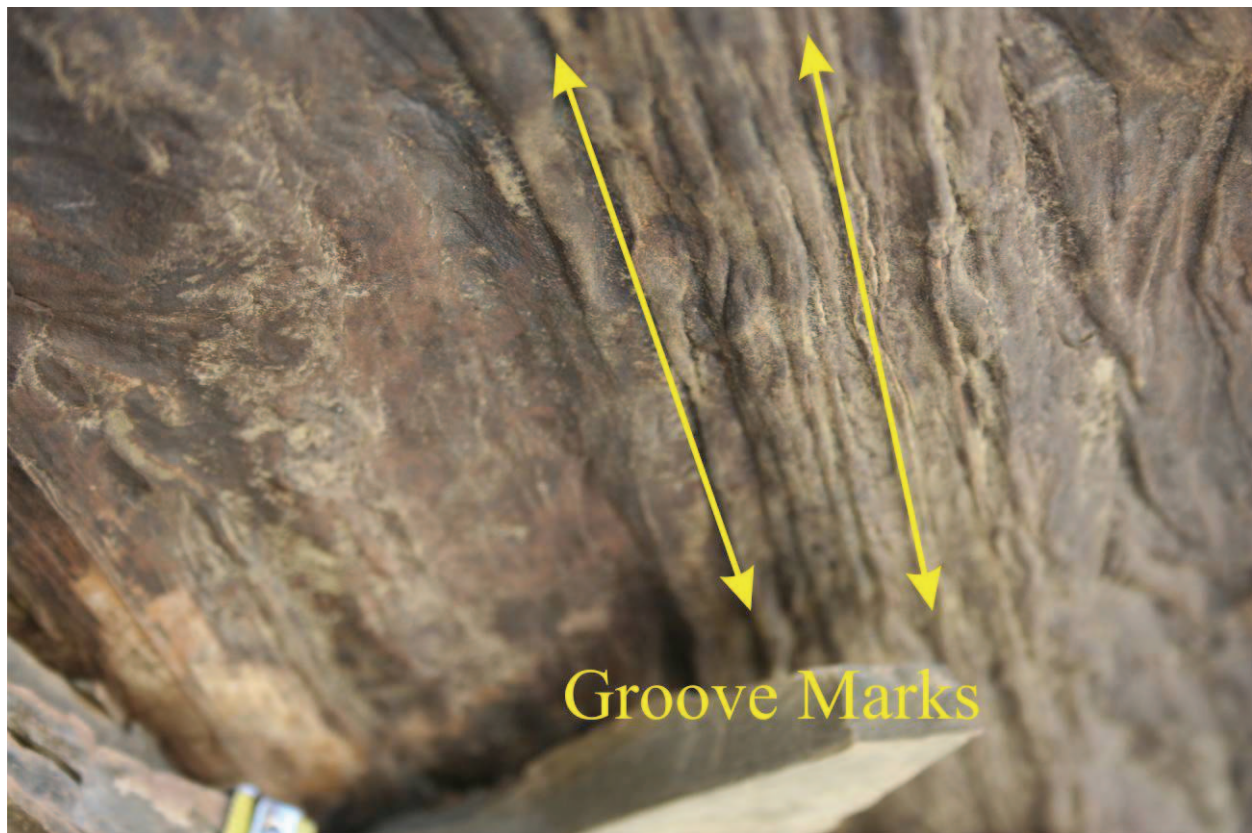


**Figure 3.5** Groove marks at the base of a structureless sandstone. These marks infer the general orientation of palaeocurrents.



**Figure 3.6** Example of a rip-up clast near the base of a thick sandstone unit. This example is near the base of Fan 3, close to the eastern margin of the fan.



**Figure 3.7** An example of a particularly large calcreous concretion. Note the concentric growth pattern.

### 3.2.4 Lithofacies 4: Structured sandstone

#### *Description:*

Structured sandstone contains either parallel- or ripple cross-lamination features. Generally these are easily distinguished from structureless sands, but in some cases the latter grades into structured sandstone (Fig. 3.8). Where no clear-cut break could be distinguished between structureless and structured sandstones, the lithofacies was classified as structured sandstone. Wherever the sandstone packages become more stratified, i.e. away from amalgamated or channelised areas, they are referred to as structured sandstone. These beds also tend to show a greater number of sedimentary features.

Where breaks can be clearly distinguished, the lithofacies can be either parallel- or ripple cross-laminated sandstone (Fig. 3.10). The bed thicknesses of these layers vary greatly. They are

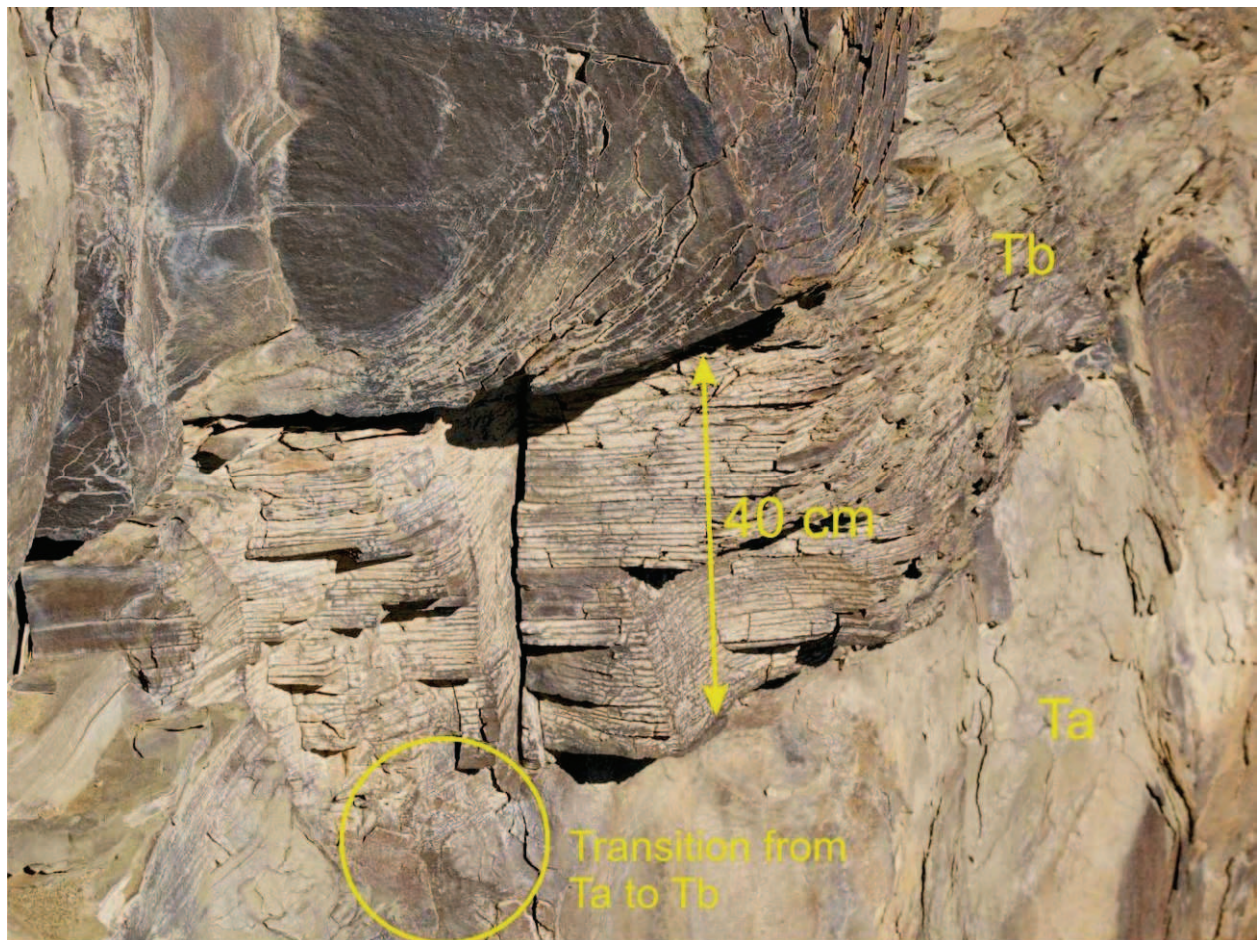


**Figure 3.8** An example of where the transition between Ta and Tb is not particularly clear-cut. The transition only becomes apparent laterally. This particular feature is fairly common along the Gemsbok River outcrop.



**Figure 3.9** An example of the sharp transition between a Tb and Tc succession.

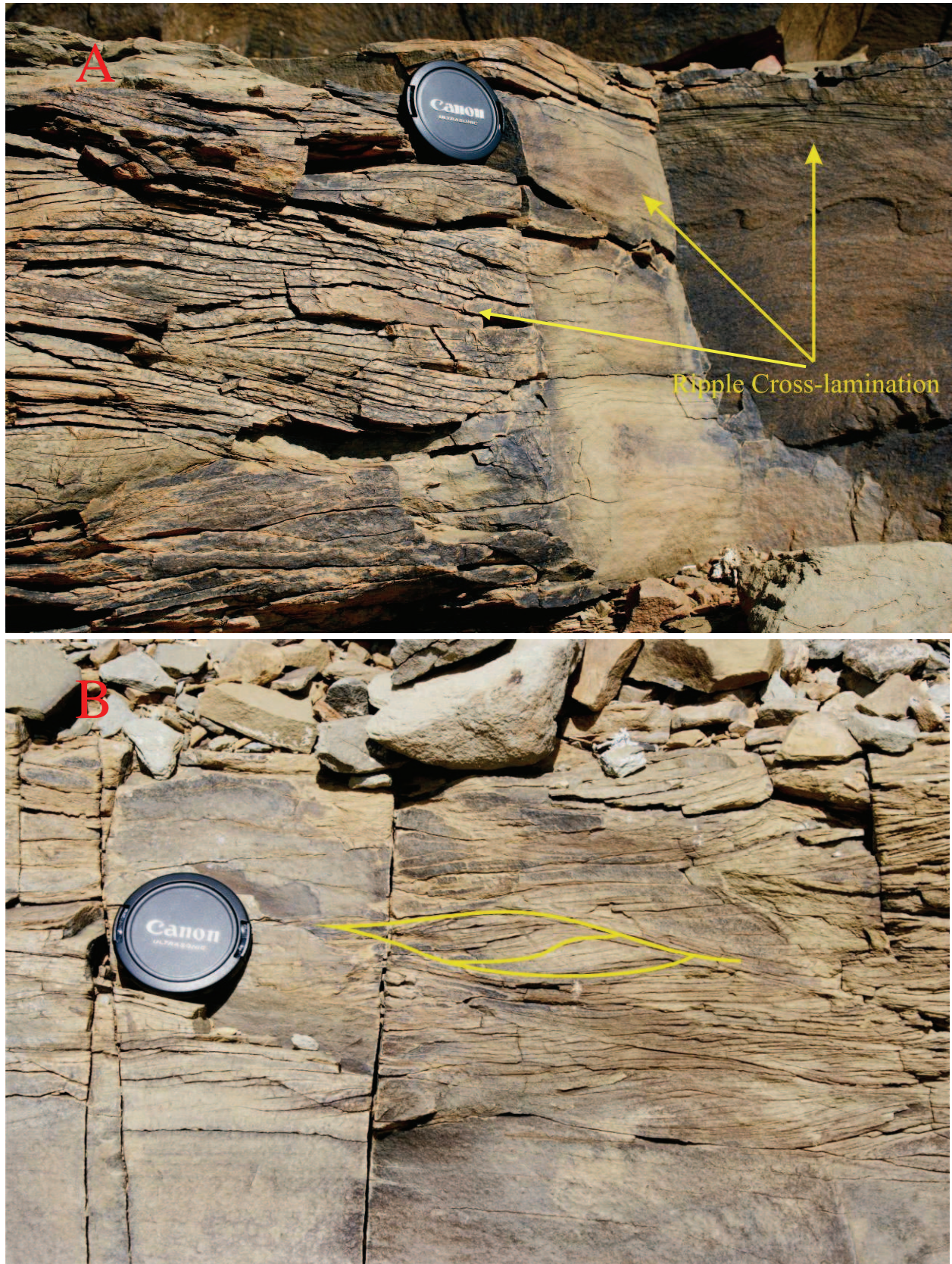


**Figure 3.10** Closer views of ripple cross-laminated sandstone: (A) Ripple cross-lamination; (B) Climbing ripple-lamination.

### 3.2.5 Lithofacies 5: Mud-clast conglomerates

#### *Description:*

The term “mud-clast conglomerate (MCC)” is a collective term used to describe a “nest” of rip-up clasts in a matrix of either sand or silt. The clasts generally appear as a collection of small (less than 5 cm) elongated slivers of mud. MCCs can be found either above or below thick sand units. They often resemble lag deposits when found below the base of sandstone beds (Fig. 3.11). All of these deposits have in common the lack of internal structure.

#### *Interpretation:*

MCCs commonly form in the thalwegs of channels as a result of bypassing of high-energy flows. Clay clasts can originate during erosive undercutting and by local rip-up by strong, high-density turbidity currents. Lag deposits, as well as debrites (MCCs with large amounts of organic material), represent the final trailing of sediment or debris pulled behind the turbidity flow. The turbulent nature of the flow ensures these are the last components to be deposited, often close to the margin of a lobe.

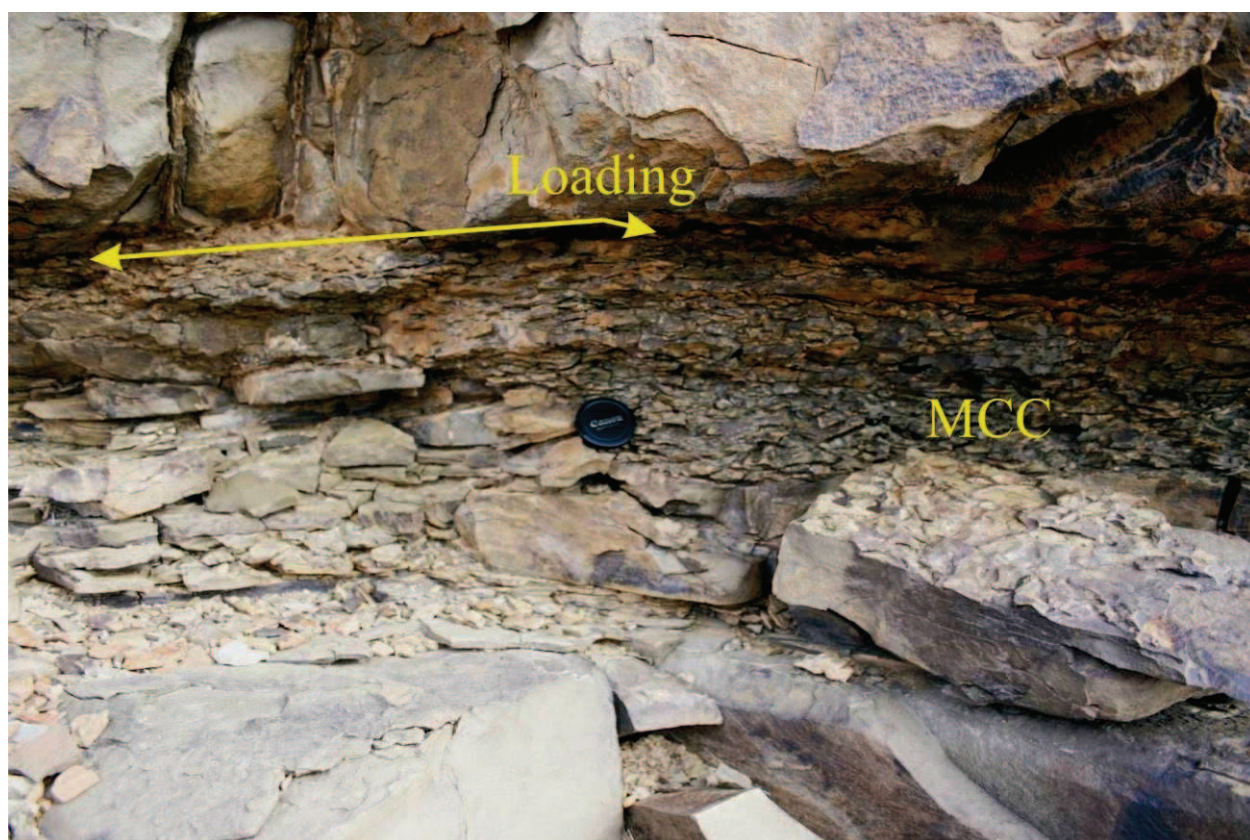


**Figure 3.11** This is how mud-clast conglomerates mostly appear in the study area. This example lies at the base of a large structureless sand, the latter loading into the MCC.

### 3.3 Stratigraphy

#### 3.3.1 Introduction

Mid- to lower Fan 3 can be subdivided into several lobes, each of which consists of one or more lobe-elements. Figure 3.12 shows the subdivision as defined in the Lobe project.

A fan is built up by a series of stacked lithological units: The initial beds and bed-sets (“bulb” deposits as described by Machado *et al.*, 2004); lobe-elements, singular discrete sedimentary units consisting of stacked beds (Deptuck *et al.*, 2008); lobes, which are separated by significant thin-bedded, fine-grained intervals (referred to as *composite lobes* by Deptuck *et al.*, 2008); and a lobe complex, or fan (Fig. 3.12). Importantly, a lobe complex will thin to a lobe, and a lobe will thin to a lobe-element, and a lobe-element will thin to an individual bed.

Six lobes have been identified to the north of the Gemsbok River (Prélat *et al.*, in review). Most of these are traceable to the northern pinch-out of Fan 3. Of these six lobes, only five are present south of the Gemsbok River. The missing lobe, Lobe 3, is rarely more than a single bed

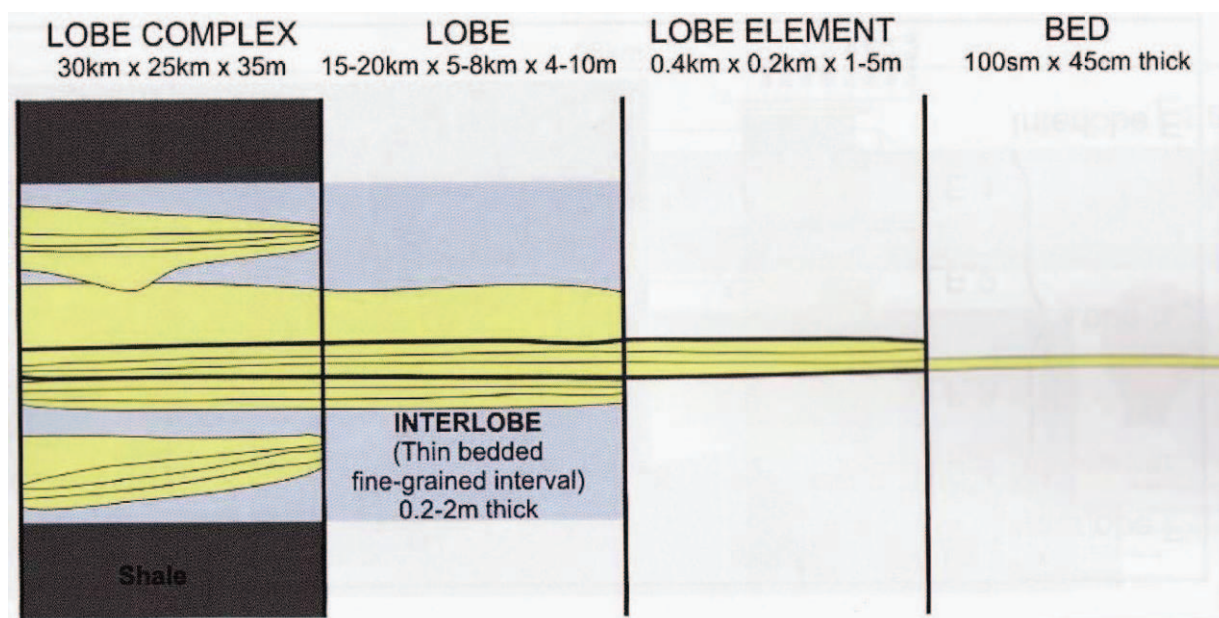
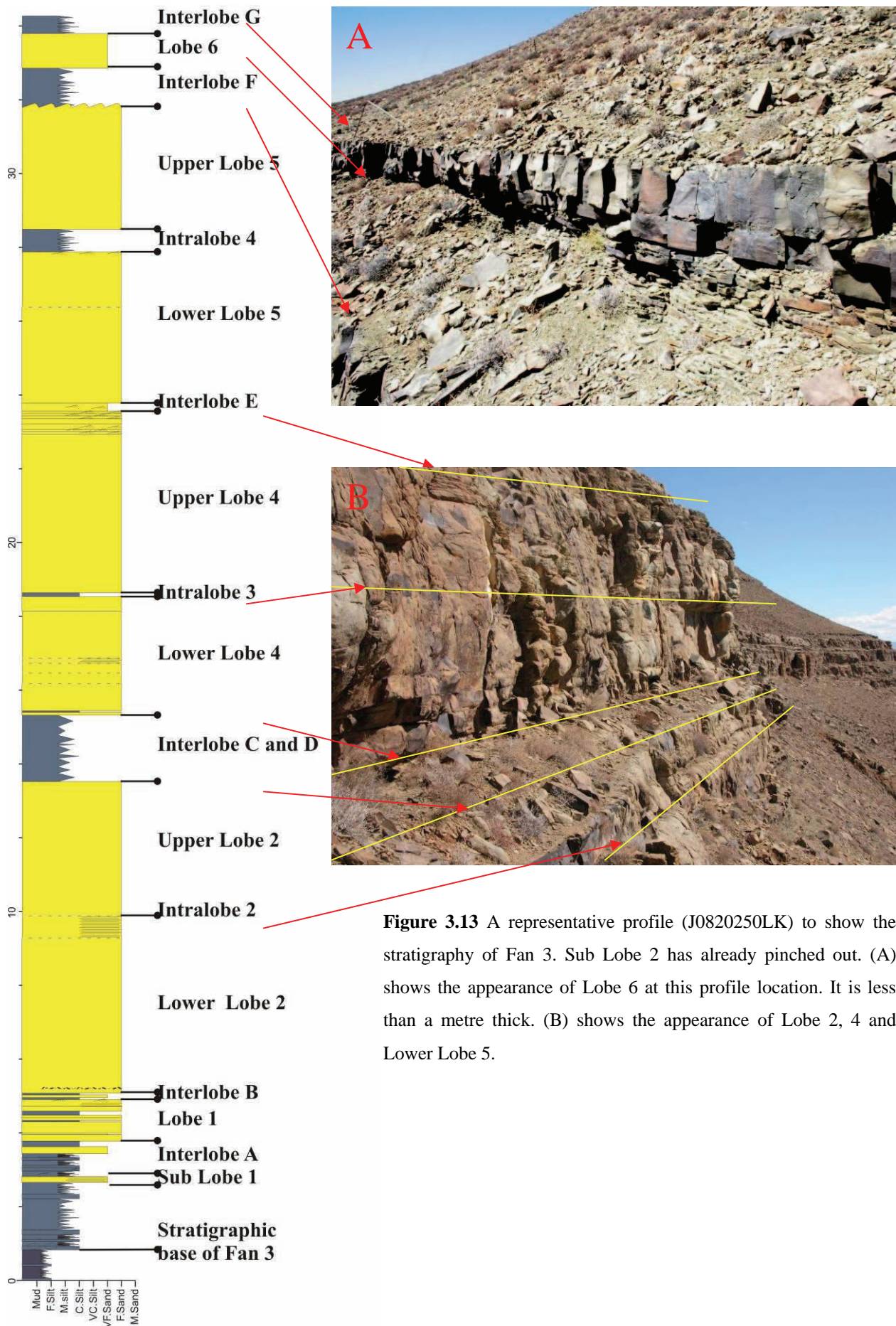


**Figure 3.12** Hierarchy of depositional elements in distributive deep-water systems. The division consists of four scales of elements, namely single beds, lobe-elements, lobes and the lobe complex (or fan) defined by the bounding fine-grained units and mappable extent, not thickness. Lobes are separated by interlobe units of fine-grained, thin-bedded siltstones (From Lobe Field Guide, © STRAT Group, University of Liverpool, June 2008).



sheets. These sheets can be anything from lobe-scale features to bed-set features, depending on their relative position to an axial zone and the thickness of a lobe.

Palaeocurrent measurements provide an important constraint in determining the depositional environment of a submarine fan (e.g. flow direction and strength), as well as constraining the 3D shape of a lobe or lobe-element. Palaeocurrent indicators include current ripple laminations, parting lineations, and sole structures. All palaeocurrent measurements within a lobe-element are grouped together to give an indication of the behaviour of a specific lobe.

The panels below provide information of the architectural behaviour of the stratigraphic units in 2D space. Panels 1 – 2, 3 and 3 – 4 are oblique strike sections along the mid-fan area (i.e. the Gemsbok River valley). Panel 12 is a dip-section roughly along the fan’s axis. The other panels are small strike sections along the length of Panel 12.

The “Panel X – Y” names represent sections where two originally separate panels were either combined (1 – 2, 8 – 9 and 10 – 11) or where a smaller section intersects a larger one (3 – 4).

Short notes are presented on each panel, focussing on important details found on each panel.

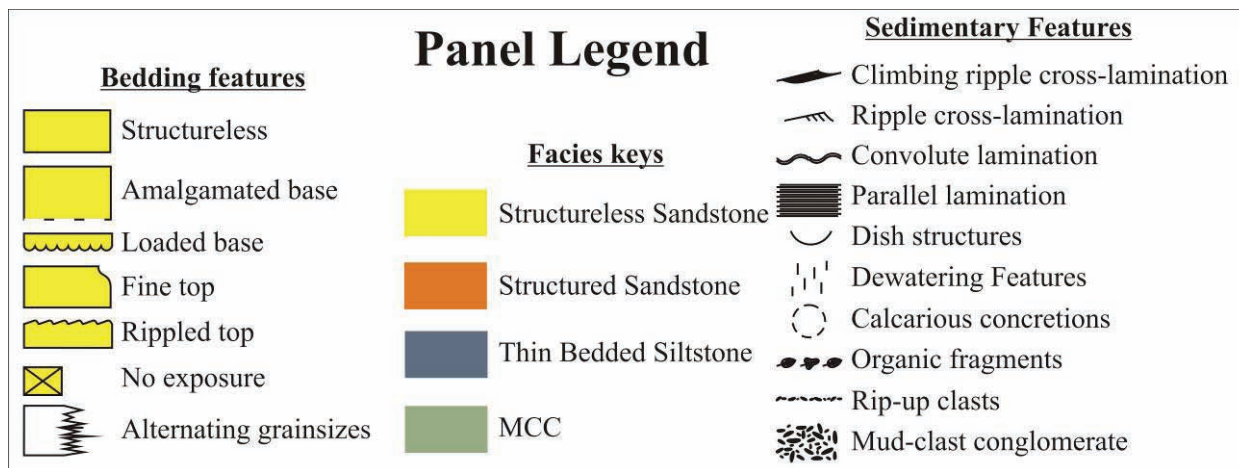


Figure 3.14 Legend for all the correlation panels.

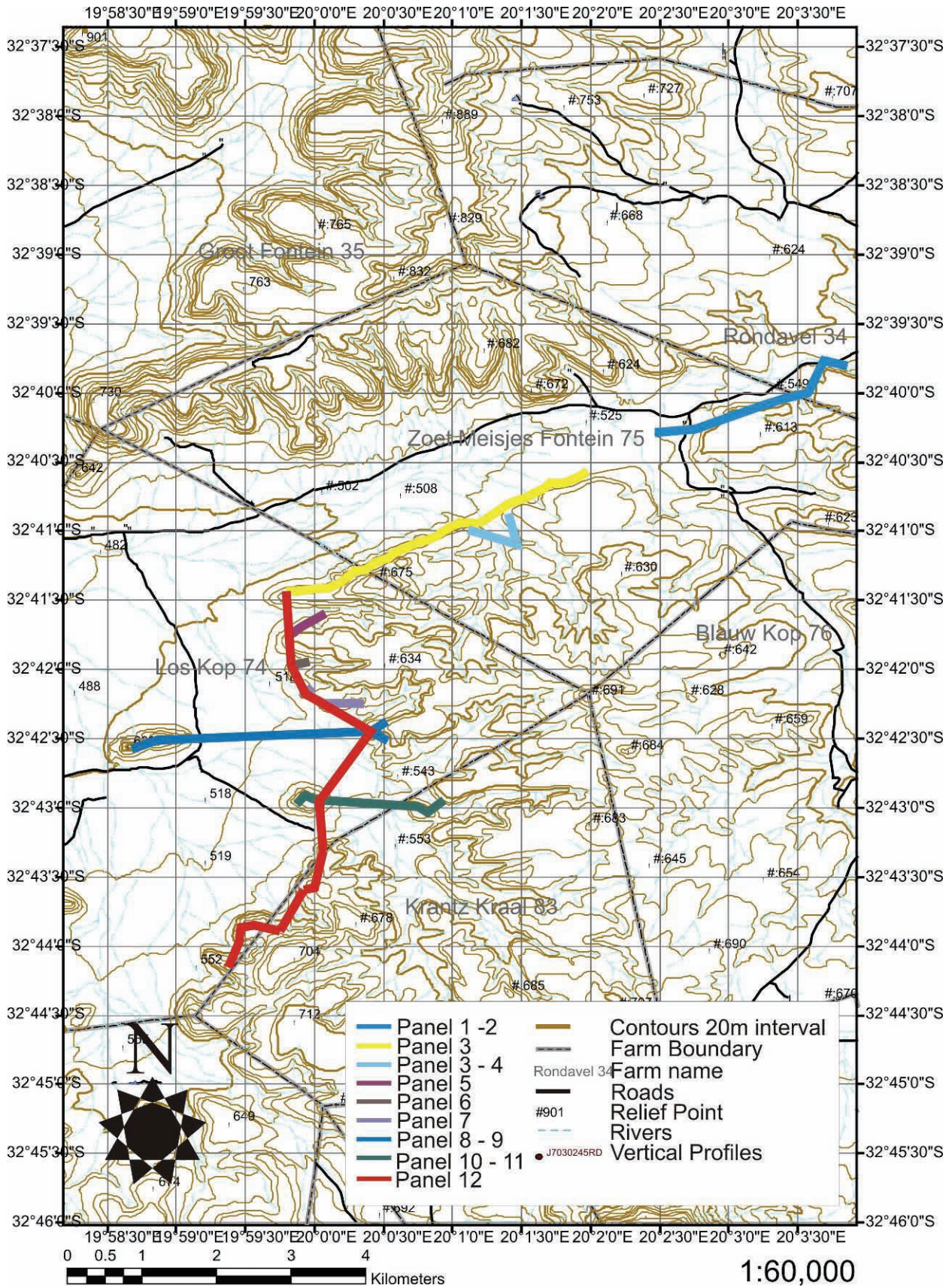
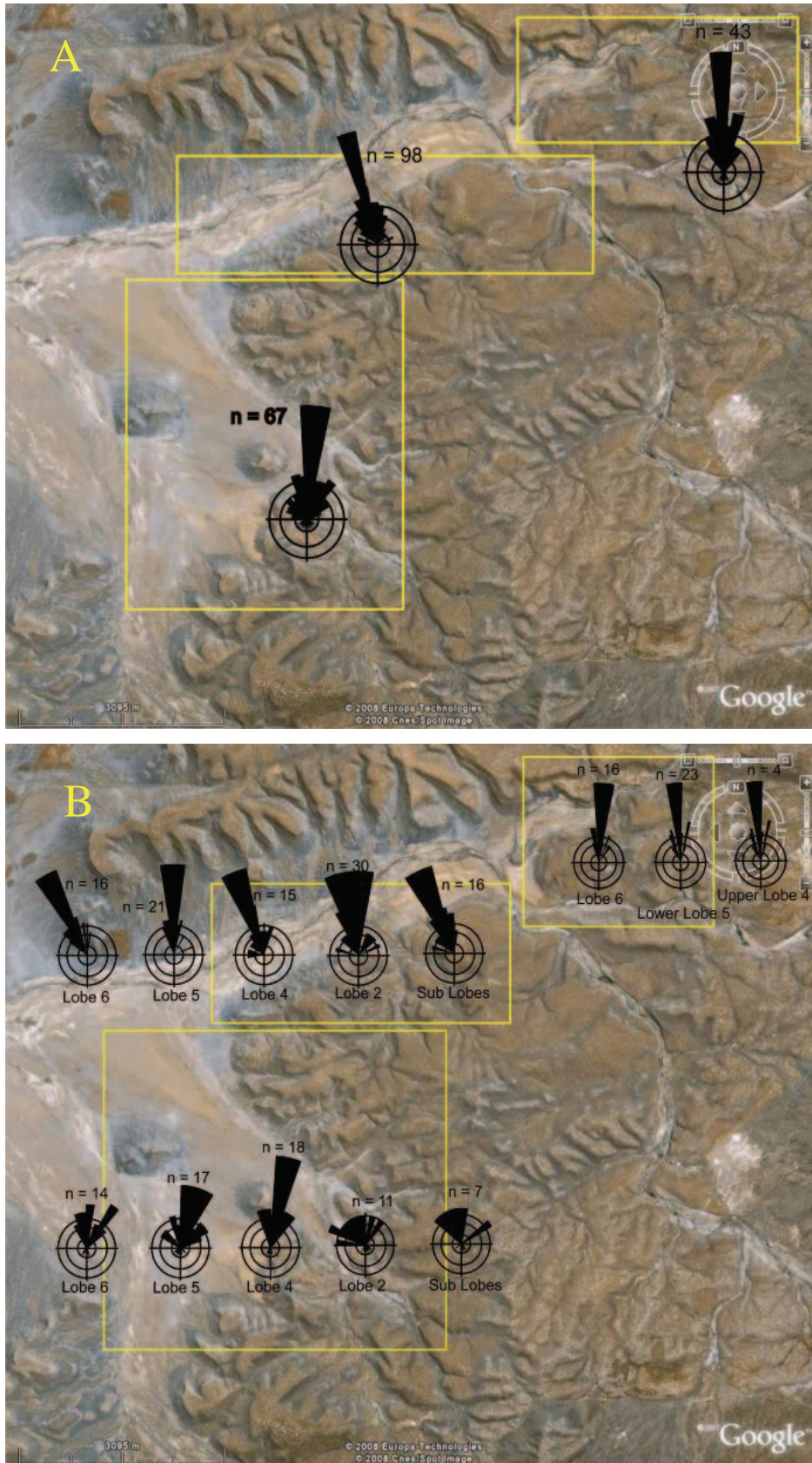


Figure 3.15 Topographical map of the area indicating the locations of the various correlation panels.



**Figure 3.25** Palaeoflow directions for Fan 3. (A) is a summary of the whole Fan 3, whereas (B) breaks down the palaeoflow into the main lobes. The yellow blocks represent the areas from which the groups of palaeoflow indicators were taken. The majority of the palaeoflow indicators are ripple laminations.

Highstand System Tracts (HST) are formed during later stages of sea level rise. The early stage of HST in deep water is characterised by hemipelagic mud deposition. This is because of the increase in accommodation space, which ensures that almost none of the coarser sediments are transported beyond the shelf edge. Turbidites can however be deposited during HST in deep water if sediments can accumulate on the shelf edge.

Lowstand System Tracts (LST) are formed during relative sea level fall. They are characterised by a basinward shift in coarser sediment deposition. Gravity processes, such as sediment gravity flows, play an important role in moving sediment beyond the shelf edge.

Transgressive System Tracts (TST) are formed during that part of relative sea level rise when the rate of accommodation space increase exceeds the rate of sediment supply into the basin. A TST is characterised by basin filling, and is contained within basinal mudstone in deep water.

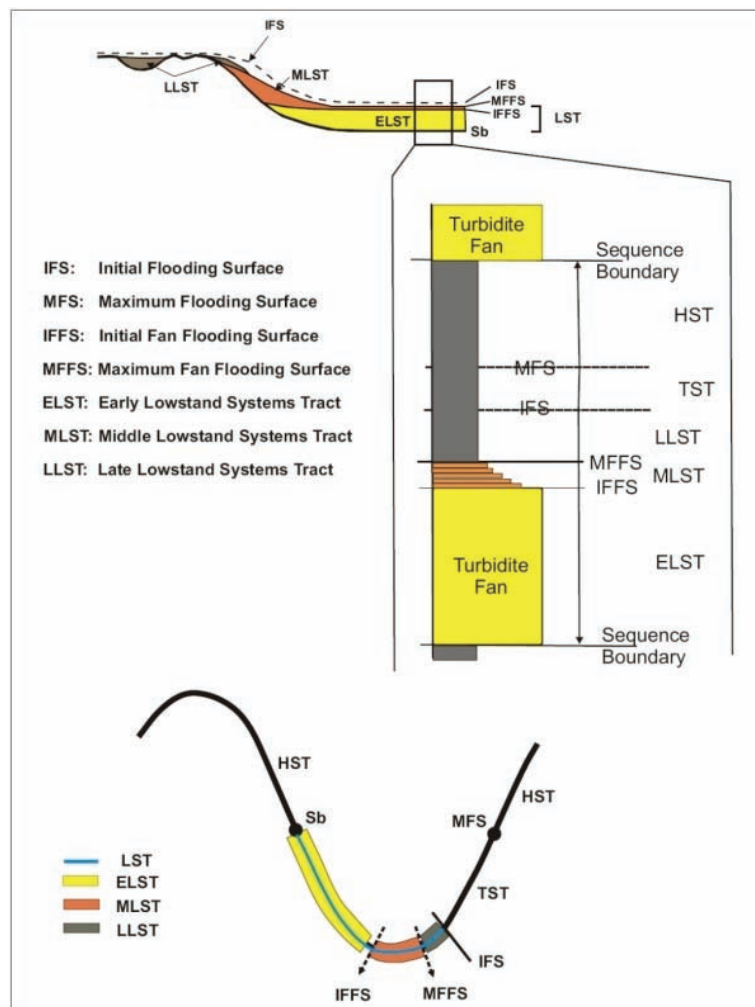


**Figure 4.1** A simple diagram from Sixsmith (2000) showing the surfaces and zones used to describe a turbidite.

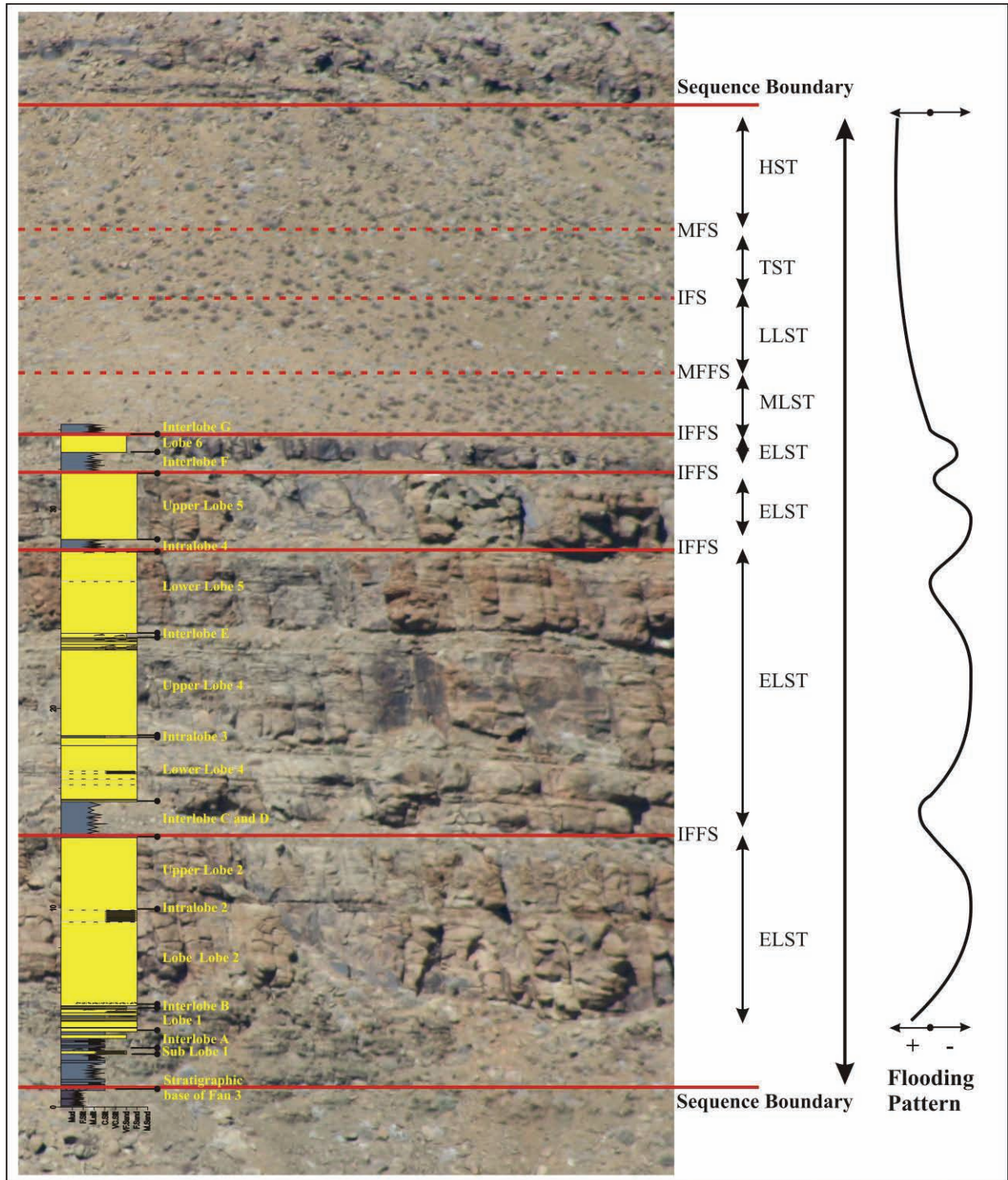


**Figure 4.2** Application of sequence stratigraphy on the outcrops of Fan 3 of the southern Gemsbok River valley.

Assuming some allogenic control over lobe deposition, a general pattern of sea-level fluctuation can be inferred. The entire lobe complex was deposited during LST (relatively shallower sea-level). On a more micro-scale, internal variation within the lobe complex shows a

pattern of variable flooding. Lobes and lobe-elements were each deposited during an early LST (ELST) followed by fine-grained deposition after an initial fan flooding surface (IFFS).

The lengths of the flooding stages correspond to the progradation-aggradation-retrogradation pattern as described by Hodgson *et al.* (2006) for Fan 3. Fig. 4.3 is a dip section schematic of the outcrops to the south of the Gemsbok River valley to the northern pinch-out of Fan 3. The figure was modified from Prélat *et al.* (in review) in order to show both Upper and Lower Lobe 4. Lobe 5 was left unchanged, as Upper Lobe 5 has a similar pattern to Lobe 6. The red box represents the observed outcrops of this study (the area south of the Gemsbok River valley). The figure is not drawn to scale. The Sub Lobes and Lobes 1 and 2 represent the progradational phase, or initial basin-ward shift of Fan 3. Lobes 4 through Lower Lobe 5 are aggradational, gradually building the bulk of the fan. This part constrains the largest part of the fan, in terms of thickness and spatial and volumetric extent. Upper Lobe 5 and Lobe 6 are more retrogradational, at least this is their appearance in the study area. Their thickness never matches that of the underlying lobes, which are much thicker down-dip. Also, Lobe 6 pinches out over almost 6 kilometres along the Gemsbok River valley, but has only a single identified axial zone and remains mostly structured away from this zone.

The above pattern is also reflected on the micro-scale. The length of the gradation stages determined the duration of the ELSTs, and as a result the volume of the lobes that were deposited during that stage. To illustrate this graphically, a line diagram is presented on the right in Fig. 4.2. A curve to the right means a relative lowering of sea-level, where as a curve to the left is a relative increase in sea-level. It should be noted that the longest ELST is again an

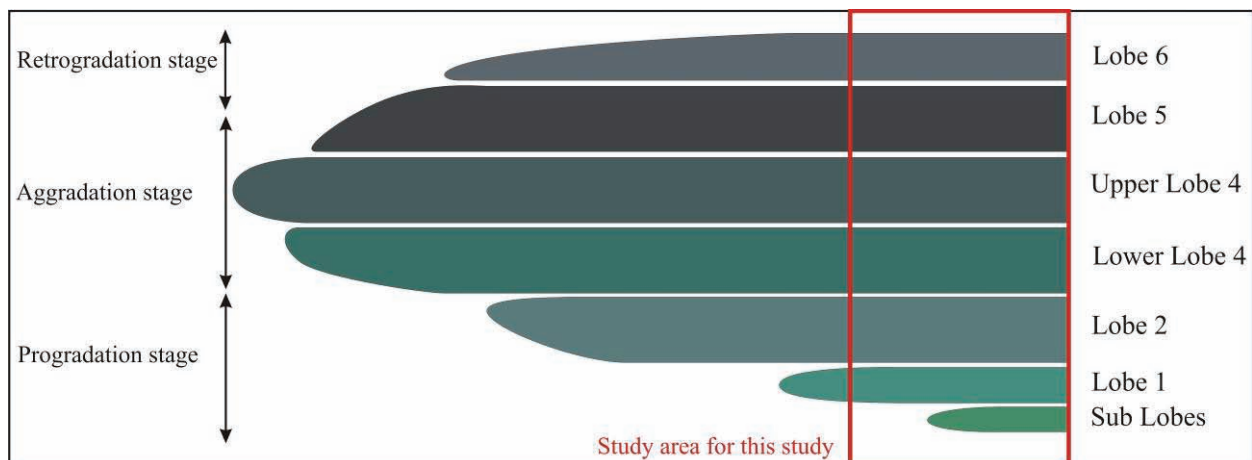


**Figure 4.3** Schematic of a dip section through mid to distal Fan 3 to illustrate the different stages of deposition. Modified from Prélat *et al.* (in review).

metres), only the top GPS coordinates were used to reference the positions of the profiles, as they are generally more accurate and display smaller errors (better overhead coverage). For this reason, the bottom coordinates, as well as the tops and bottoms of every bed in relation to the top GPS coordinates, were calculated in Excel for later use. GPS measurements were taken using UTM standards.

The data gathered in the field proved more difficult to use in Petrel than expected. None of the lobes had the same regional extent (E-W and N-S extent). Figure 5.1 shows an example of what the final spreadsheets looked like. It shows the tops and bases of all individual lobes and lobe-elements defined for use in Petrel. These numbers were calculated by subtracting measured thicknesses from the topmost GPS coordinate.

Profile Name	X Coordinate	Y Coordinate	Top	Top L6	Base L6	Top UL5	Base UL5	Top LL5	Base LL5	Top UL4	Base UL4	Top LL4	Base LL4
J7030245RD	412255	6385599	568	568.00	558.85	558.31	558.31	557.77	555.91	554.56	552.56	552.36	552.36
J6830263RD	411967	6385745	561	563.30	561.40	561.20	561.20	561.00	559.53	559.53	556.96	556.76	556.76
J6450245RD	411817	6385234	586	586.00	582.51	581.46	581.46	580.41	578.56	578.24	575.69	575.49	575.49
J6180245ZM	411553	6385156	593	593.00	586.80	586.00	586.00	585.19	583.59	583.39	581.39	581.19	581.19
J5940245ZM	411283	6385083	582	581.30	574.13	573.16	573.16	572.18	570.23	569.69	567.69	567.49	567.49
J5030246ZM	410522	6384661	567	567.00	562.28	561.73	561.73	561.18	557.89	557.39	554.83	554.63	554.63
J4930248ZM	410499	6384466	576	576.00	571.03	570.50	570.50	569.96	565.84	565.12	562.34	562.14	562.14
J4860243ZM	410236	6384795	556	558.30	556.40	556.20	556.20	556.00	551.14	550.46	546.74	546.54	546.54
J4800242ZM	410181	6384778	560	560.00	559.20	558.90	558.90	558.59	553.91	553.47	547.79	547.59	547.59
J4710243ZM	410103	6384732	560	562.30	560.40	560.20	560.20	560.00	556.07	555.53	551.31	551.11	551.11
J3730245ZM	409310	6384105	567	567.00	564.05	563.53	563.53	563.00	558.64	558.04	553.32	553.12	553.12
J3570245ZM	409185	6384023	572	572.00	568.79	568.41	568.41	568.02	565.24	564.79	559.67	559.14	558.32
J3430245ZM	409052	6383961	568	568.00	564.74	564.05	564.05	563.35	559.63	558.82	552.30	552.11	550.21
J3270245ZM	408888	6383941	571	571.00	570.36	569.95	569.95	569.54	564.74	564.11	557.76	556.89	556.32
J3150245ZM	408815	6383872	569	571.30	569.40	569.20	569.20	569.00	565.26	564.66	556.76	556.76	553.56
J2920246ZM	408596	6383745	563	567.40	565.50	565.30	565.30	565.10	563.20	563.00	557.59	556.67	554.32
J2760256ZM	408578	6383217	550	550.00	548.34	548.30	548.30	548.26	544.96	544.96	539.66	539.66	538.33
J2750246ZM	408435	6383682	565	569.40	567.50	567.30	567.30	567.10	565.20	565.00	563.59	563.00	559.76
J2690255ZM	408512	6383242	555	557.30	555.40	555.20	555.20	555.00	550.80	550.28	545.38	545.38	543.50
J2660254ZM	408482	6383272	552	556.40	554.50	554.30	554.30	554.10	552.20	552.00	546.68	546.68	545.66
J2340249ZM	408094	6383398	576	580.40	578.50	578.30	578.30	578.10	576.20	576.00	572.41	570.74	567.68
J2130246ZM	407872	6383410	589	591.10	589.20	589.00	588.44	588.11	585.24	584.76	581.77	581.67	577.67
J2030246ZM	407788	6383363	593	593.00	592.22	591.18	590.35	589.98	587.65	587.03	582.87	582.49	579.07
J1930246ZM	407670	6383315	601	601.00	599.41	598.21	597.55	597.08	594.00	593.16	589.87	589.64	585.34
J1800247ZM	407605	6383233	607	607.00	605.30	603.68	602.75	602.00	599.98	599.25	596.21	595.84	592.04
J1700248ZM	407517	6383184	602	604.10	602.20	602.00	601.72	601.35	597.46	597.09	594.10	593.80	588.25
J1600248ZM	407427	6383149	609	611.60	609.70	609.50	609.02	609.00	604.44	603.80	599.66	599.08	595.22
J1500248ZM	407332	6383110	617	619.10	617.20	617.00	616.31	616.11	613.01	612.46	606.62	606.42	604.52
J1400247ZM	407237	6383062	628	628.00	625.20	623.74	622.74	622.20	619.10	618.57	613.95	613.78	610.51
J1300248ZM	407143	6383021	633	632.80	630.54	629.70	628.80	628.50	624.41	624.41	620.62	620.62	618.82
J1200249ZM	407058	6382967	636	636.00	634.55	633.53	631.63	631.23	629.15	629.15	623.55	623.55	621.85
J1100249ZM	406984	6382993	637	637.00	636.20	635.18	632.72	632.52	630.98	630.98	629.09	629.09	623.76
J1030252ZM	406903	6382875	635	635.00	634.10	632.97	630.51	630.16	627.46	627.46	622.16	622.16	619.33
J0920253LK	406808	6382816	625	625.00	624.20	623.04	620.14	619.95	615.30	615.20	610.55	610.35	608.45
J0820250LK	406709	6382801	622	621.52	620.58	619.52	616.22	615.61	612.11	611.89	606.97	606.87	603.72
J0620258LK	406552	6382653	626	626.00	626.00	625.80	623.76	622.94	618.69	618.65	617.15	616.95	612.86
J0450266LK	406396	6382558	616	618.30	618.30	618.10	616.20	616.00	611.97	611.97	609.33	609.13	605.96
J0350269LK	406277	6382534	615	619.40	619.40	619.20	617.30	617.10	615.20	615.00	612.20	612.20	608.80
J0100292LK	406025	6382520	623	625.30	625.30	625.10	623.20	623.00	622.43	622.33	619.68	619.68	616.80
J0000000LK	405933	6382519	625	625.20	625.20	625.00	624.45	624.33	622.31	622.31	620.41	620.41	616.31
J0500312LK	406350	6382216	574	578.40	578.40	578.20	576.30	576.10	574.20	574.00	570.54	570.54	570.19
J0560002LK	405949	6381967	604	606.30	606.30	606.10	604.20	604.00	600.82	600.82	598.66	598.66	598.14
J0500345LK	406102	6382069	598	600.30	600.30	600.10	598.20	598.00	591.96	591.96	589.96	589.96	588.16
J0950345LK	406185	6381585	585	587.10	585.20	585.00	583.80	583.63	572.78	572.58	571.93	571.93	571.28
J0950357LK	406005	6381558	576	578.10	576.20	576.00	574.08	573.92	566.88	566.68	566.16	566.16	565.63
J1270348LK	406227	6381286	578	582.20	580.30	580.10	578.20	578.00	576.51	576.51	573.49	573.49	571.49
J1330352LK	406145	6381193	578	582.20	580.30	580.10	578.20	578.00	572.01	571.81	570.83	570.83	569.85
J1490345LK	406359	6381089	583	587.20	585.30	585.10	583.20	583.00	581.74	581.61	579.13	579.13	577.42

**Figure 5.1** Part of one of the spreadsheets used to calculate top and base values for use in Petrel. The yellow cells represent areas where no data were present in the initial construction of the spreadsheet. The values were calculated during the later stages of modelling in order to facilitate the process in Petrel.

The yellow cells in Figure 5.1 represent areas where no data were present in the field, i.e. either through lack of outcrop, erosion or pinch-out, or where lobe-sets were too amalgamated to separate (between white cells). The values in these cells were calculated in order to give all lobes the same regional extent. This makes using them in Petrel a lot easier.

In general, one basic rule was followed: the thickness of the siltstones-breaks separating lobes were set to 20 cm in areas where no outcrop data were present. To keep things simple, it was assumed that the sandstones were amalgamated, which is probably not far from reality.

In some cases the sand-prone lobes pinched out. For these instances the 20 cm siltstone breaks

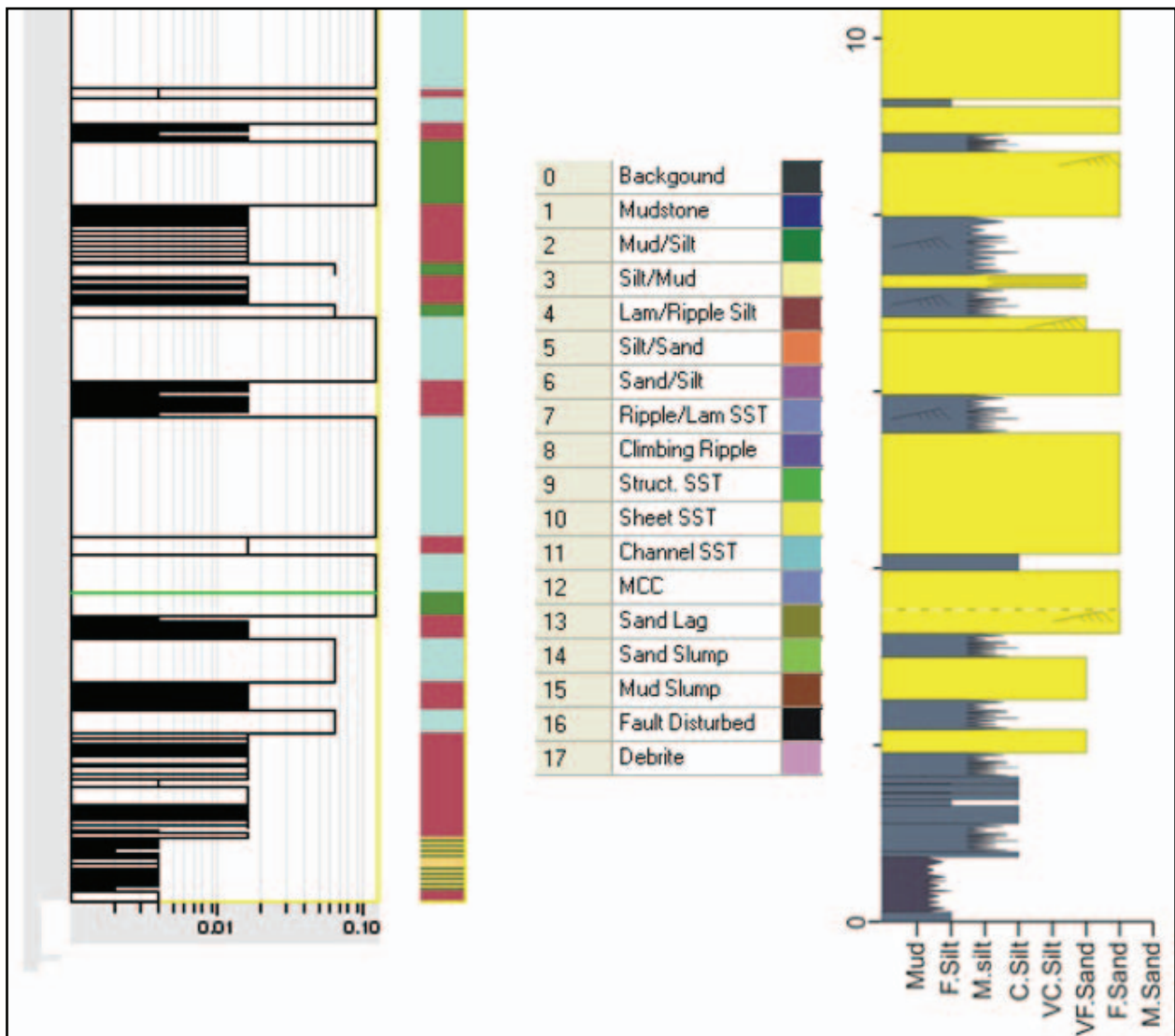


**Figure 5.2** An example of how DSL (left) and CorelDraw (right) displays the same vertical profile, in this case J4930008LK. DSL’s digital usage of data makes it very useful for exporting into other programs, whereas CorelDraw provides a better visual display of the data.

## Deposition of Fan 3

### 6.1 Introduction

This chapter will attempt to explain some of the depositional features described in previous chapters, particularly Chapter 3. The 2D outcrop maps will be used in conjunction with the isopach maps generated in Petrel.

A “fan” is not the immediate result of a turbidity deposit, but rather the combination of many smaller events. A study by Machado *et al.* (2004) outlined three distinct deposits (based on age

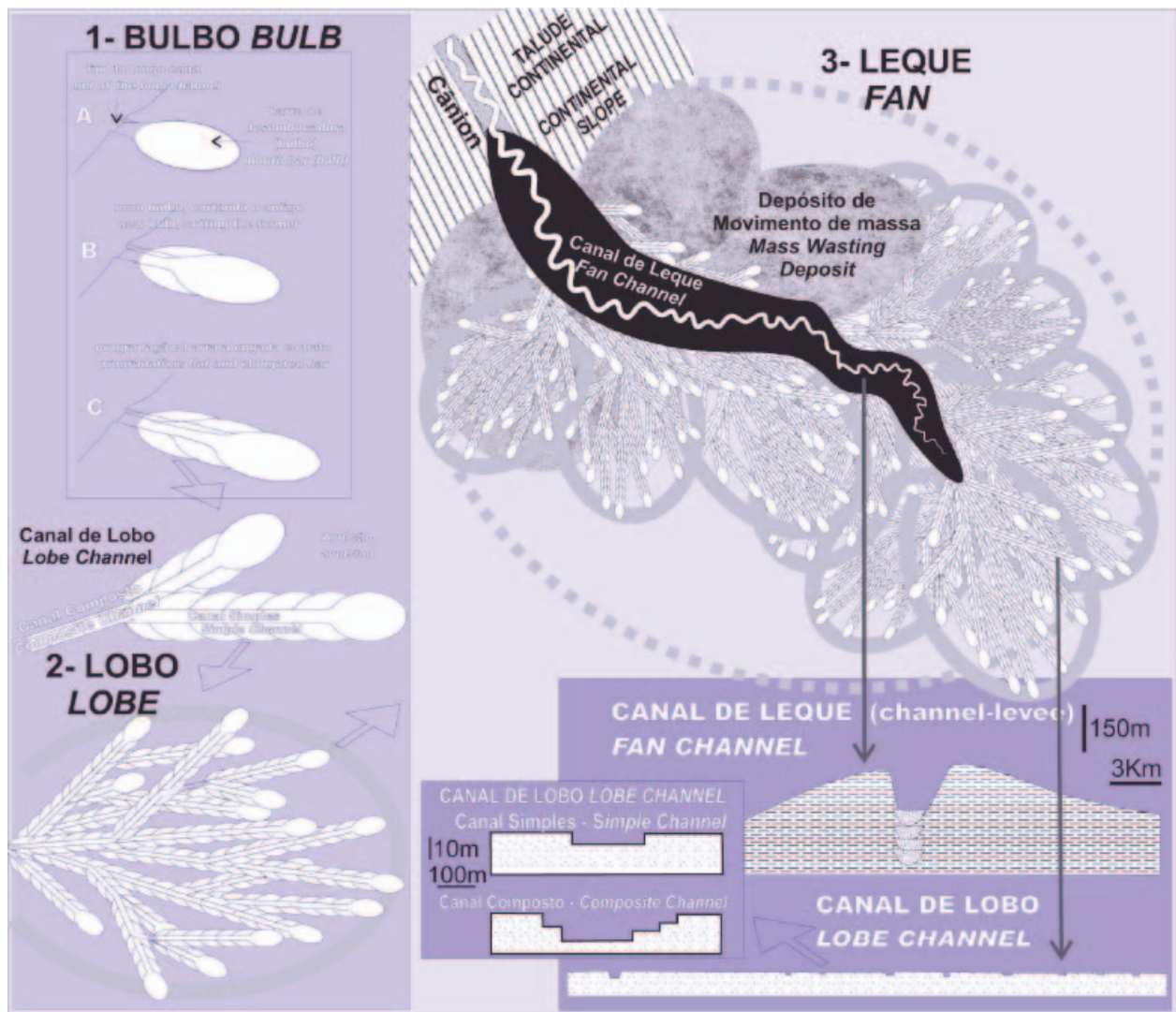


**Figure 6.1** Three depositional models for turbidity currents as suggested by Machado *et al.* (2004). These models are based on age and complexity. Initially, a turbidity current forms a bulb. Given time and a constant sediment supply, several bulbs can build a lobe.

and complexity) based on studies of the modern Mississippi, Amazon and Indus deltas, as well as the Paraíba do Sul/ Carapebus (Fig. 6.1). These deposits can build upon themselves in order to form the larger deposits. In other words, several relatively small “bulb” deposits (singular turbidity flow deposits, equivalent to beds and even lobe-elements) can form a lobe channel. If enough of these lobe channels are present, a “lobe” can form. A fan is then the final product of several lobes stacked together. As an ancient analogy the Tanqua Fan Complex is a prime example.

### 6.2 Finger-shaped deposits of Fan 3

The pattern suggested by Machado *et al.* (2004) gives lobes a more “finger-like” appearance near the distal parts and margins, as opposed to a “classic” lobe shape. These features are shown in Figure 6.1. Several such features have been observed by the Liverpool teams to the north of the Gemsbok River, closer to the pinch-out of Fan 3 (Prélat *et al.*, in review). These features are present in Lobes 4, 5 and 6, the last lobes to pinch out. In outcrop, they appear as major thickenings of a lobe after a steady thinning. They can appear within less than a hundred metres, and disappear just as fast, thickening a lobe by several metres within a very short distance (up to 8 metres within less than a hundred metres in the study area).

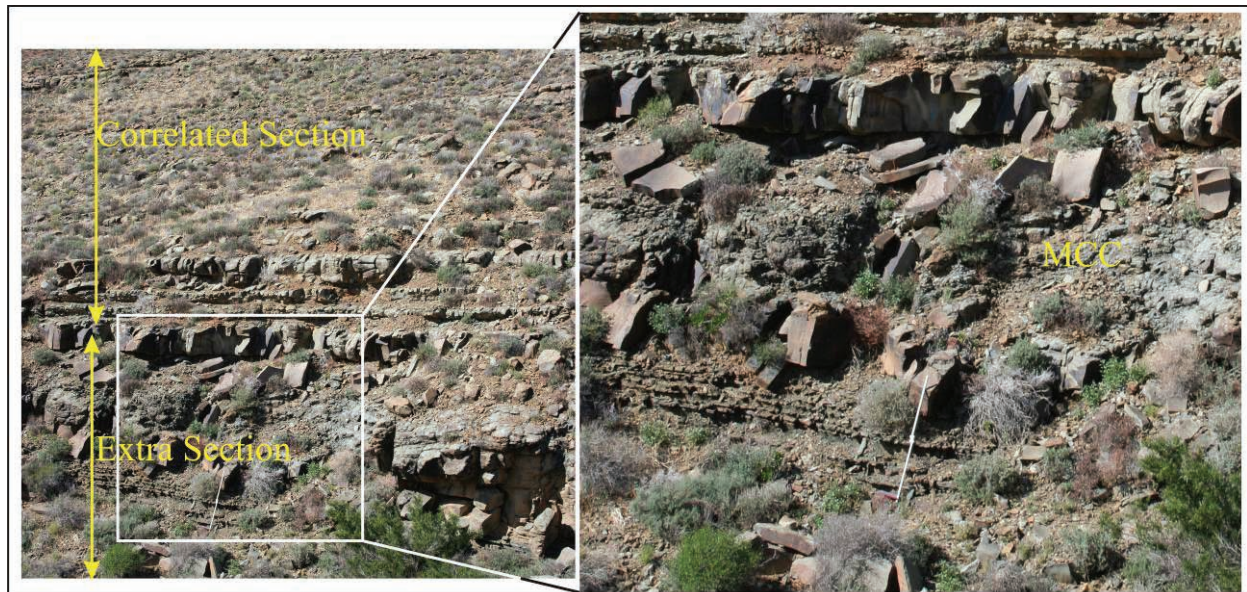


**Figure 6.2** Example of the bedded nature of the finger-shaped axial zones. The correlated section at the top can be traced for hundreds of meters along strike, whereas the “extra” section at the base is very localised, with less than a hundred metres lateral extent. Note the large amount of mud-clast conglomerates at the top of the thickest sandstone. Here it resembles a debrite, with significant amounts of organic material.

Generally, these features are well structured (Fig. 6.2), with beds and lobe-elements clearly defined and separated by siltstone or claystone (mostly claystone, whereas the rest of the lobe is separated almost exclusively by siltstone). They can also appear as structureless sandstone, with large concentrations of dewatering features. What they all have in common are the mud-clast conglomerates, located at the top and above the thicker sandstones, and the lack of major scouring at the base. In the study area this thickening would erode less than 2 metres compared to more than 8 meters of thickening. It should be noted that the outcrop in Fig. 6.2 did show more than 2 metres of erosion, however, this was into the underlying muds, and not into sandstones. Nowhere in the study area do these features (the axial zones in the central section) erode into older sandstone units.

Also, some display features that resemble a squeeze effect, where mud or sand is forced into plastic (soft-sediment) deformation by a relatively sudden increase in overburden. To the north, these features were observed within the lobe. In the study area, one such feature was identified in the claystones 2 metres below the thickest sections of sandstone. Figure 6.3 shows such a feature, located in the claystones below the lobe.

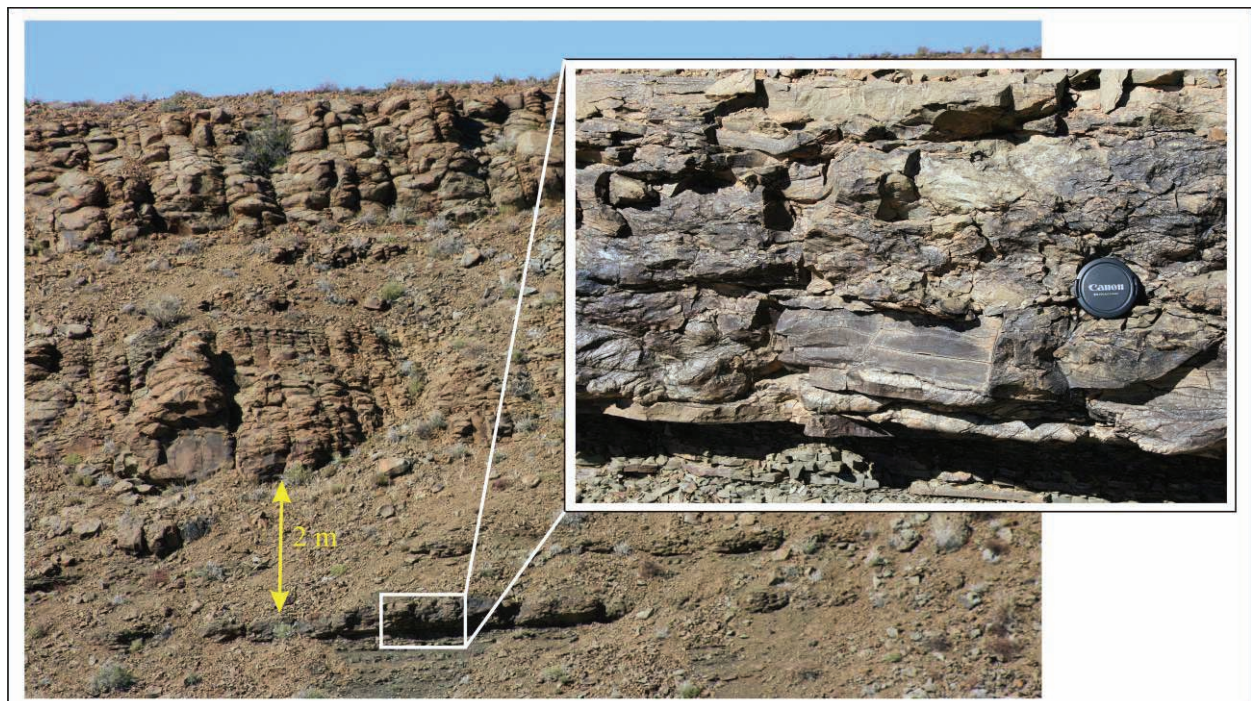


**Figure 6.3** Example of the plastic (soft-sediment) deformation observed in the units below a finger-shaped axial zone. This example is a siltstone located in the claystones about 2 meters below a significantly thickened lobe (Upper Lobe 4).

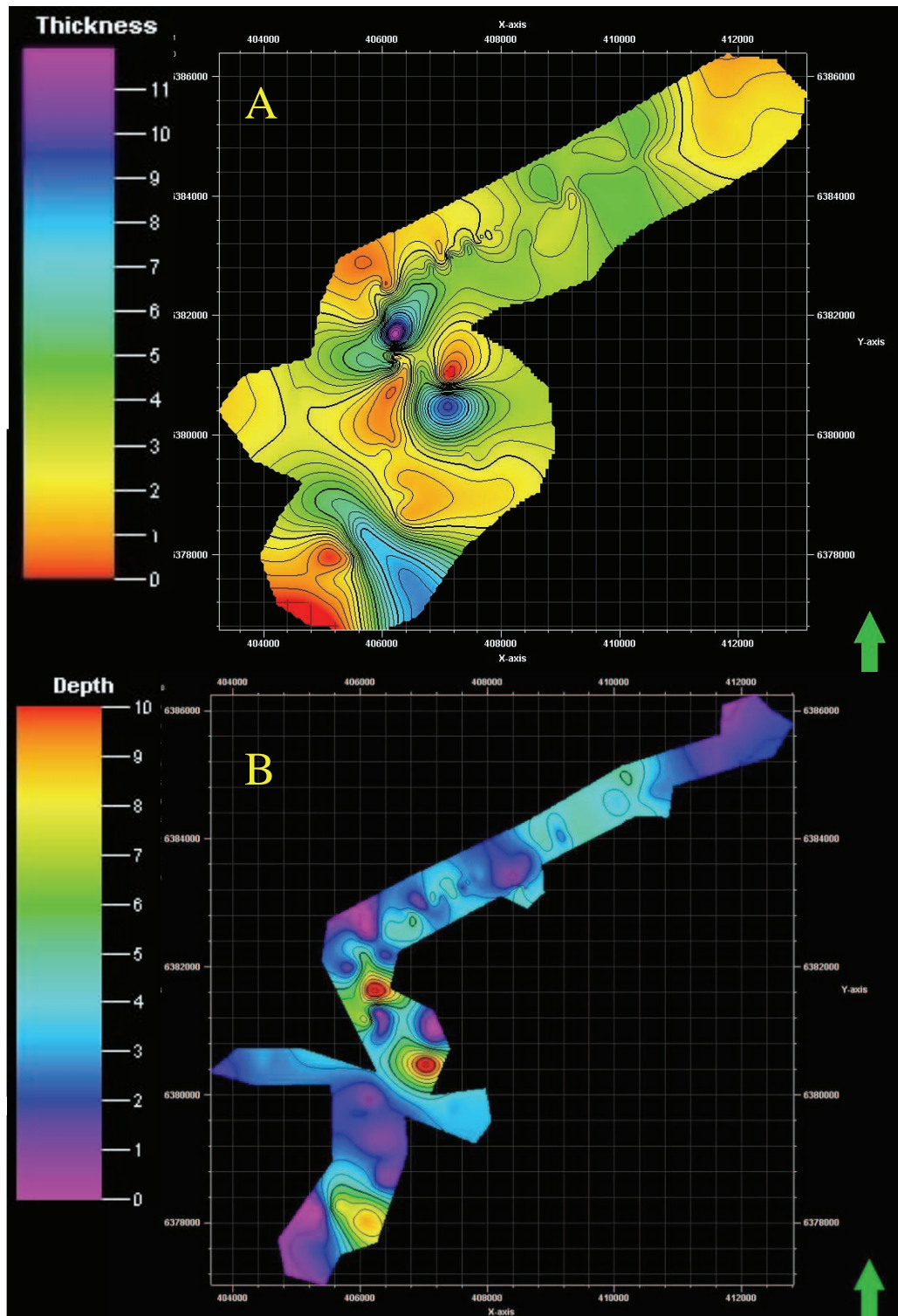


**Figure 6.4** Example of the difference between the first isopach maps and the final product. Both represent Lower Lobe 5. (A) used the old, larger polygon, and the colour scales were automatically adjusted to the minimum and maximum values. (B) used the constrained polygon and the colour scale was manually set to 10 metres. The results may appear similar, but there are some significant differences: (B) has a much smaller degree of contouring. The purple in (B) is both a result of outcrop not revealing the whole of the lobe (in the west and south), as well as true thinning (east).

accomplished by using Upper Lobe 5 and Lobe 6 as single axial zone analogies, and Lobes 2, 4 and Lower Lobe 5 as multiple axial zone analogies.

Single axial zones are the mid-fan continuations of channels which are mostly restricted to more proximal locations. A general appearance is an area of focussed flow, characterised by

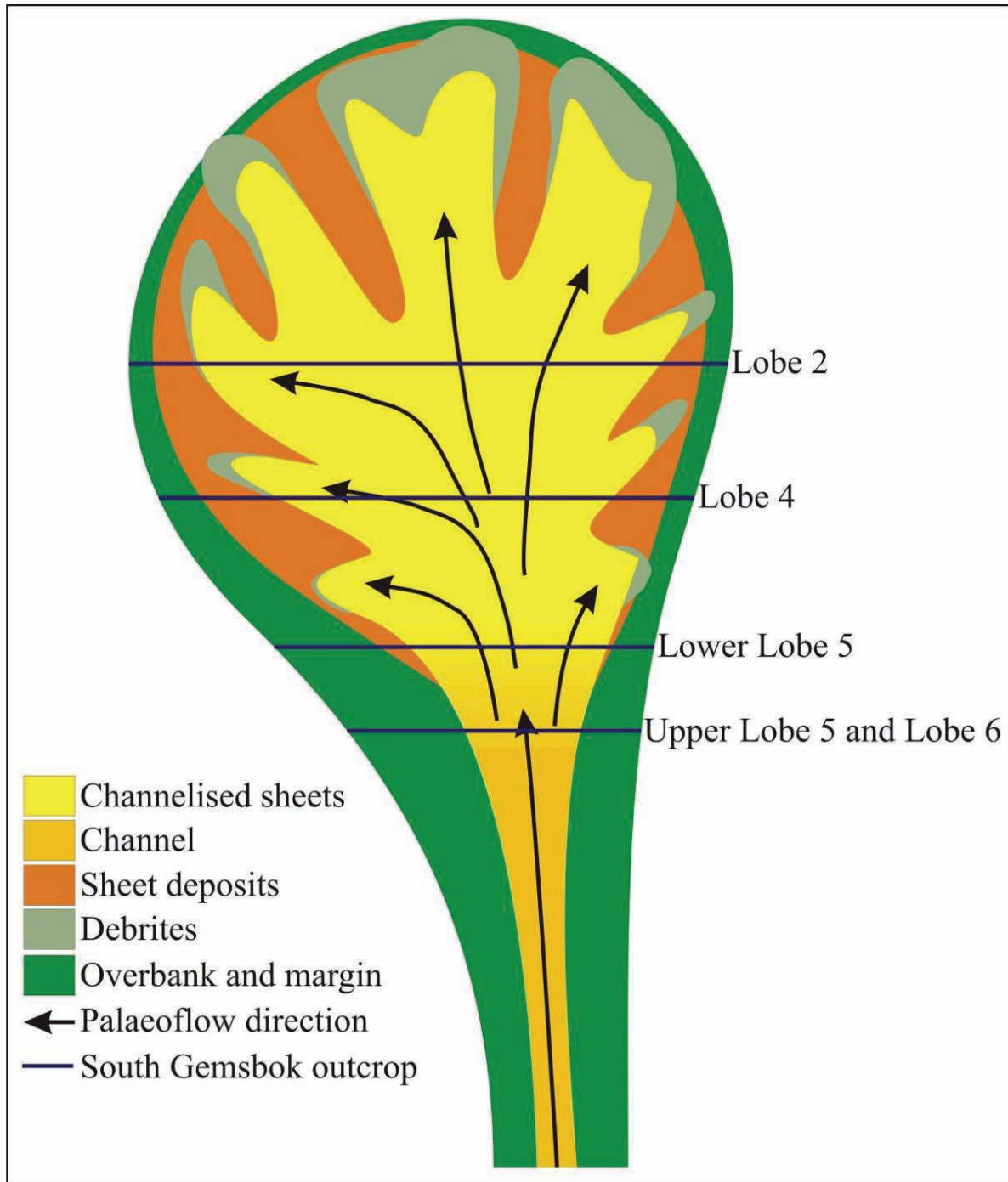


**Figure 6.6** Schematic of the structure of a lobe. The diagram illustrates the transition from channel to channelised sheets, and channelised sheets to sheets. The single axial zone is the transition zone from confined flow to unconfined floor spreading. Also indicated is the position of the southern Gemsbok Valley outcrop in relation to Lobes 2, 4, 5 and 6.

shape. Note that there are no “hard lines” separating the zones. The reason for this is that the transitions are often not abrupt, and grading between them is common.

#### 6.4.1 Lobe stacking

Topography can have a major influence on the flow direction of sediment gravity flows, ranging from diverting to complete damming of flows (Kneller and Buckee, 2004; Prather *et al.*, 1999; Pickering *et al.*, 1989). Topography can constitute a basin floor feature, or result from the presence of a previous deposit. In a distributive system, a deposit from a single flow has the appearance of a thickened “mid-section”, the equivalent of a channel, with thinning sheet deposits moving away from the centre. The channelised area would constitute a topographic high, and the sheet deposits topographic lows. Basic physics dictates that a flow should follow the path of least resistance. A new flow would therefore divert around the obstacle. The exact behaviour of a turbidity current in such a situation depends on the forward velocity of the flow, the height of the topographic obstruction, the density of the flow, and the density stratification of the flow (Alexander and Morris, 1994; Lane-Serff *et al.*, 1995). The result of such behaviour would appear in a strike section as laterally or vertically stacked flows, or a combination of stacking patterns.

The mid-fan strike section stacking pattern of all the lobes is shown in Figure 6.7. Note that this diagram is not to scale, and that anything to the right of the red line is unknown (the line represents the western end of the Gemsbok River valley outcrop). The lobes of mid Fan 3 show a

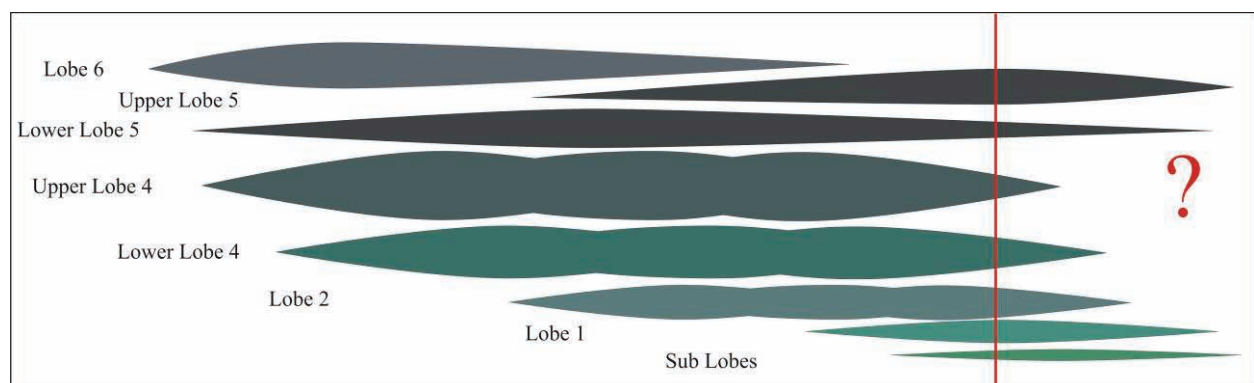


**Figure 6.7** Schematic to illustrate the strike section stacking pattern of Fan 3 in the mid-fan area (southern Gemsbok River valley) The red line represents the western end of outcrop in the valley. Not to scale.

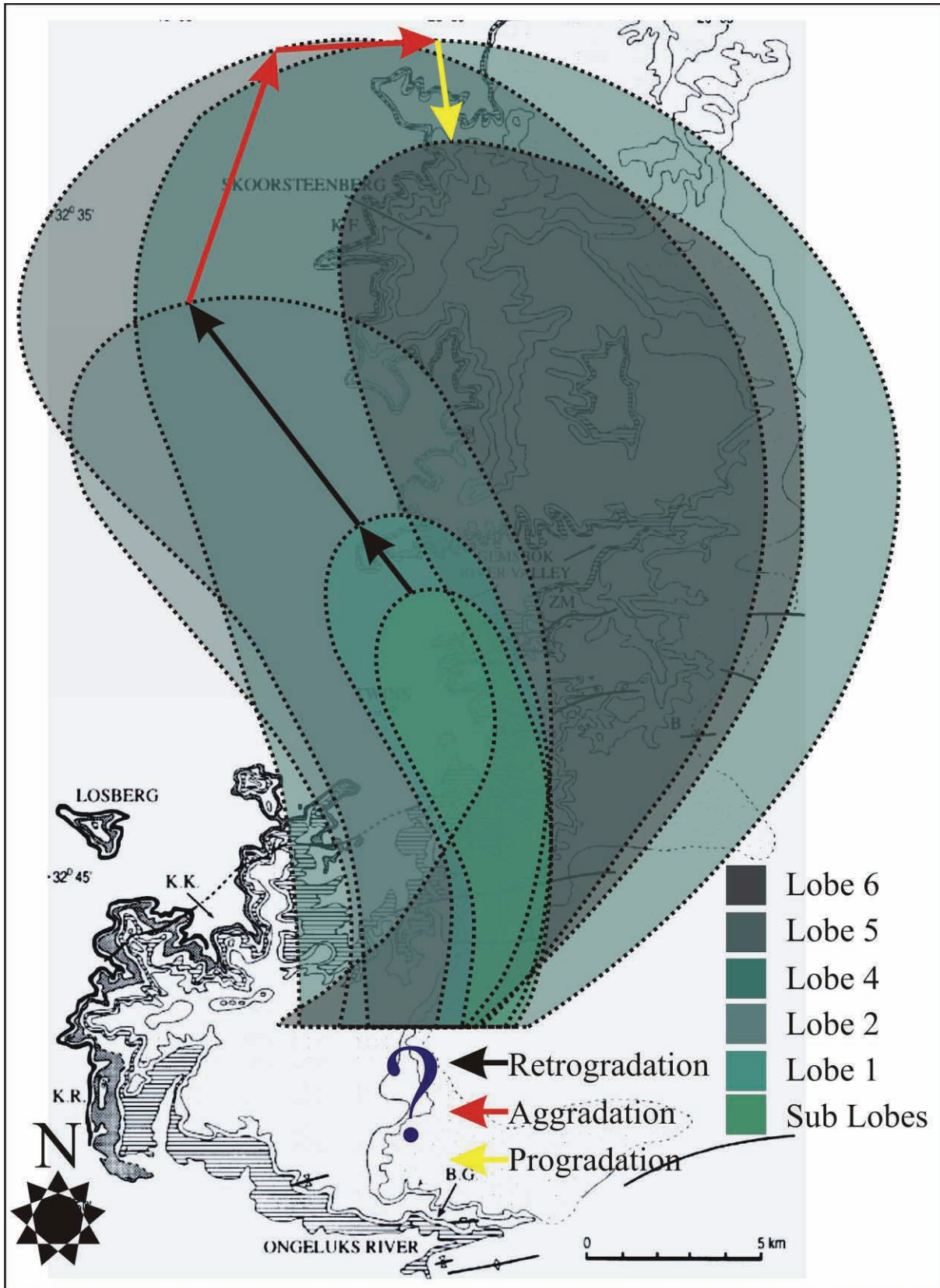


**Figure 6.8** Schematic of the probable locations of the Lobes in order to illustrate their positions relative to each other. Also shown is the inferred stepping pattern for the lobes. The black arrows represent basinward stepping (progradation), the yellow arrows represent aggradation, and the red arrows represent back stepping.

- Isopach map building (Chapter 6)
- Surface creation
- Static model grid building
- Lithofacies distribution modelling

This chapter will focus on several aspects of the modelling process. First the data will be discussed, providing examples of all the different forms used. Then the modelling process with Petrel will be discussed in detail, as well as the methods used and the limitations encountered. Lastly the results of these manipulations shall be discussed.

## 7.2 Petrel Modelling

Schlumberger's Petrel is a powerful software package capable of modelling most aspects of a petroleum reservoir. It includes a myriad of algorithms developed to create visual representations of complex physical features in 3D. For this project, only a small part of the program's capabilities was exploited, namely the grid building and facies modelling features and the ability to create isopach (thickness) maps. The aim here was to create a 3D representation of the conceptual depositional model (Chapter 6). For a short description of some of the algorithms

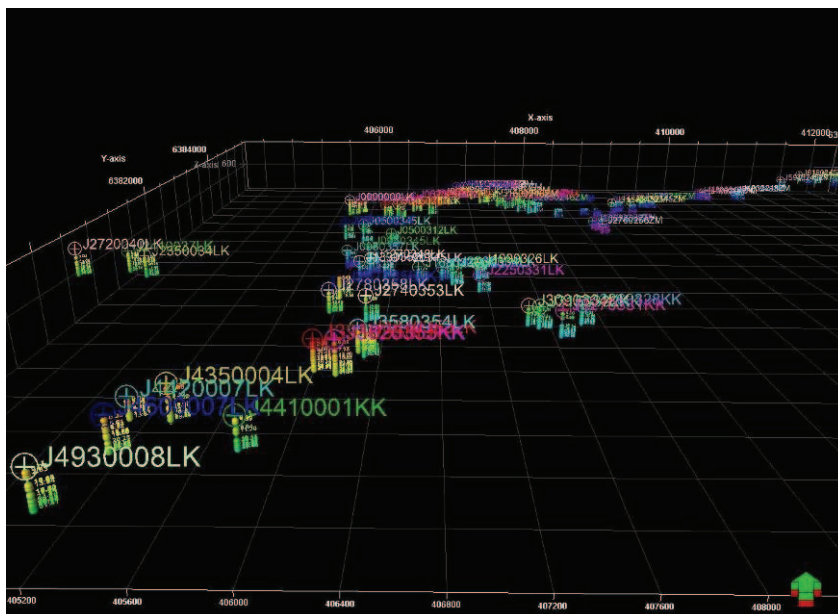


**Figure 7.1** A 3D view in Petrel, looking north, of the wells and well-tops used. These data represent all 72 vertical profiles (wells).

used by Petrel to create the features, based on Petrel's Online Help files, please refer to Appendix E.

### 7.2.1 Field size

Figure 7.1 is a view from the south, showing the entire study area. Both the wells and their associated well tops are shown. The entire study area covers an area of almost 10 kilometres from east to west, and about 7 kilometres from north to south. The entire area could not be included as is for the initial modelling attempts. The layout and positions of lobes and lobe-

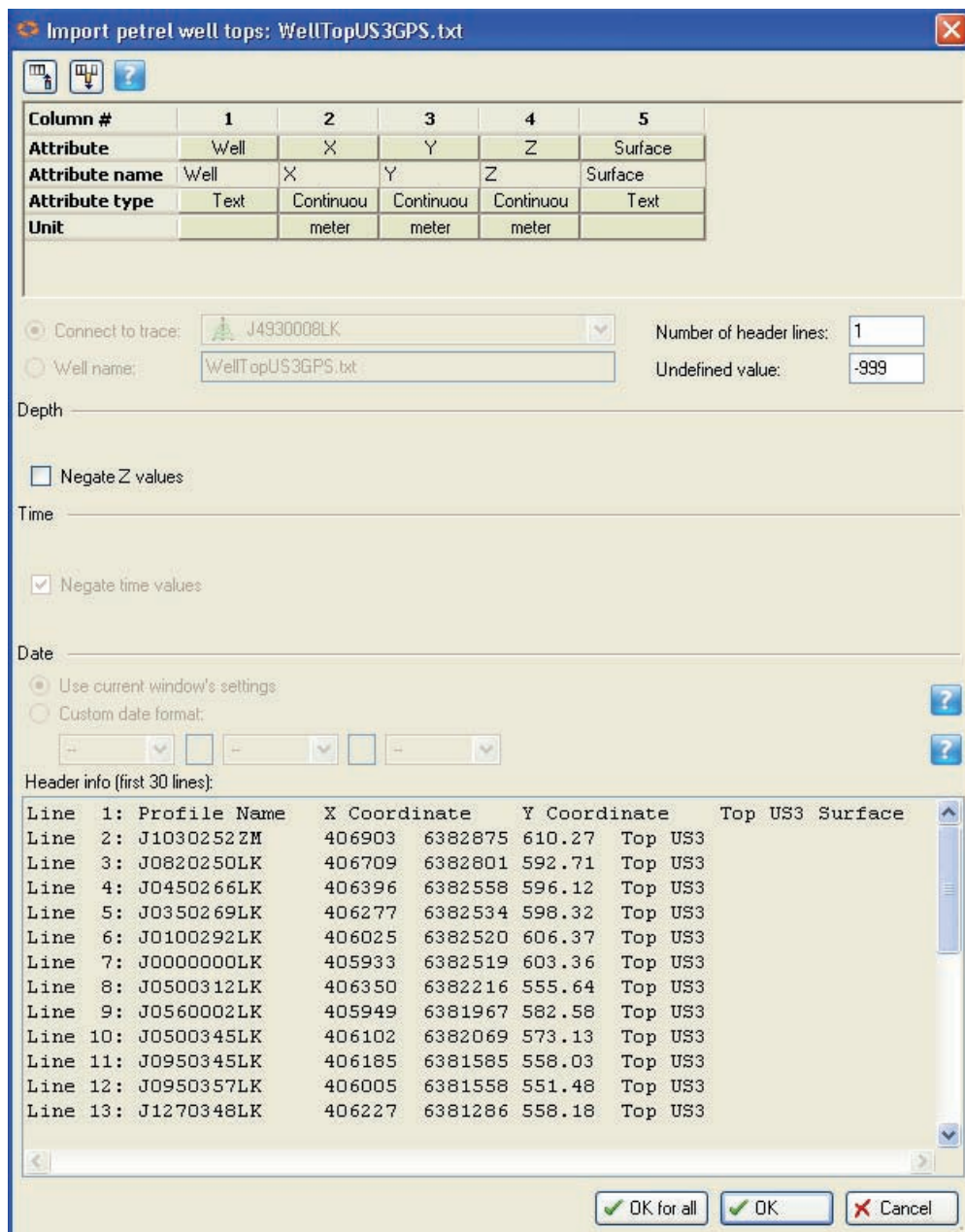
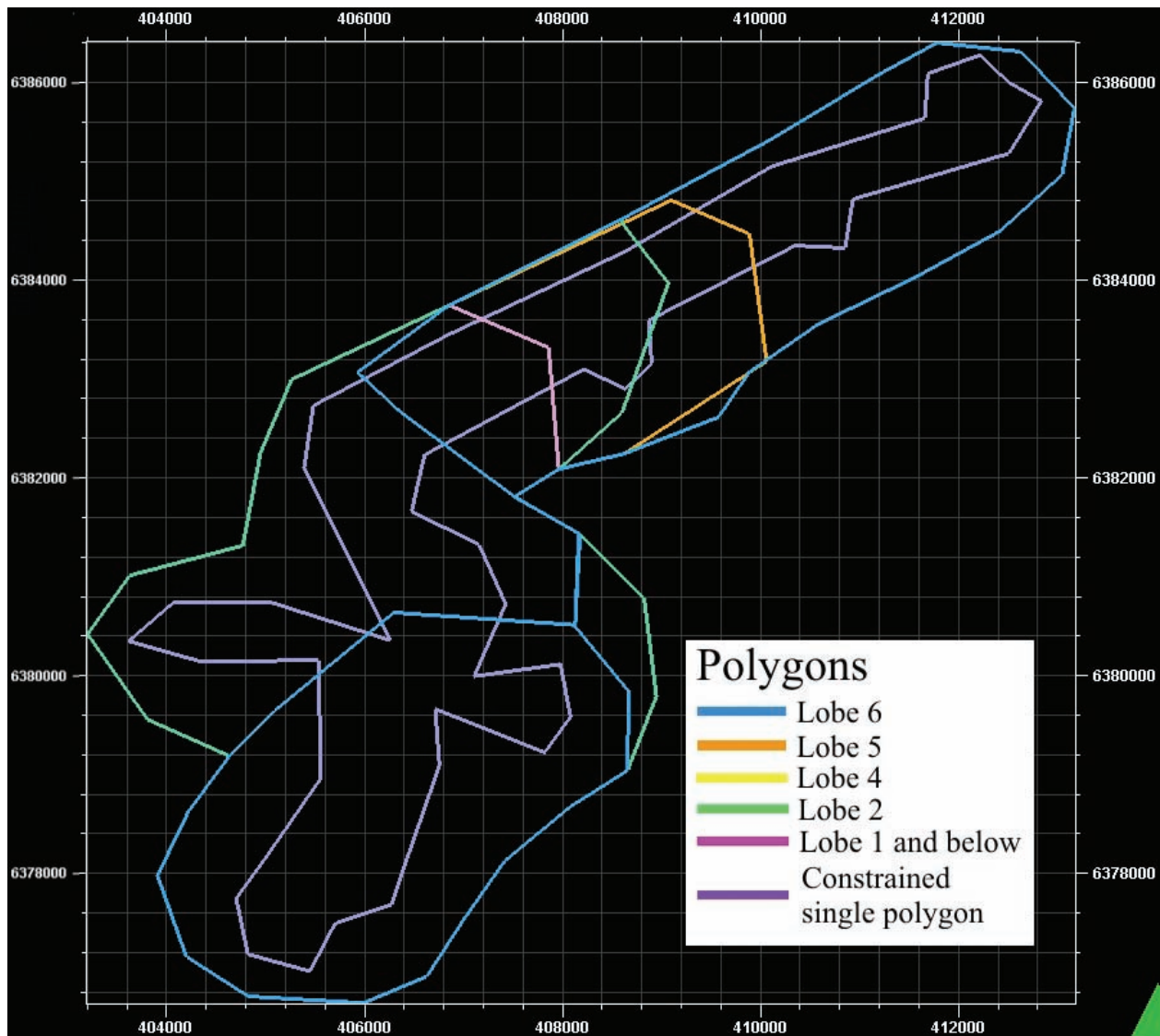


Figure 7.2 Example window of how data appear when imported from text files into Petrel.

While the Kriging algorithm is useful, the nature of the input data from this study makes it difficult for the algorithm to function properly (according to Petrel's Online Help files). For this reason, the Convergent Interpolation algorithm, which is the default algorithm, was used to form the surfaces used in building the grid for modelling. This algorithm was far more accurate in keeping to the data (Fig. 7.4 B). To make it even more accurate, a "well adjustment" was completed by adding the well tops as a constraint. The result was a surface that made contact with all the data points, even though it had a bit of a bulleted appearance (most detail centred around wells).

In order to illustrate the problem with the Kriging algorithm with this data-set, Appendix D



**Figure 7.3** The different polygons used in various runs in Petrel. The constrained polygon was used for the final product.

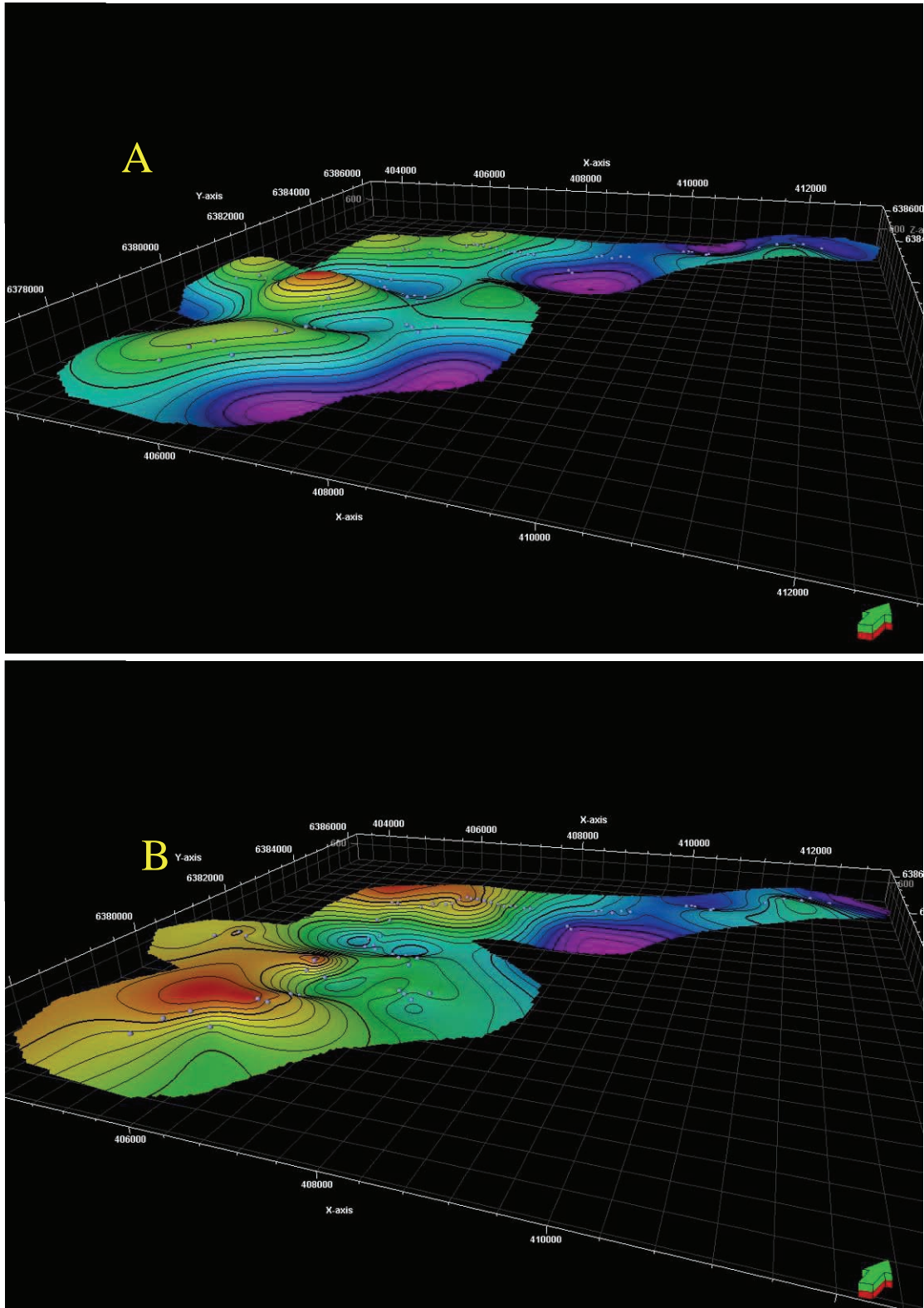


**Figure 7.4** Two of the initial surfaces created in Petrel. (A) used the Kriging algorithm, whereas the Convergent Interpolation (CI) algorithm was used for (B). Note the difference in surface shape between the two methods: Kriging created a much smoother surface but was unable to keep to the data, whereas CI managed to honour the data points to an acceptable degree.

### 7.2.4 Grids, Zones and Layering

Grids, zones, and layering are key features used to define a model. A grid is defined by using the surfaces created above (after Z adjustments), and providing the x and y dimensions for each cell. In this case, the dimensions were set to 20 metres a side. Because of computational constraints, the cells could not be any smaller. They need not be smaller for this model, as all wells are located far enough apart that a grid of 20x20 metres would place each well in its own cell (wells should not share a cell). The second problem with the original data arises here: all the data were used for the grid, but only a part of the western part of the field area was used, as this is the only place where all 5 boundary polygons overlap. Thus the grid was much smaller than intended.

The grid is defined in the z-axis by zones, the Petrel analogue for architectural elements such as lobes. They were built by using the “conformable” command, which forces them to follow the correlated well tops. Fig. 7.5 is an example of these zones as created in the initial runs.

Layering can be seen as the z-dimension of the cells. For the first few attempts it was set to 20 centimetres, and layered using the “Follow-top” command, which sets the cell layering parallel to the top of the zone. The choice between “follow top” and “follow base” was based on the fact that all the data used were based on the top z-value for each well, but refer to whether a unit should show top-lap or down-lap. Again the layering thickness was limited by the computer’s processing ability. This layering will also be used to up-scale (block) the lithofacies from the well-logs. The thickness of the layers determines whether a field measured feature will be visible or not. The DSL logs included all measured layers, but a too low resolution during layering in Petrel will average out these layers, resulting in a loss of data.

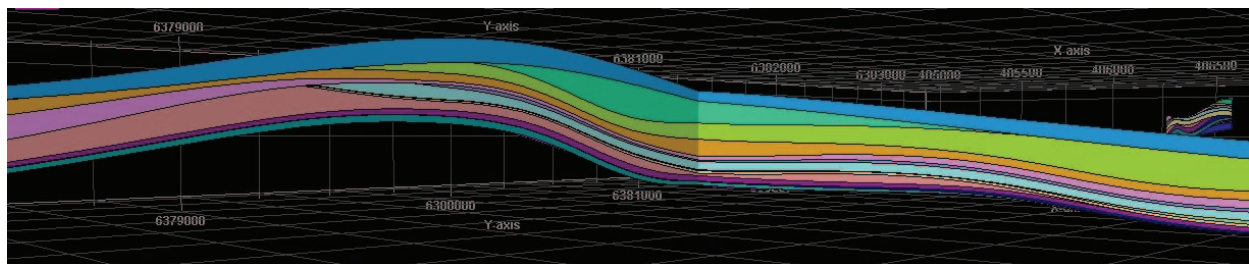


**Figure 7.5** This figure shows the zones created in the first grid run. The surfaces created from the larger polygons caused some major pinch-out features when grouped together. One of the reasons for this is because they used different polygons, and as such the Z values could not be correctly adjusted.

DSL Lithofacies	Reduced Lithofacies	Chapter 3 Lithofacies
Background	Background	Hemipelagic Suspension Deposits
Mudstone		
Mudstone / Siltstone (>50%)		
Siltstone / Mudstone (>50%)	Siltstone	Parallel- and ripple- cross-laminated siltstone
Laminated / Rippled Siltstone		
Siltstone / Sandstone (>50%)		
Sandstone / Siltstone (>50%)		
Laminated / Rippled Sandstone	Structured Sandstone	Structured Sandstone
Climbing Ripple Lam. Sandstone		
Structured Sandstone		
Structureless Sandstone (Sheet)		
Structureless Sandstone (Channel)	Structureless Sandstone	Structureless Sandstone
Channel Lag (Mud-clast conglomerate)	MCC	Mud-Clast Conglomerate
Channel Lag (Sand-clast conglomerate)		
Slump (sandstone)		
Slump (Mud)		
Debrite		

**Table 7.1** Summary table of the lithofacies used. The DSL lithofacies were grouped in order to better match the lithofacies descriptions as given in Chapter 3.

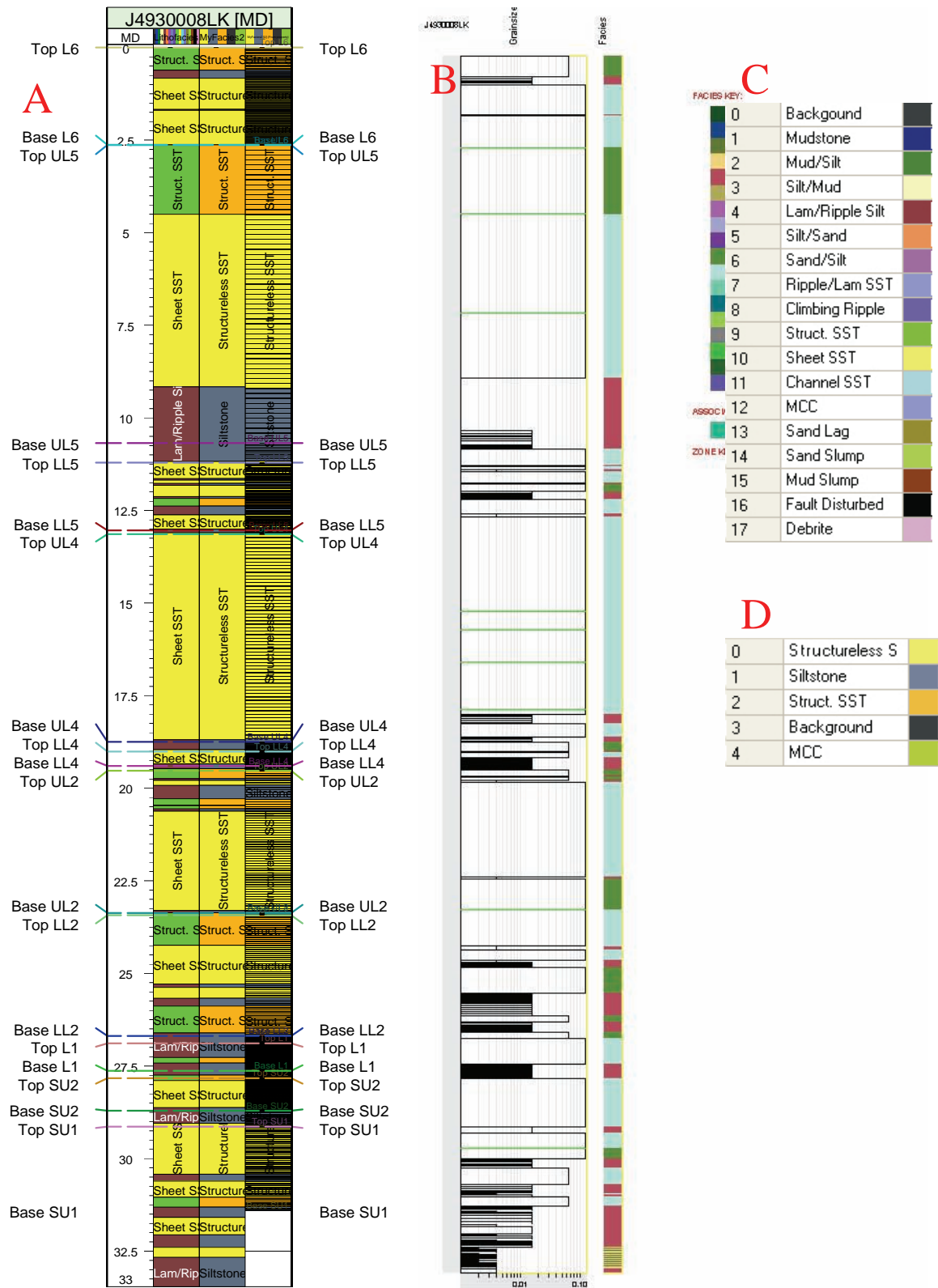


**Figure 7.6** Well J4930008LK. The detailed representation (A) is from Petrel. It shows both lithofacies lists used, namely the DSL lithofacies in the left column (lithofacies group C) and the reduced lithofacies in the middle column (lithofacies group D). The column to the right shows the result of proportional layering. The DSL profile (B) is again provided as a comparison.

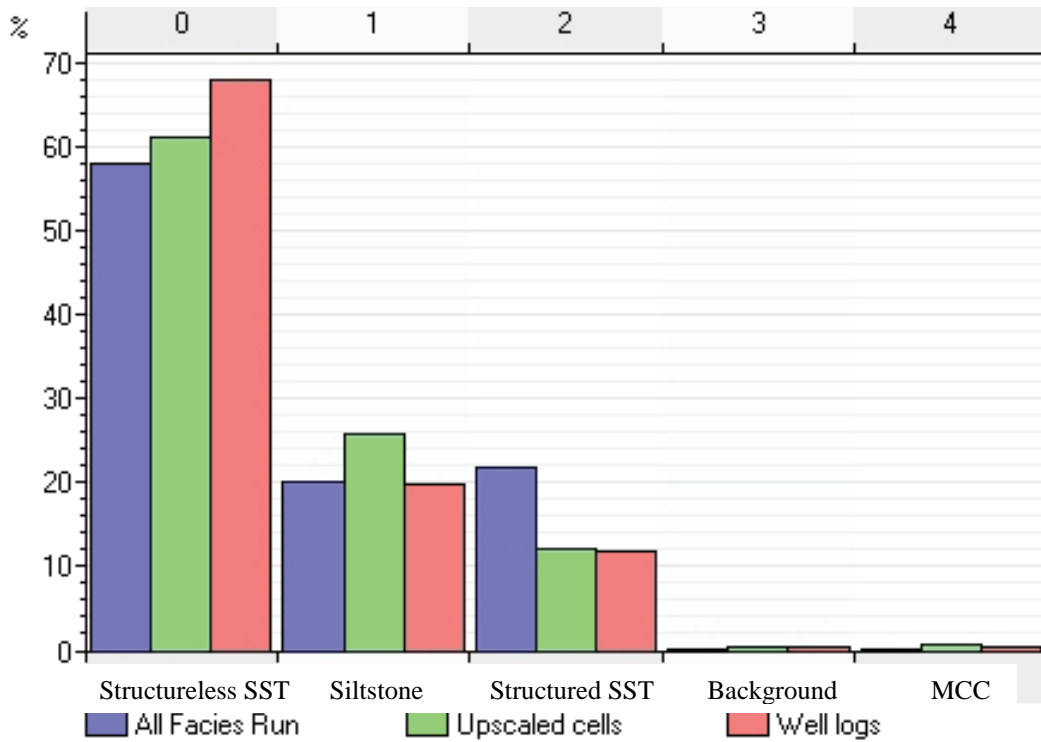


**Figure 7.7** The proportion of lithofacies present before and after lithofacies modelling. The percentage of a lithofacies present is shown on the y-axis, and the lithofacies are listed on the x-axis. The red column represents the original 1D lithofacies as provided by the well logs (reduced from the DSL lithofacies); the green represents the lithofacies proportions after up-scaling (the blocked wells); and the blue logs are the proportions (in 3D) after the lithofacies have been modelled in 3D. The aim is for the 3D model lithofacies to honour the 1D input data in 3D. The results, however, show a decrease in structureless sandstone and a proportional increase in structured sandstone.

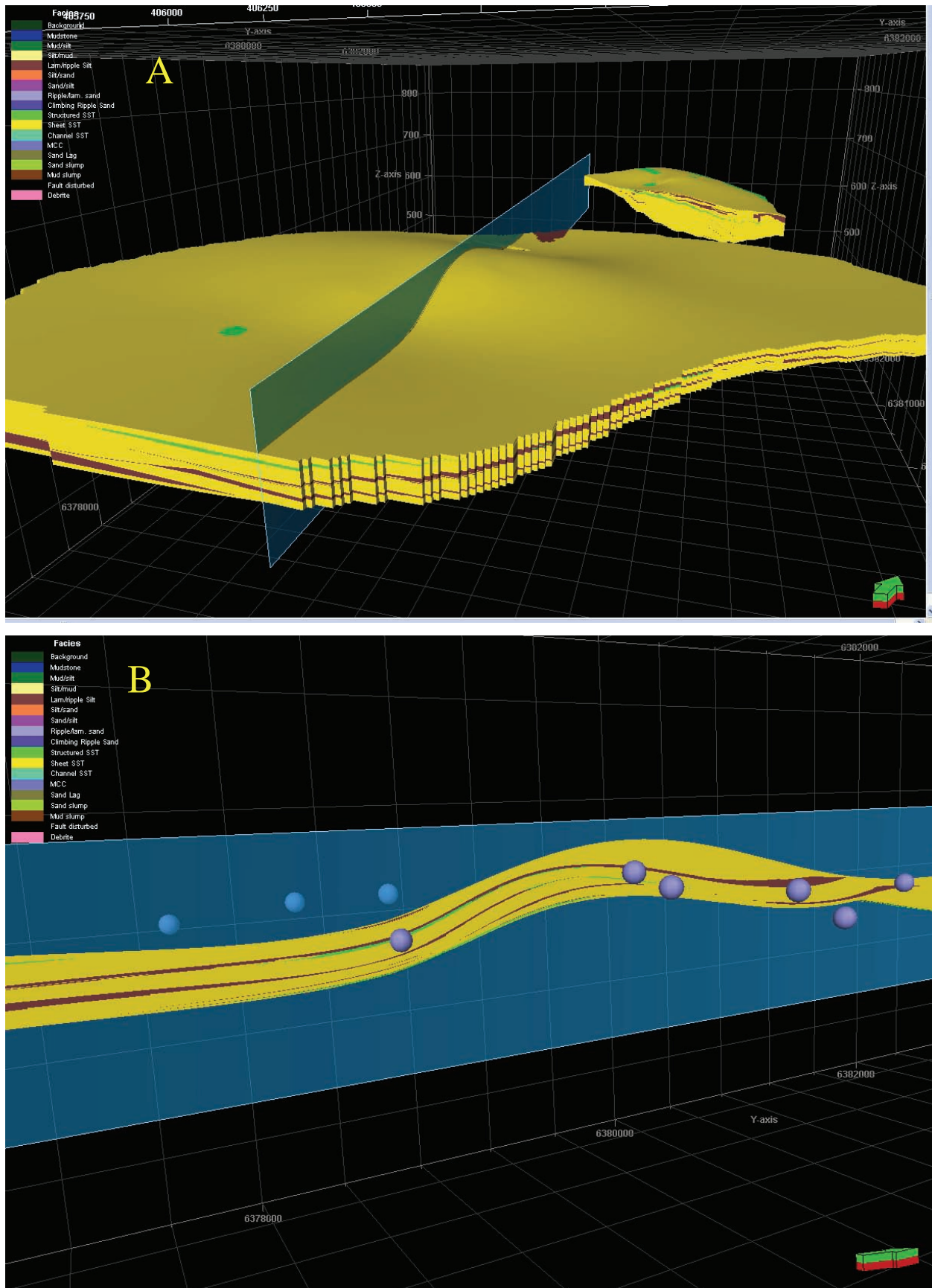


**Figure 7.8** The results of the first facies model run, using the Kriging algorithm, and it is immediately evident that too little variation is present (17 lithofacies were used, yet only 3 are visible). (B) is the cross-section through (A). The purple balls represent well data points.

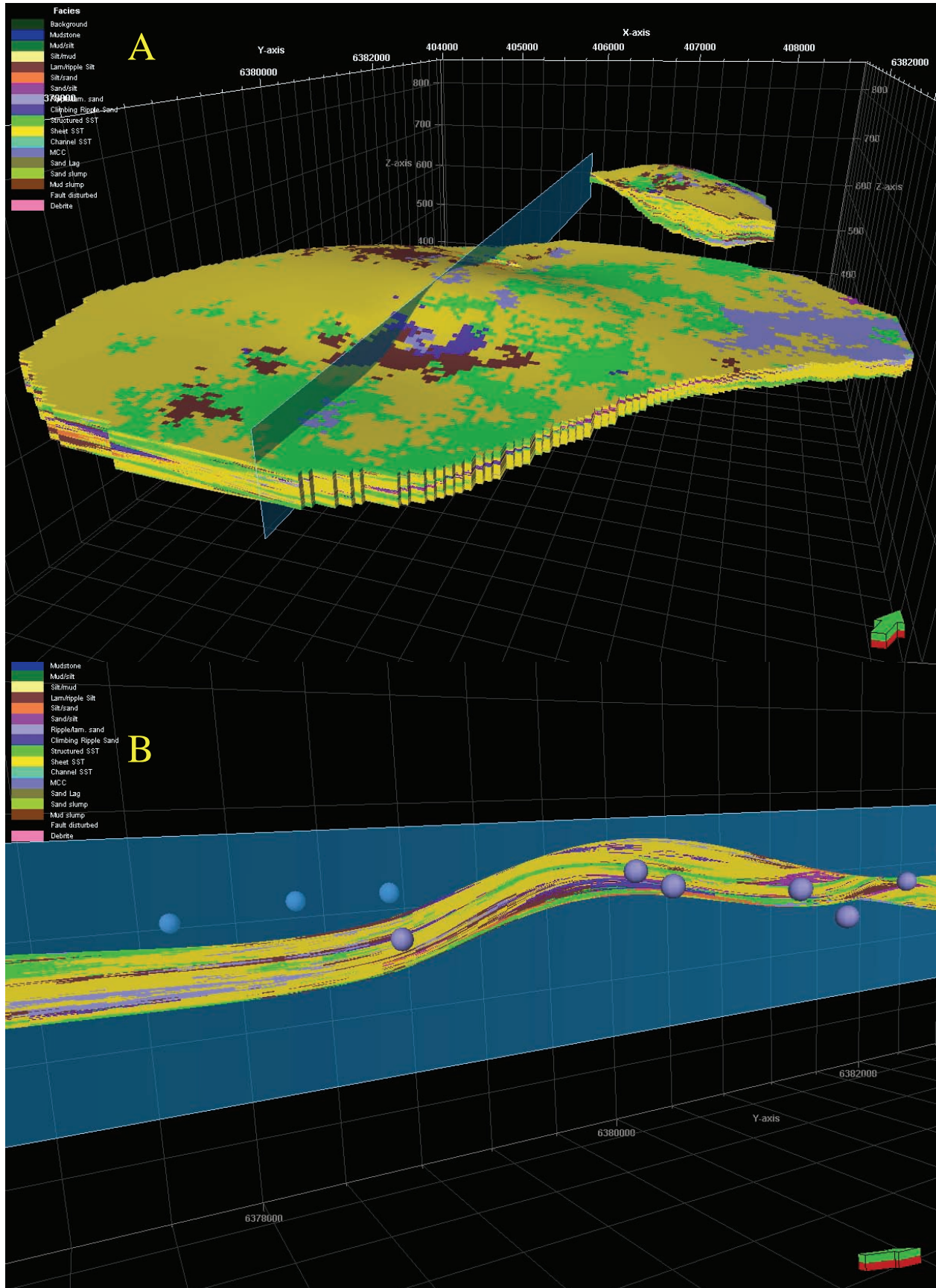


**Figure 7.9** The facies model using the Sequential Gaussian algorithm. (B) is the cross-section through (A). Note the large variation in lithofacies that can be observed, as opposed to the Kriging model in Fig 5.12.

1. The quality and nature of the input data are critical. While good data can be gained from a 2D outcrop, or even 1D well-logs, without decent 3D spread of data it is near impossible to get a truly accurate and reliable representation of information in 3D data analysis.
2. Close quality control of the data and results is important. Modelling is a highly iterative process, and errors can occur at any level of the process.
3. The scale at which 3D data analyses can be done relies heavily on the hardware that is available. Without decent computing ability much data can be lost simply because of too low resolutions. This can have major consequences when the presence or absence of barriers to hydrocarbon movement is critical to the productivity of a field.
4. Knowing what to use and where to use it makes the final output more reliable.

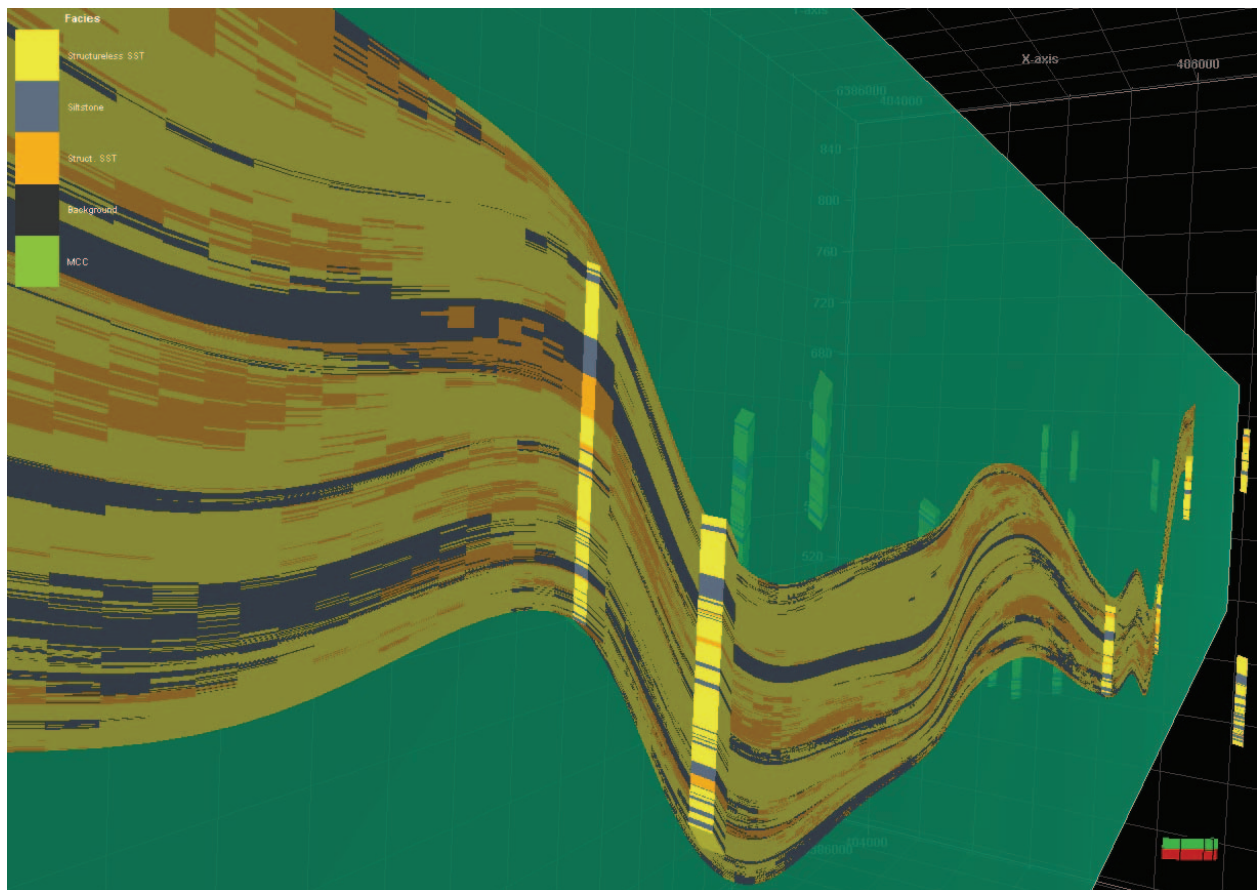


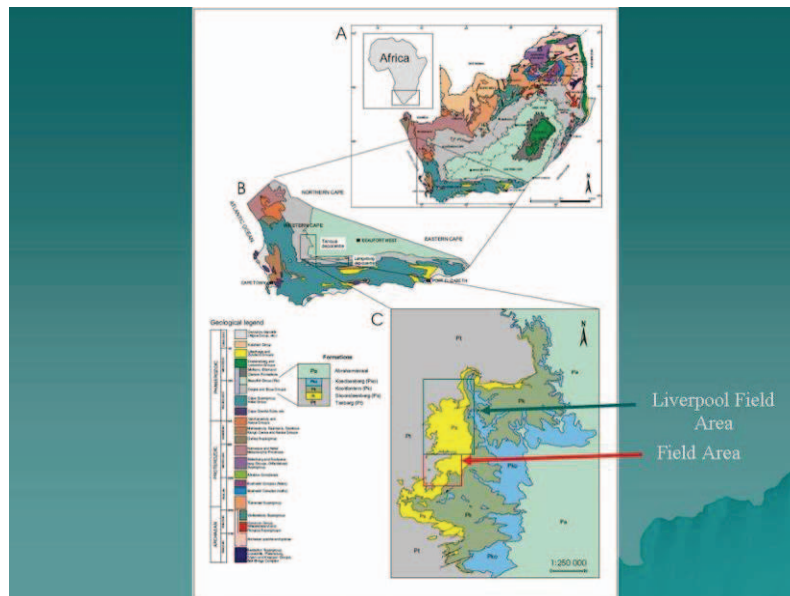
**Figure 7.12** This figure attempts to show the accuracy with which Petrel created the facies model in regards to the up-scaled wells. With enough wells to constrain the algorithms, Petrel can produce accurate and realistic facies models

## PetroSA Presentation

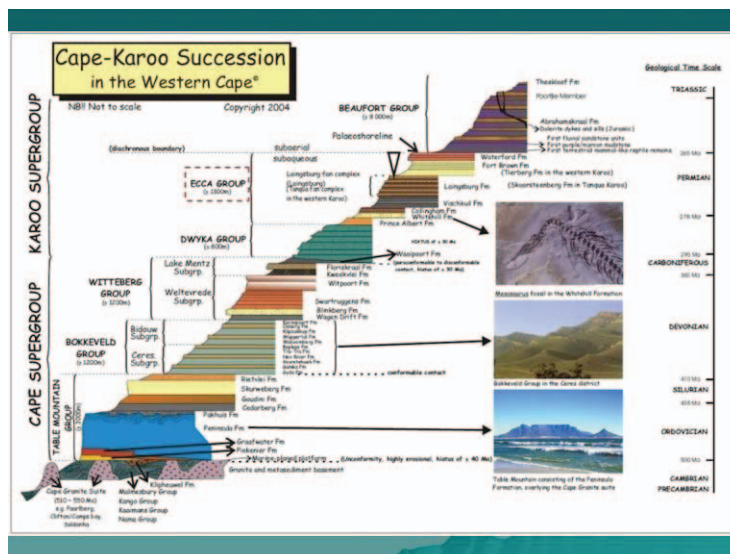
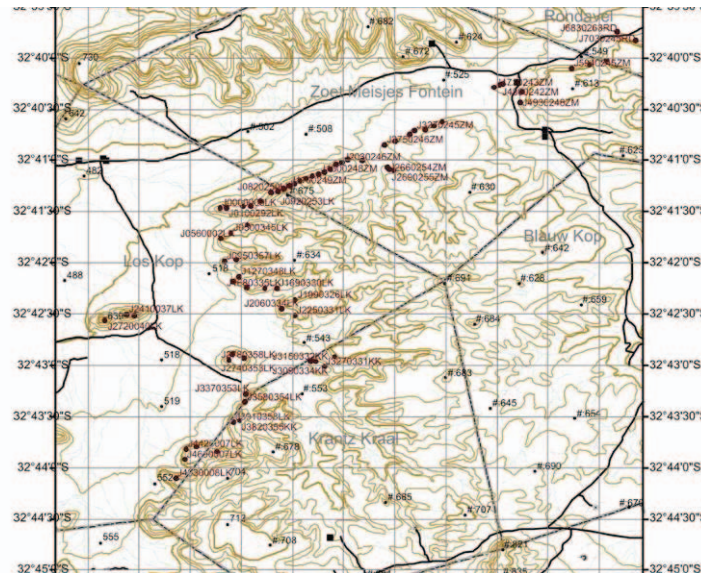
The presentation was given as per agreement with PetroSA for the aid provided with the modelling section of this project.

# Stratigraphic evolution of the channel-lobe transition zone: a high resolution study of mid- to distal Fan 3, Tanqua Karoo, South Africa

Jaco Neethling

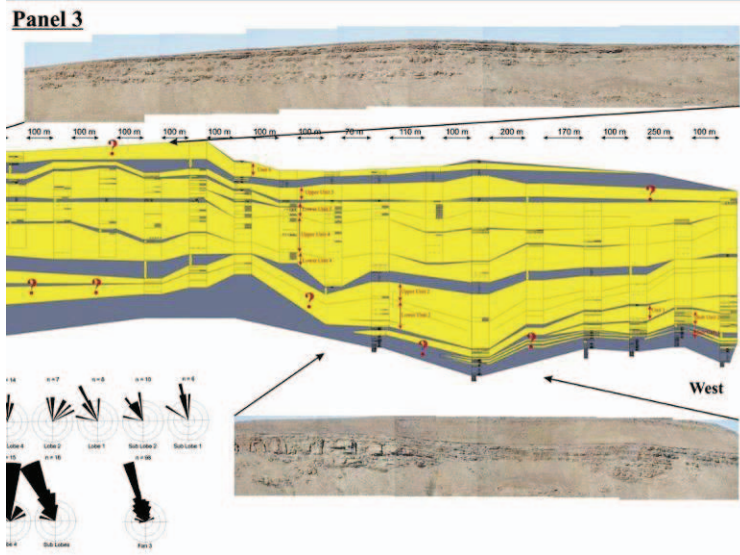


# Appendix B PetroSA Presentation

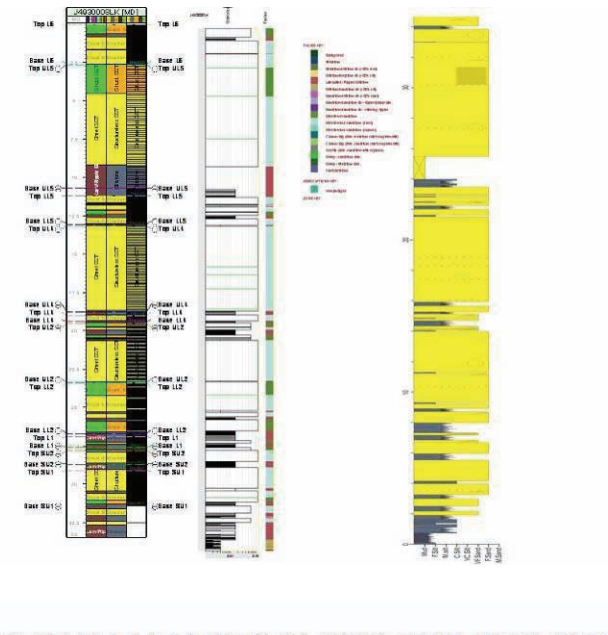


## Aims

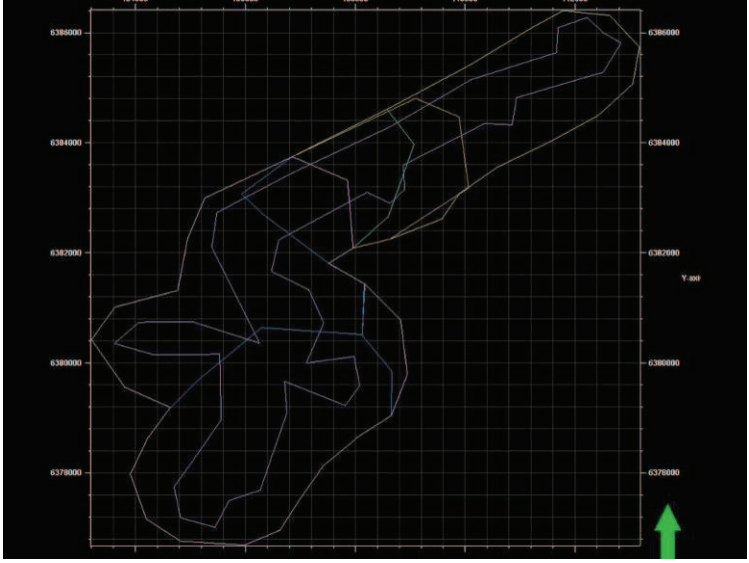
- ◆ Assessment of the transition of channelised lobe deposits into sheet deposits downdip
- ◆ Production of a high-resolution outcrop map, detailing the internal architecture, facies association and lobe-set characteristics of mid-fan Fan 3.
- ◆ Incorporation of mapping and borehole data collected during current studies in the area, namely the Lobe project
- ◆ Data manipulation in Petrel



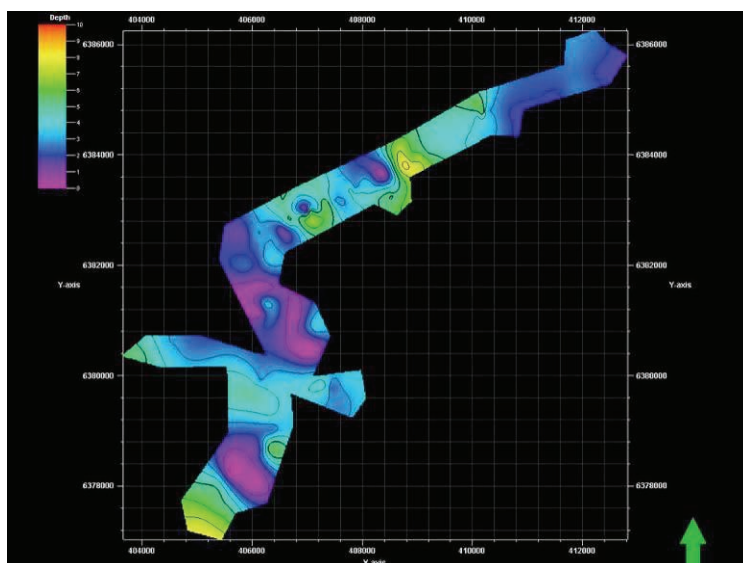
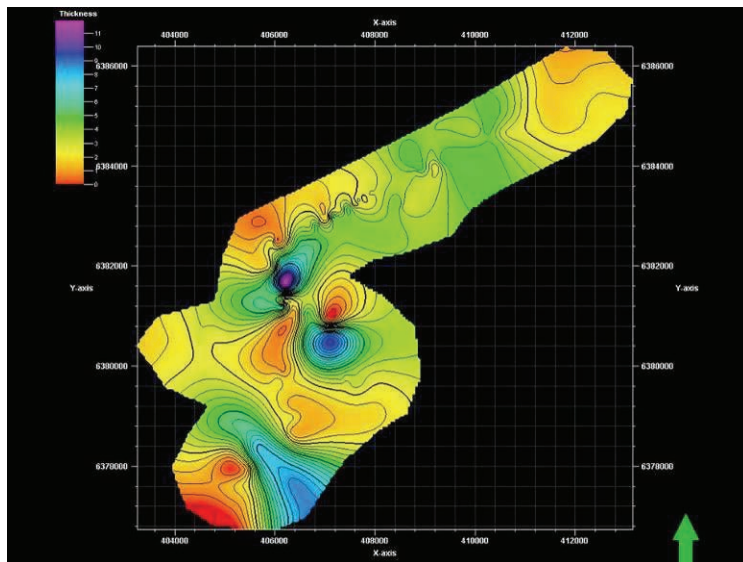
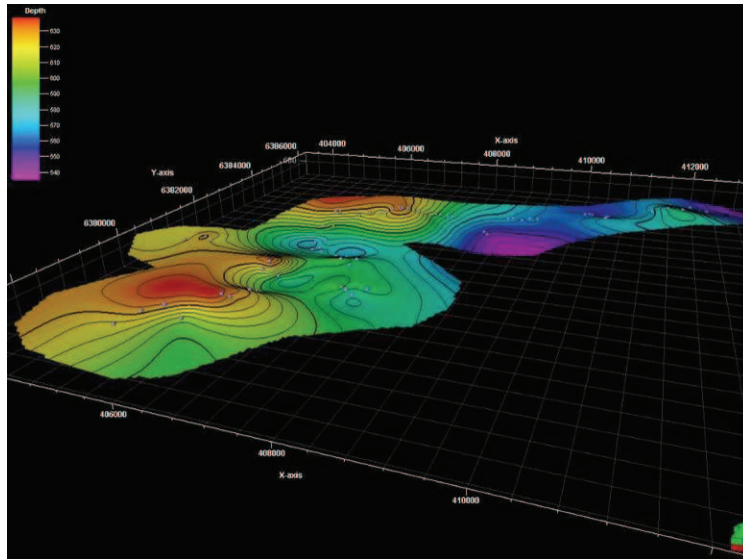
# Appendix B PetroSA Presentation



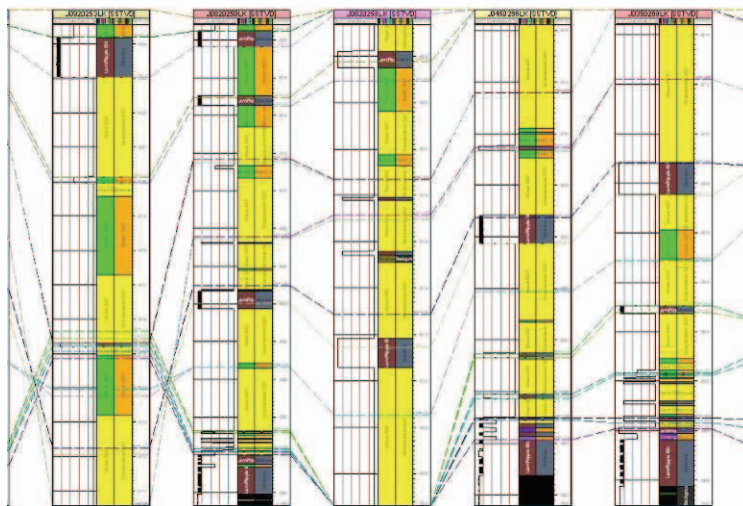
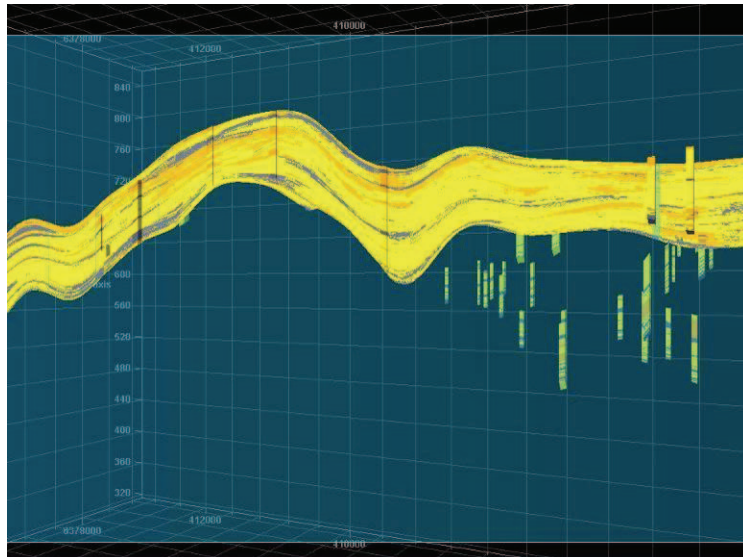
Profile Name	X Coordinate	Y Coordinate	Top L4	Base L4	Top U4	Base U4	Top L5	Base L5	Top U4	Base U4	Top L4	Base L4	Top U2	Base U2	Top L2	Base L2
J7000456R	412255	6209500	580	580.00	595.05	595.31	590.21	657.77	655.91	654.66	652.00	652.36	652.16	652.16	651.06	
J6500356R	411657	6209740	561	565.00	561.48	561.30	561.20	561.00	569.25	559.03	556.38	556.76	556.70	555.56	555.00	555.35
J4500452H	411517	6209224	598	595.00	592.51	591.48	591.85	600.61	578.95	579.24	579.69	579.46	579.20	579.20	579.20	579.00
J4100452H	411553	6209150	593	593.00	590.00	590.00	590.00	605.18	583.59	583.39	581.38	581.18	581.18	580.69	580.00	580.79
J4000452H	411589	6209080	588	585.00	584.18	584.18	584.18	612.18	578.23	580.69	587.60	587.60	587.20	587.20	587.00	587.00
J3900452H	412222	6209051	587	587.00	582.23	581.73	581.73	611.18	557.39	557.39	554.03	554.03	554.43	554.43	554.43	554.23
J4800452H	410499	6209400	576	576.00	571.03	570.50	570.50	599.66	565.84	565.12	562.34	562.34	562.34	561.64	561.64	561.74
J4800452H	410526	6209705	596	595.00	596.20	596.20	596.20	656.00	551.18	550.96	548.74	548.54	548.54	548.24	548.14	548.14
J4900452H	410181	6209770	590	590.00	589.20	589.20	589.20	609.59	563.81	563.47	547.79	547.59	547.59	547.29	547.19	547.19
J47100452H	410163	6208732	580	580.00	580.81	580.20	580.20	600.00	586.03	585.63	581.31	581.11	581.11	580.91	580.91	580.71
J3700452H	410210	6209100	587	587.00	584.00	583.03	583.03	603.00	566.04	565.04	563.12	563.12	562.92	562.92	562.72	562.72
J4000452H	410588	6208203	572	572.00	568.79	568.81	568.81	608.02	566.24	564.79	560.67	560.44	560.32	560.32	560.12	560.12
J2400452H	410252	6209381	589	589.00	594.74	594.05	594.05	603.25	569.63	569.62	562.23	562.11	562.02	562.01	561.91	561.89
J3700452H	410888	6208341	571	571.00	570.35	569.25	569.25	609.54	564.73	564.11	557.70	556.99	556.32	555.46	555.00	555.07
J1100452H	410185	6208772	589	589.00	589.33	589.20	589.20	600.00	585.28	584.88	586.78	586.78	583.88	583.18	583.28	583.38
J2000452H	410596	6209740	583	583.00	580.00	580.00	580.00	603.20	560.70	559.07	556.02	554.02	553.02	552.02	551.04	549.04
J2700452H	410878	6209217	590	590.00	588.33	588.33	588.33	606.26	544.50	544.06	539.09	539.06	538.23	538.23	538.76	538.66
J2700452H	410905	6209002	595	595.00	597.60	597.31	597.31	607.16	566.38	565.00	563.00	562.76	562.66	562.66	562.66	562.66
J2600452H	410512	6208242	595	595.00	595.41	595.20	595.20	605.00	590.80	590.28	546.38	545.38	544.90	544.24	543.73	543.53
J2600452H	410922	6208272	582	582.00	584.80	584.30	584.30	591.10	562.22	562.00	546.88	546.88	546.88	546.88	546.28	546.28
J2500452H	410584	6208388	576	580.00	575.50	575.30	575.30	578.30	578.30	576.00	572.41	570.74	567.00	564.67	562.00	562.00
J2100452H	410772	6208381	589	591.00	586.20	586.00	586.00	609.11	595.28	594.78	581.77	581.67	577.67	575.66	572.04	571.64
J2000452H	410768	6208383	593	593.00	592.22	591.18	591.18	609.68	587.05	587.03	582.87	582.88	578.07	576.63	574.18	574.18
J1800452H	410770	6208315	601	601.00	598.41	598.21	597.95	607.08	584.00	583.16	580.87	580.84	580.34	580.22	580.00	580.12
J1800452H	410768	6208223	607	607.00	605.30	605.00	602.75	602.00	589.80	589.25	586.21	585.84	585.04	584.04	583.74	583.54
J1700452H	410712	6208144	602	604.00	602.00	602.00	601.72	601.25	597.46	597.19	584.10	583.80	583.25	582.65	582.15	582.15
J1600452H	410727	6208140	609	611.00	609.70	609.50	609.02	609.00	604.49	603.90	590.89	590.08	589.22	588.52	588.02	588.72
J1500452H	410732	6208110	617	619.00	617.00	617.00	616.21	616.11	613.01	612.46	600.02	600.02	599.32	599.12	599.02	599.02
J1400452H	410737	6208082	628	628.00	625.20	623.74	622.74	622.20	616.10	615.87	613.06	613.78	613.61	613.61	613.61	613.61
J1300452H	410743	6208021	633	632.00	630.54	629.70	629.00	629.50	624.41	624.11	620.02	620.02	619.02	618.72	617.20	617.20
J1200452H	410756	6208067	636	636.00	634.90	633.85	633.00	633.10	628.19	627.99	623.05	623.05	621.85	621.65	620.25	620.25
J1100452H	410884	6208092	627	627.00	626.20	626.19	625.72	625.62	620.90	620.09	620.00	620.00	620.76	620.76	619.06	619.06
J1000452H	410903	6208076	635	635.00	634.19	633.97	633.51	633.16	627.45	627.46	622.16	622.16	619.33	617.76	615.19	615.19
J0800452H	410908	6208215	625	625.00	624.20	623.04	622.14	619.05	615.30	615.20	610.55	610.25	612.25	612.05	611.95	611.95
J0600452H	410970	6208201	622	621.00	620.06	619.82	619.22	619.11	612.11	611.59	606.97	606.97	600.72	600.54	599.20	599.20
J0600452H	410952	6208203	628	628.00	627.00	626.80	626.75	622.94	619.89	619.65	617.15	616.65	613.85	613.85	613.85	613.85
J0400452H	410958	6208250	616	616.00	615.30	615.10	615.20	616.00	611.07	611.07	609.23	609.13	606.96	604.65	602.25	602.25
J0200452H	410977	6208234	615	615.00	614.40	614.20	614.20	617.20	615.00	615.00	612.30	612.20	609.00	607.50	604.80	604.80
J0100452H	410905	6208203	623	623.00	622.30	622.10	622.20	623.00	622.40	622.33	619.88	619.68	616.80	616.80	616.80	616.87
J0000452H	410920	6208215	625	625.00	624.20	624.00	624.00	622.31	622.31	620.41	620.41	616.31	616.31	616.31	616.31	616.31
J0000452H	410940	6208215	614	614.00	613.40	613.20	613.10	616.10	614.00	613.60	610.64	610.64	610.14	609.64	609.14	609.14
J0000452H	410948	6208187	604	604.00	603.30	603.10	603.00	604.00	600.02	600.02	596.00	596.00	594.14	594.74	594.74	594.74
J0000452H	410910	6208090	608	607.30	606.60	606.40	606.30	608.00	591.50	591.68	589.59	589.68	588.16	587.11	586.00	586.00
J0000452H	410915	6208055	595	597.10	596.20	596.00	596.00	603.80	572.76	577.04	566.00	572.10	571.20	571.00	568.04	565.74
J0000452H	410900	6208050	576	576.10	575.30	575.00	574.20	573.52	566.88	570.16	564.33	567.63	566.03	565.43	564.41	565.41
J12700452H	410527	6208120	578	582.20	580.40	580.10	579.20	579.00	578.51	578.51	573.49	573.49	571.46	569.69	568.54	568.54
J1200452H	410146	6208180	570	582.20	580.30	580.10	579.20	579.00	578.21	578.16	573.16	573.16	569.65	568.55	567.27	567.27
J14800452H	410259	6208190	587	580.20	586.40	586.70	586.20	593.00	581.74	581.61	576.13	576.13	577.42	575.38	572.05	571.85



# Appendix B PetroSA Presentation



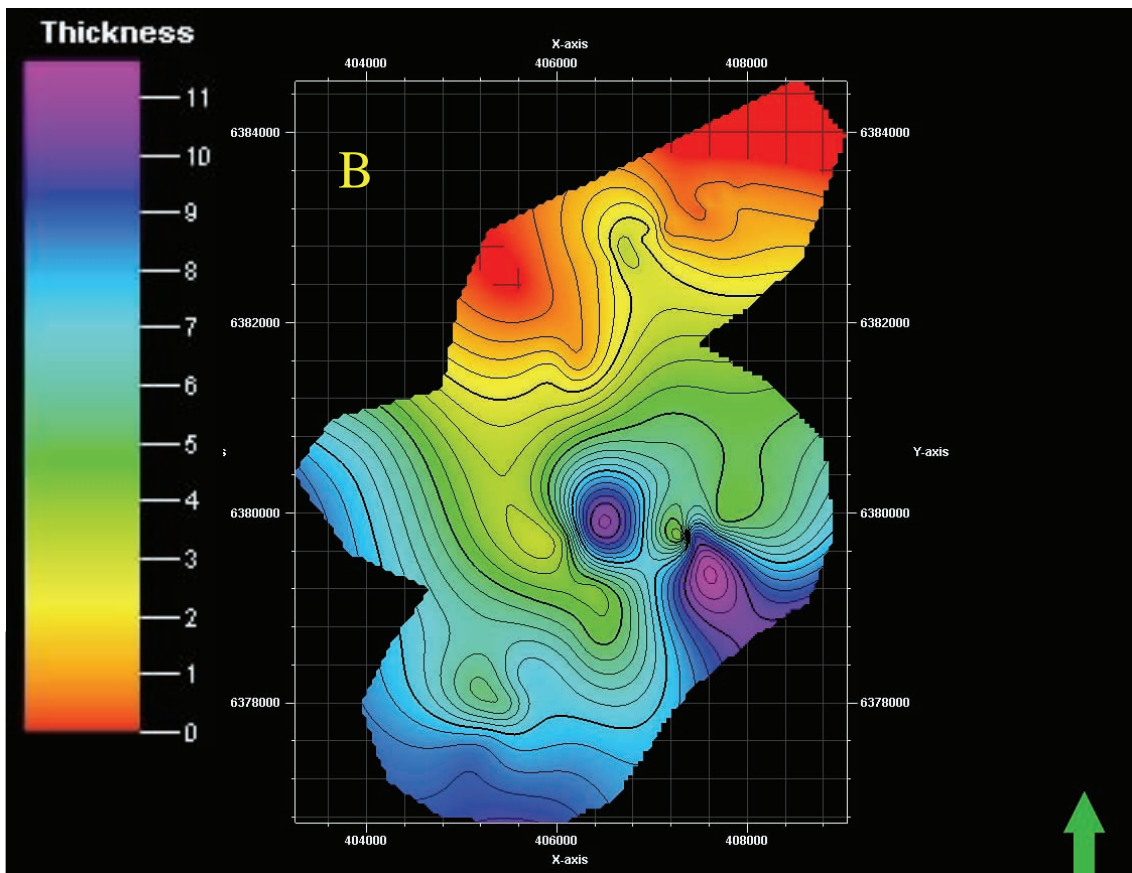
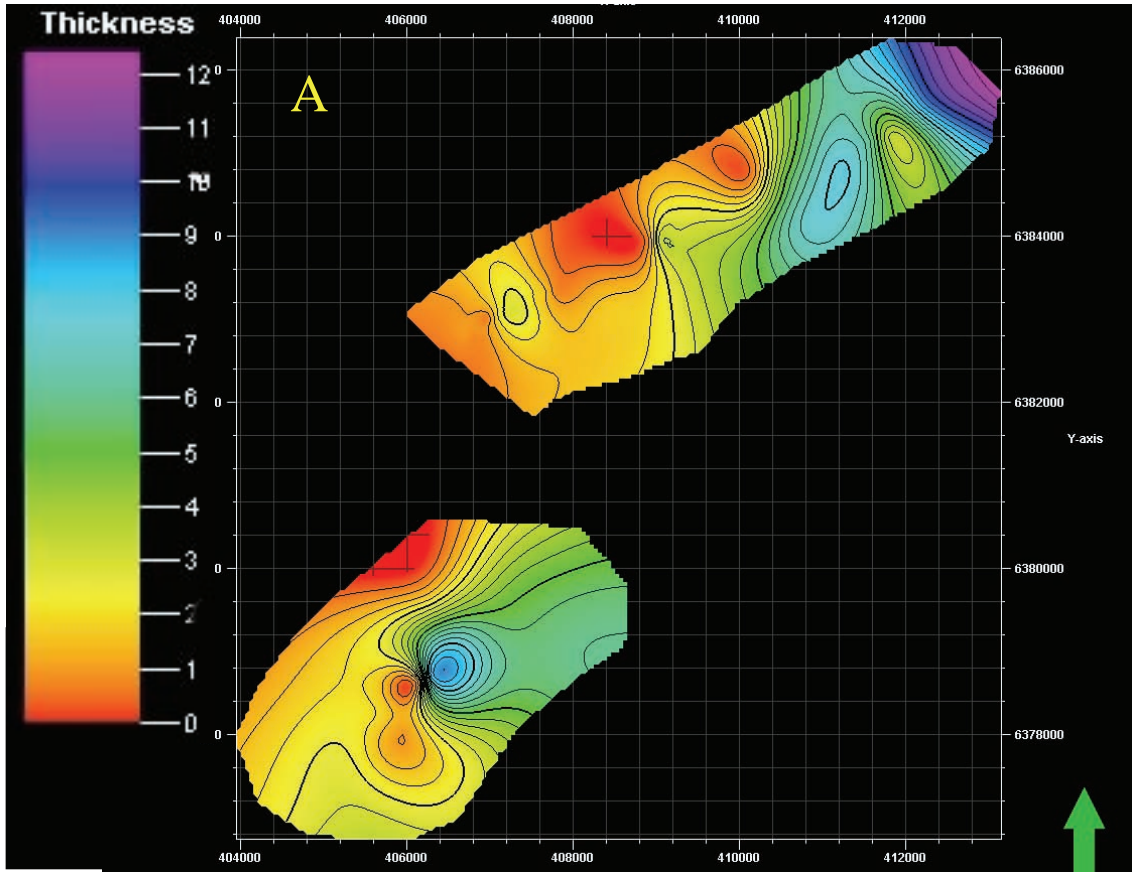




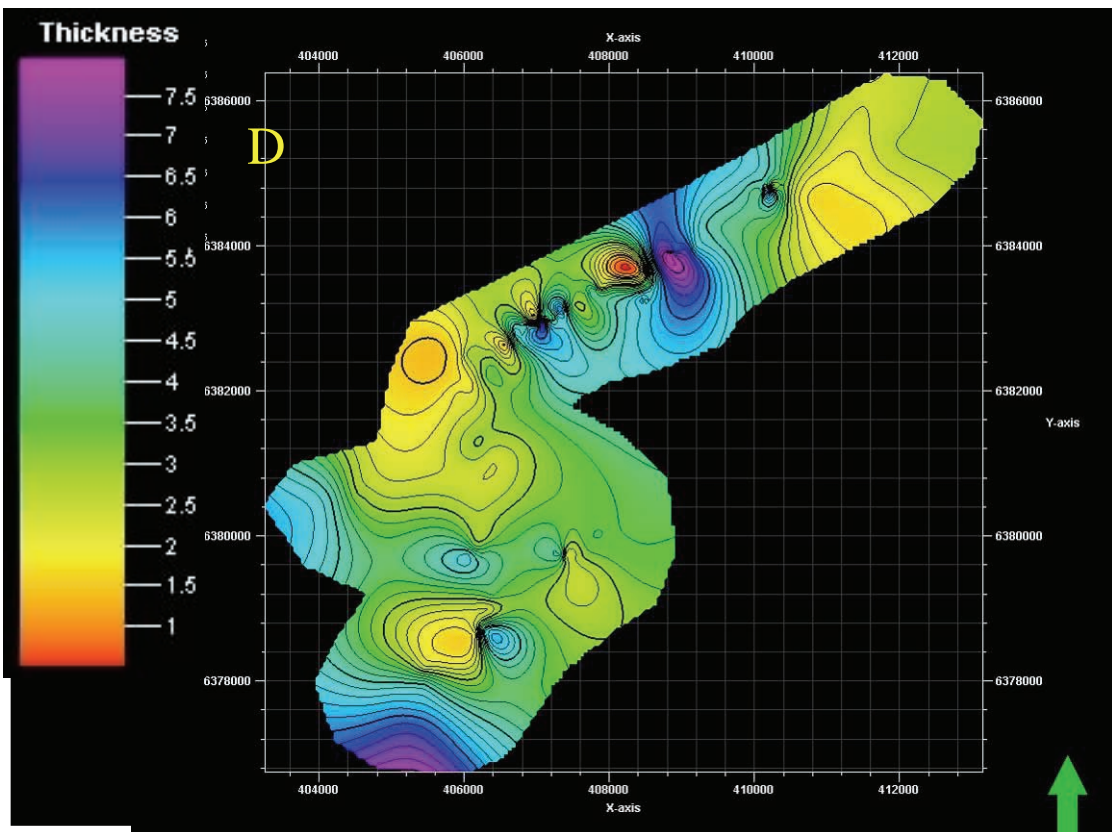
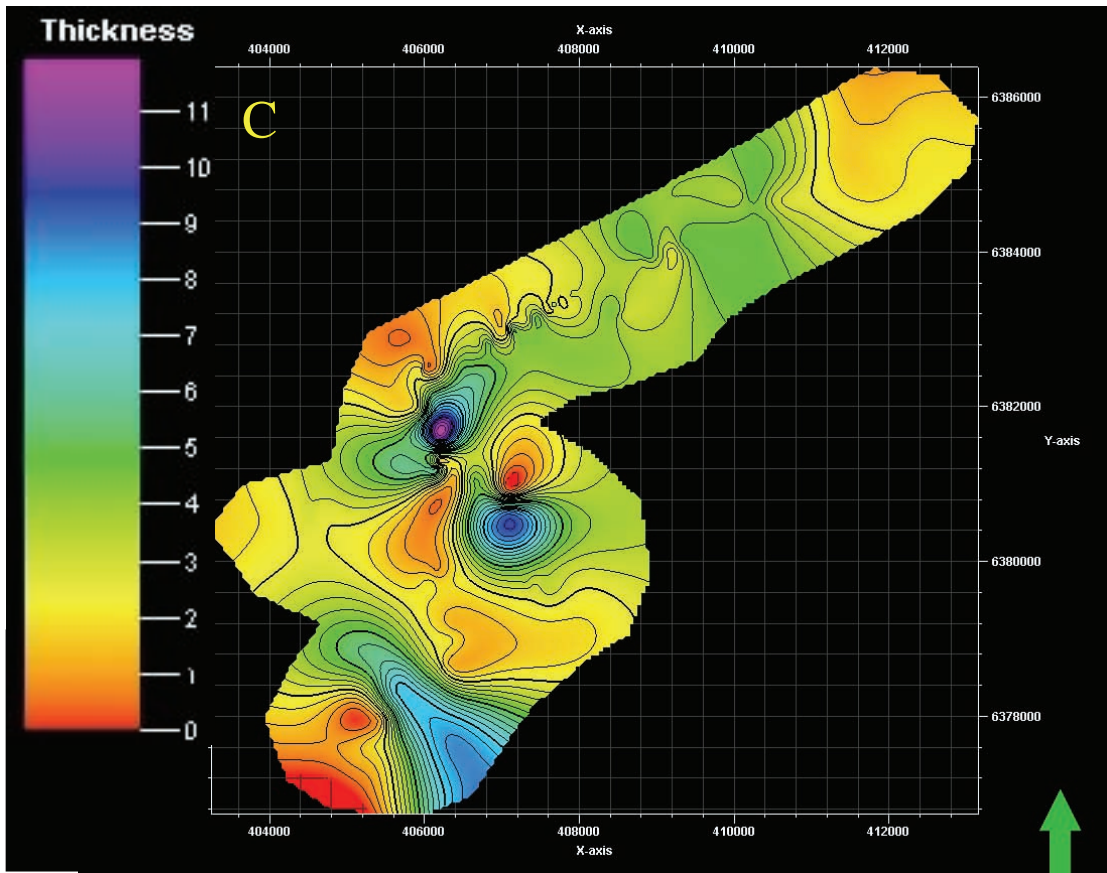
## Current work

- ◆ Project hand-in: 1 September 2008
- ◆ Finishing Write-up

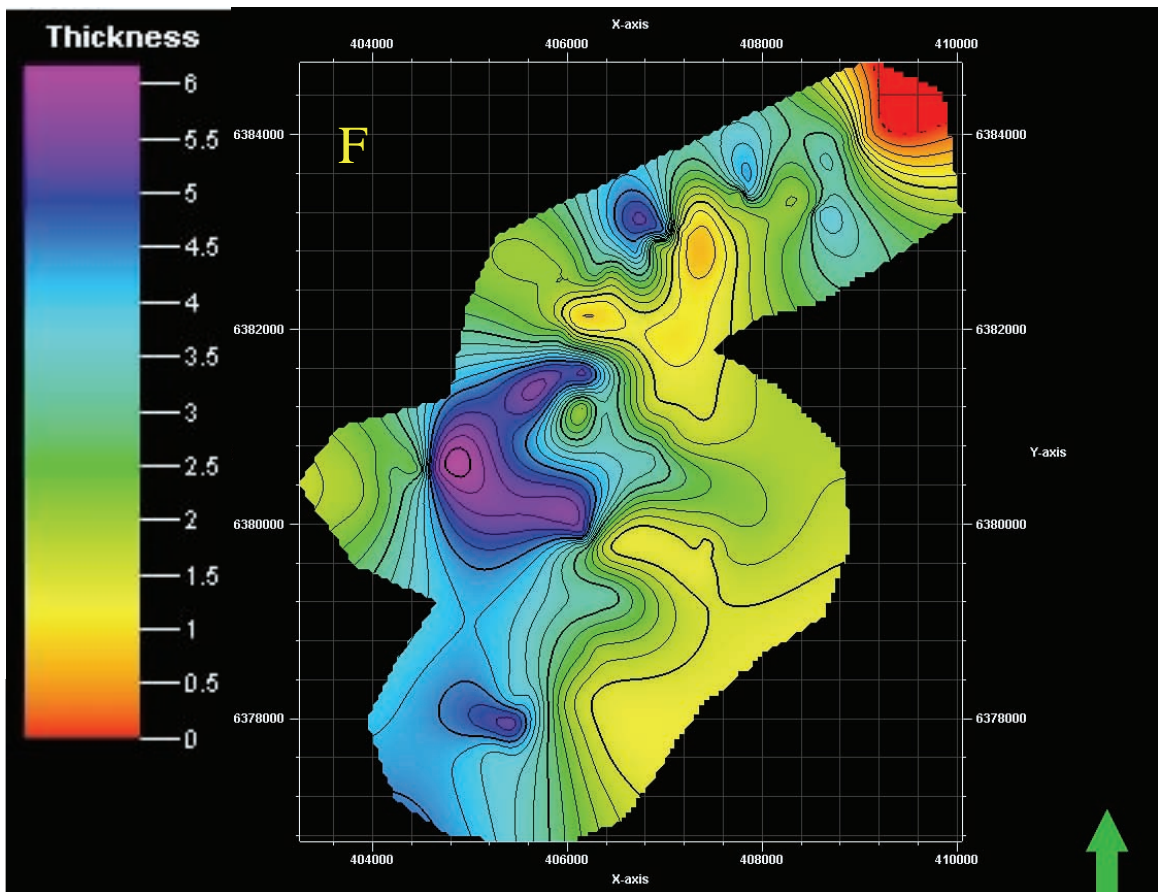
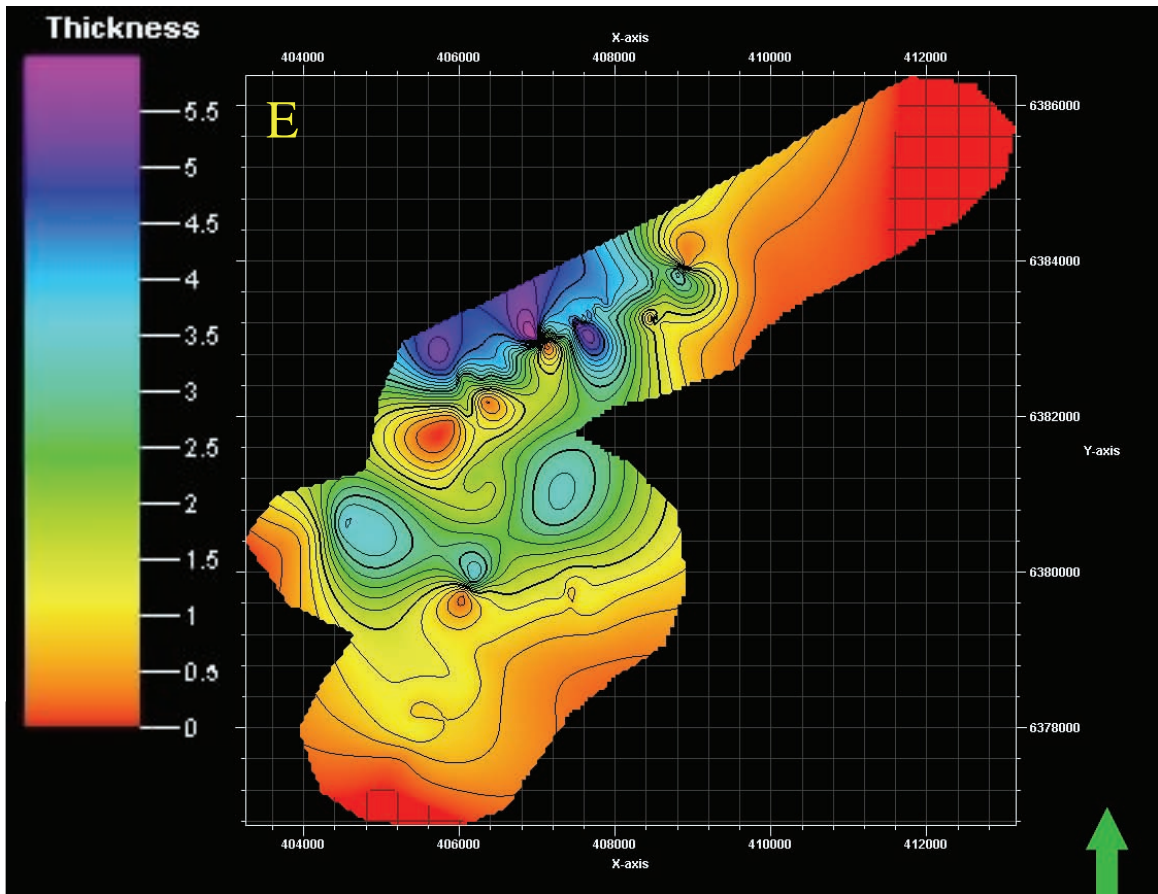
Appendix C Petrel Thickness Maps



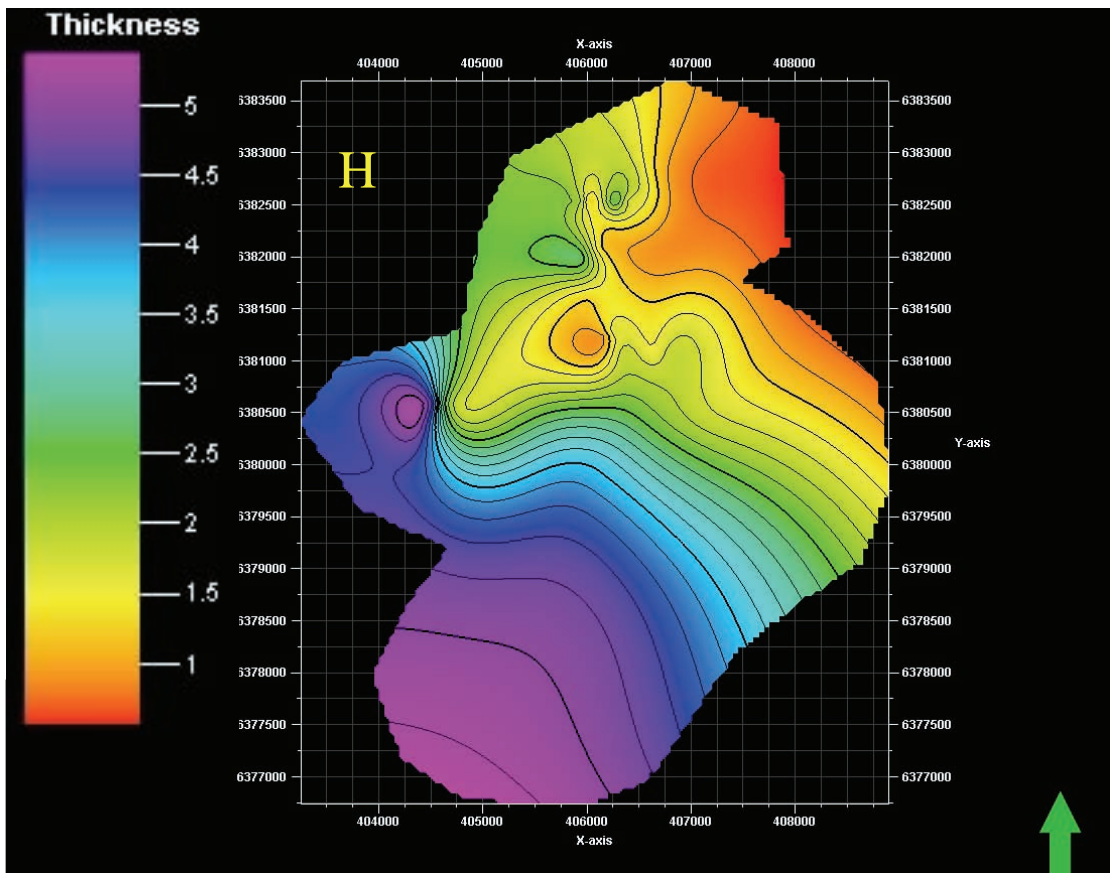
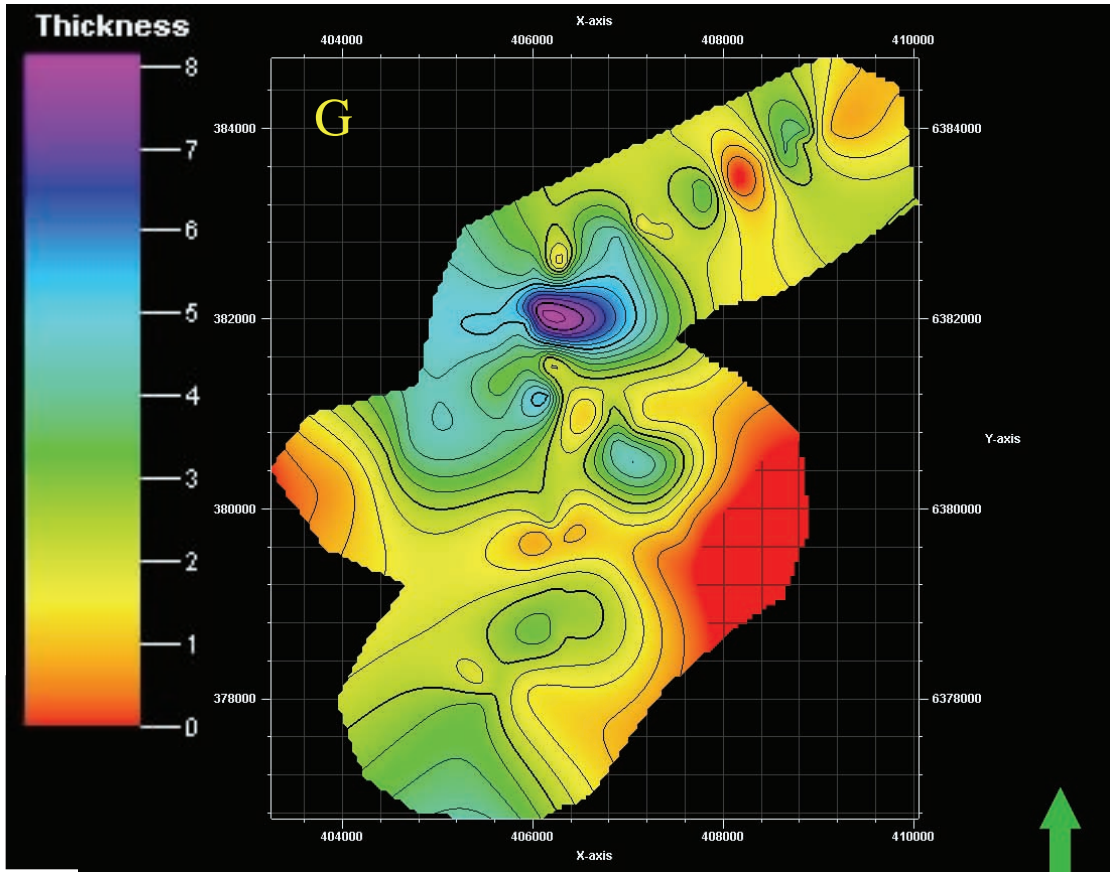
Appendix C Petrel Thickness Maps



Appendix C Petrel Thickness Maps



Appendix C Petrel Thickness Maps



Appendix C Petrel Thickness Maps

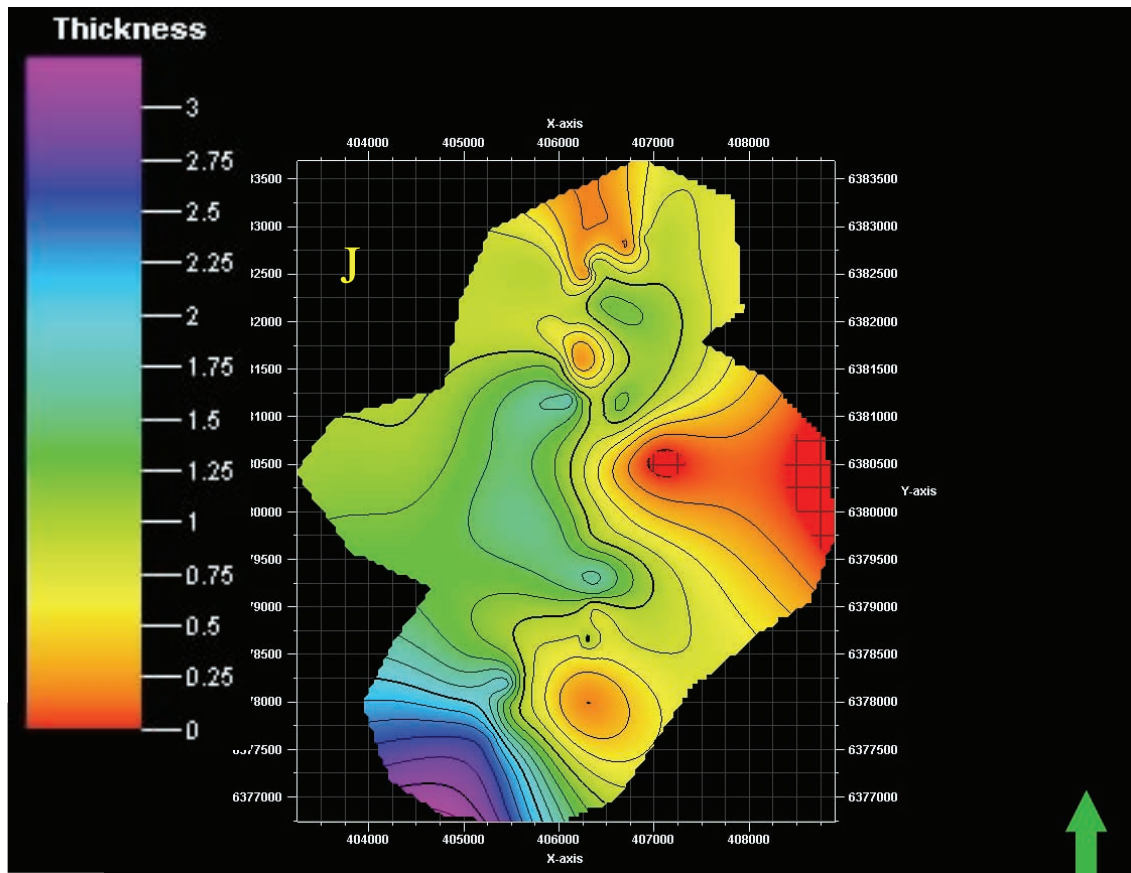
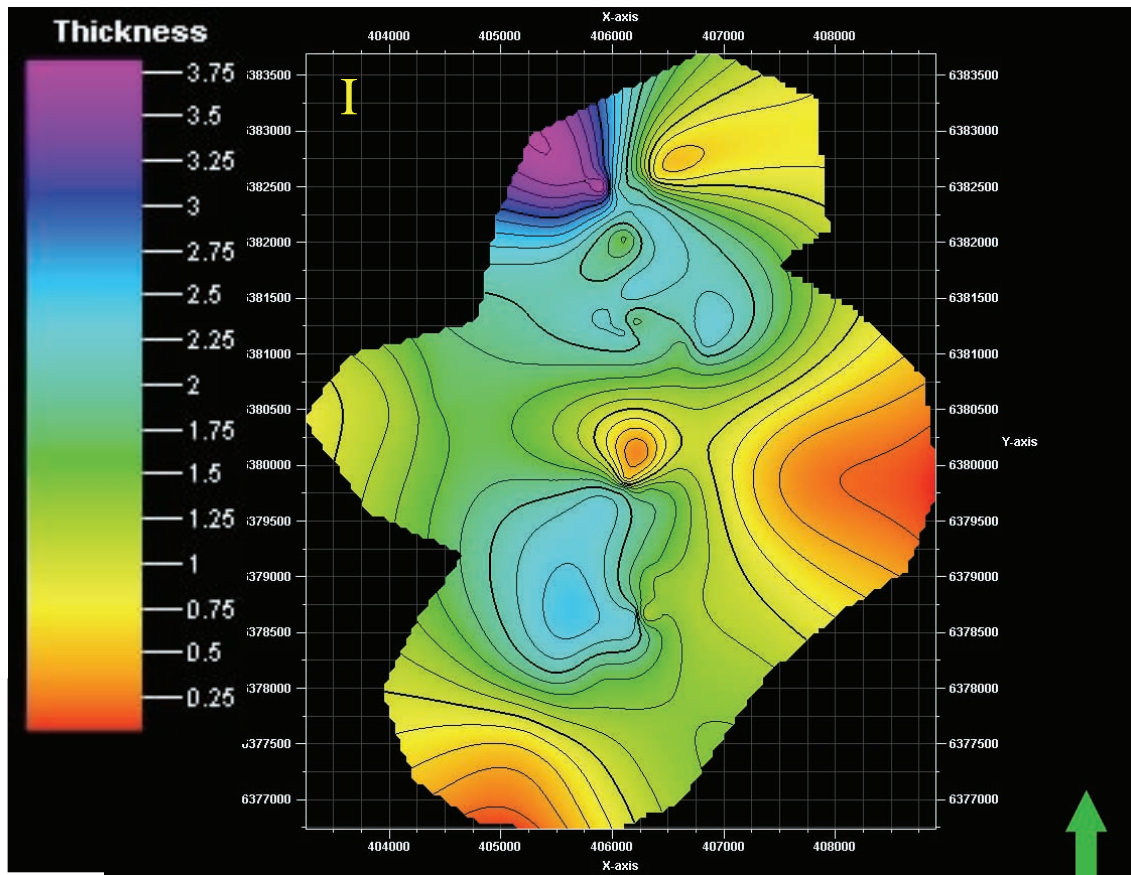
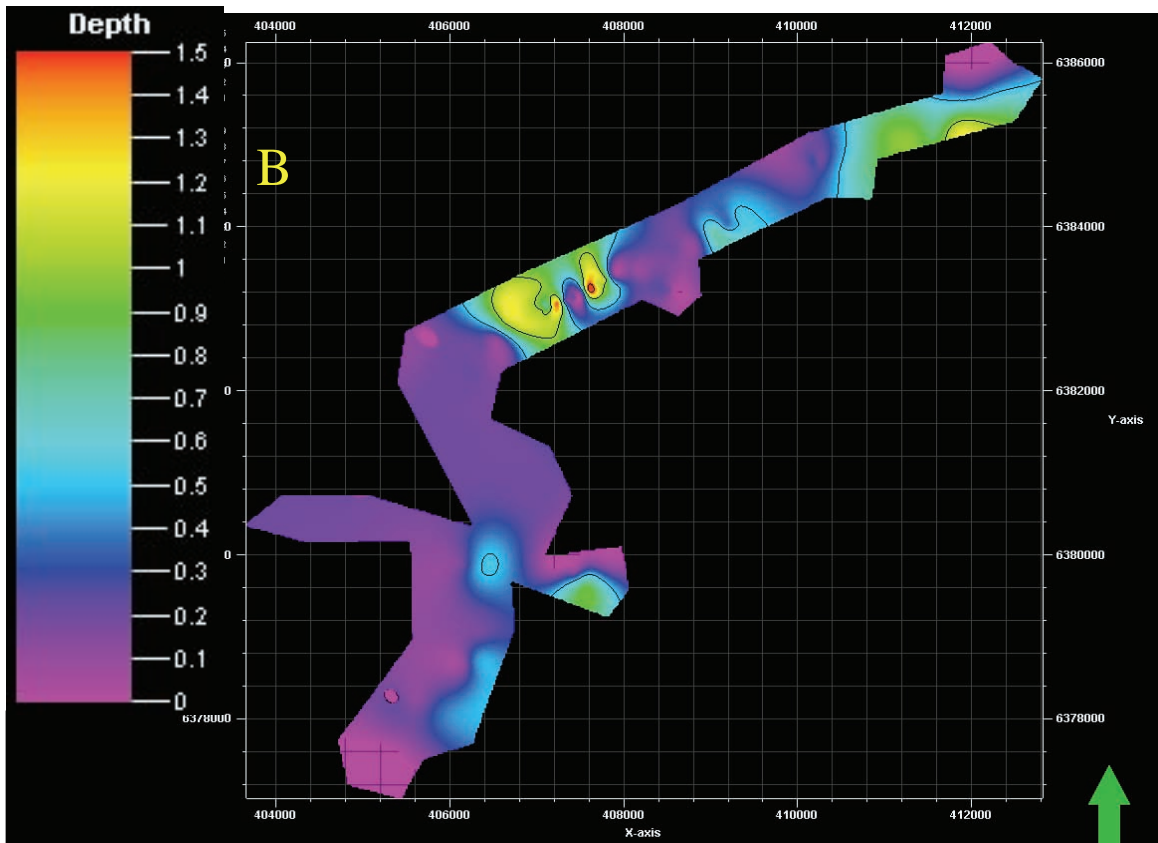
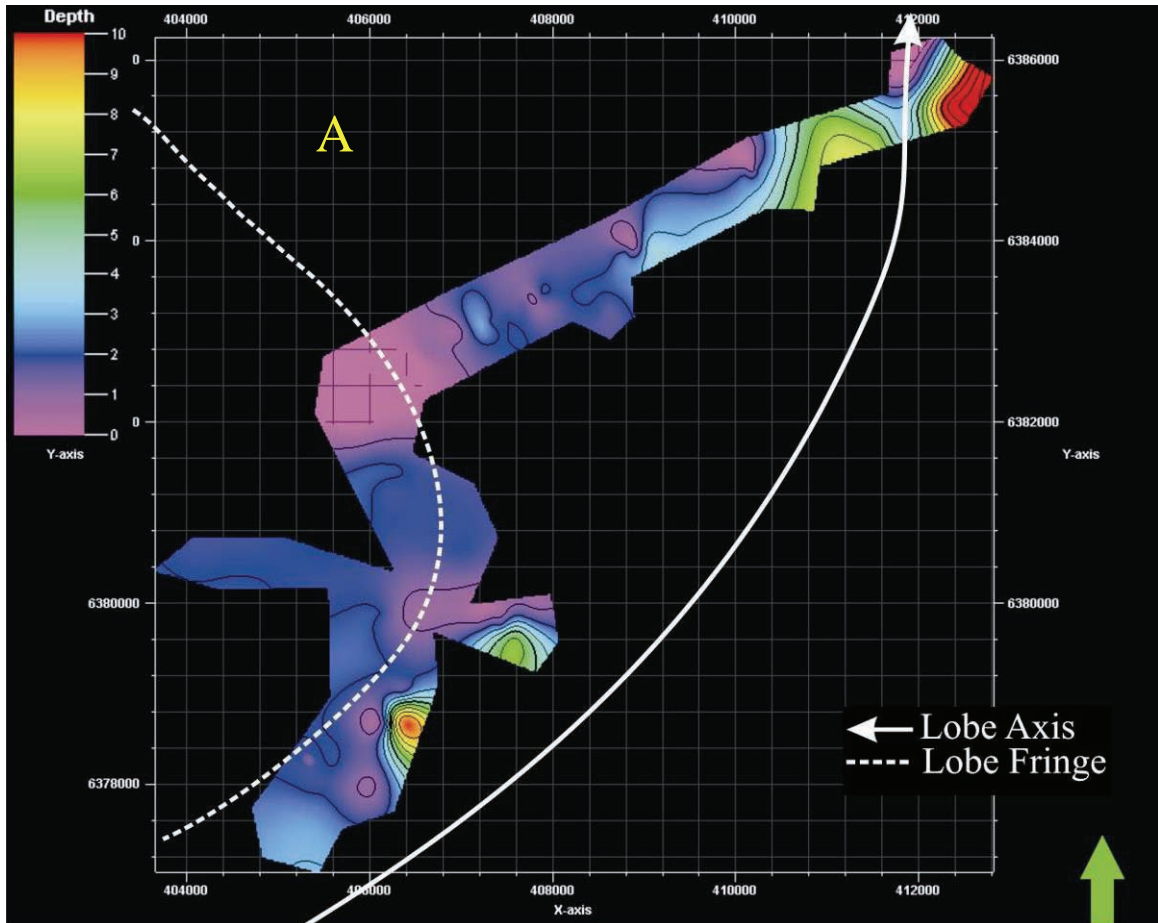
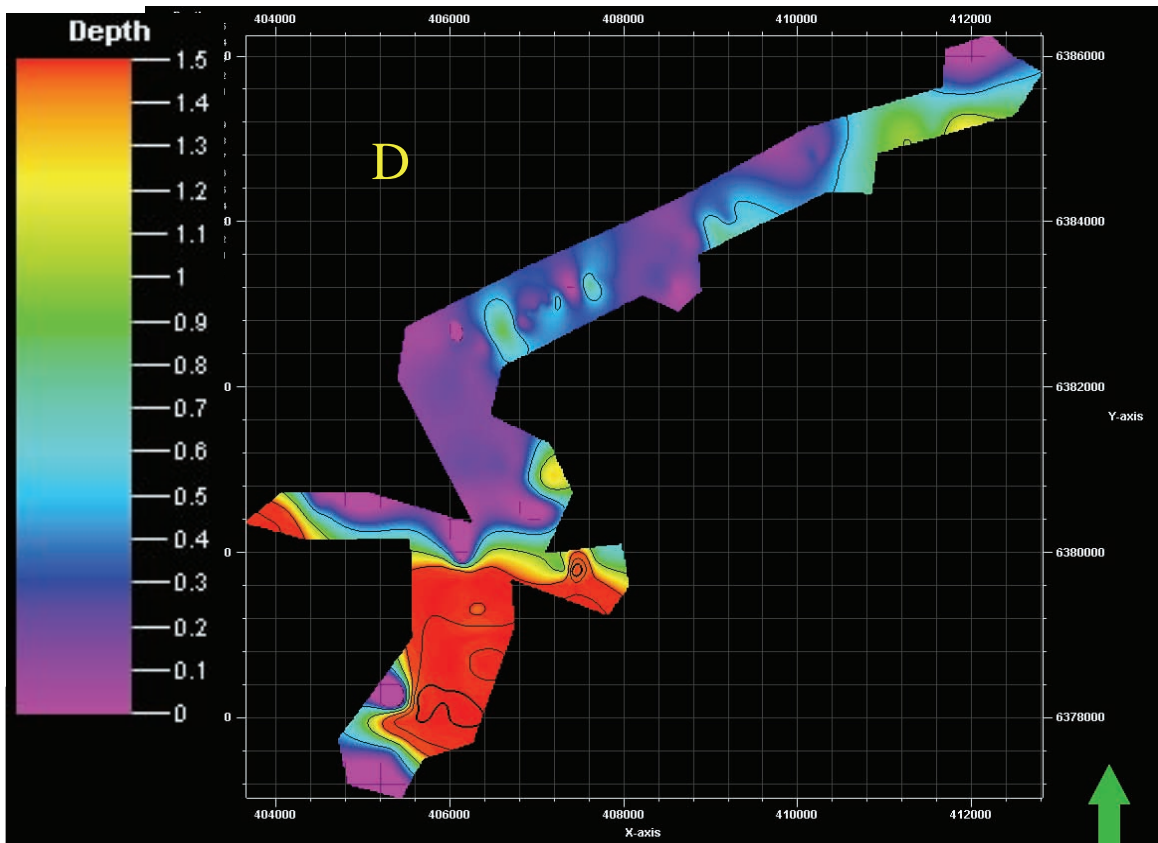
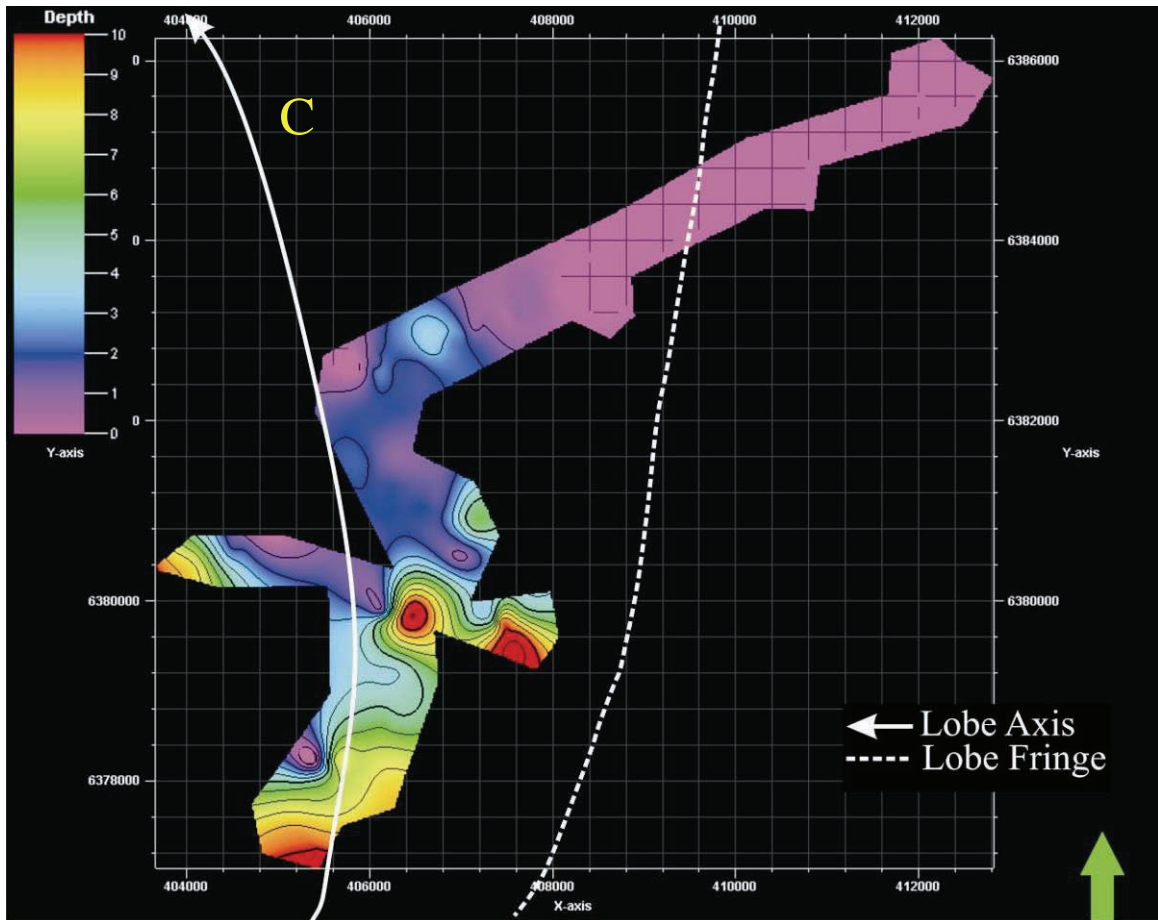


Figure C.1 The first set of Thickness Maps.

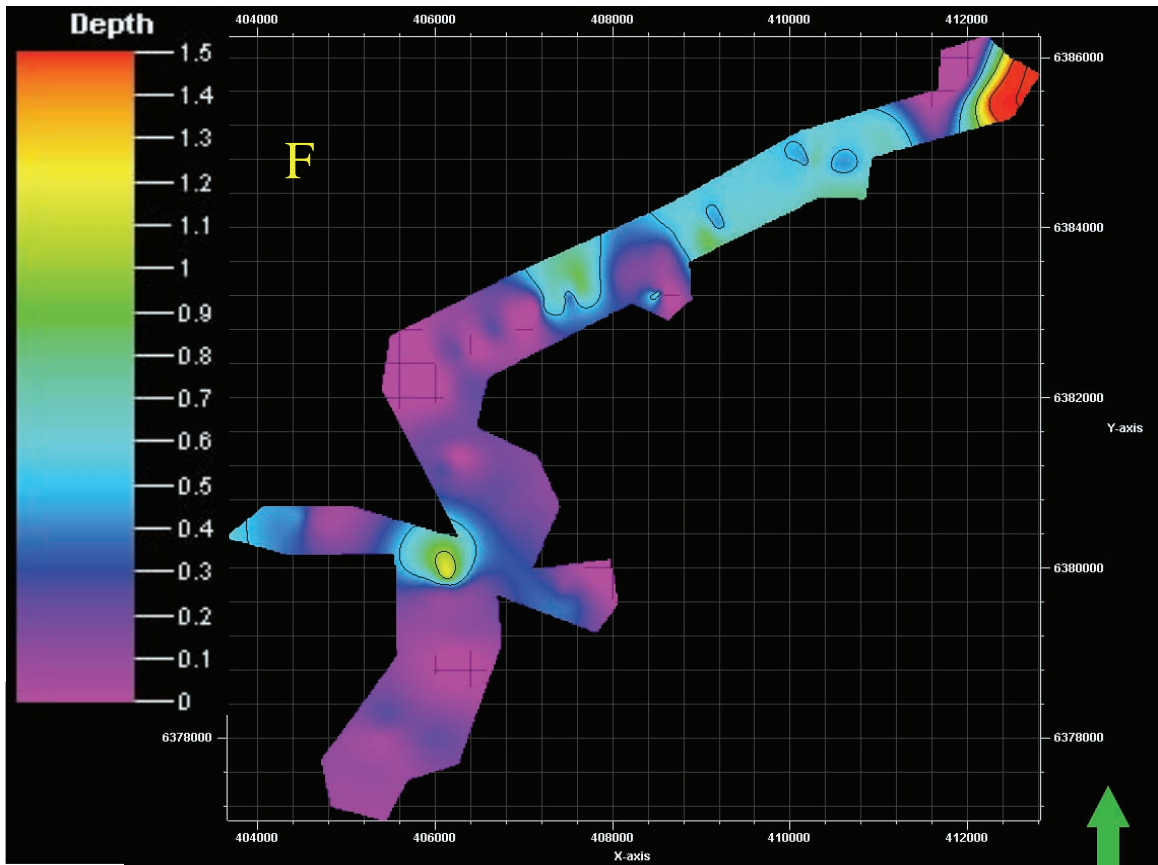
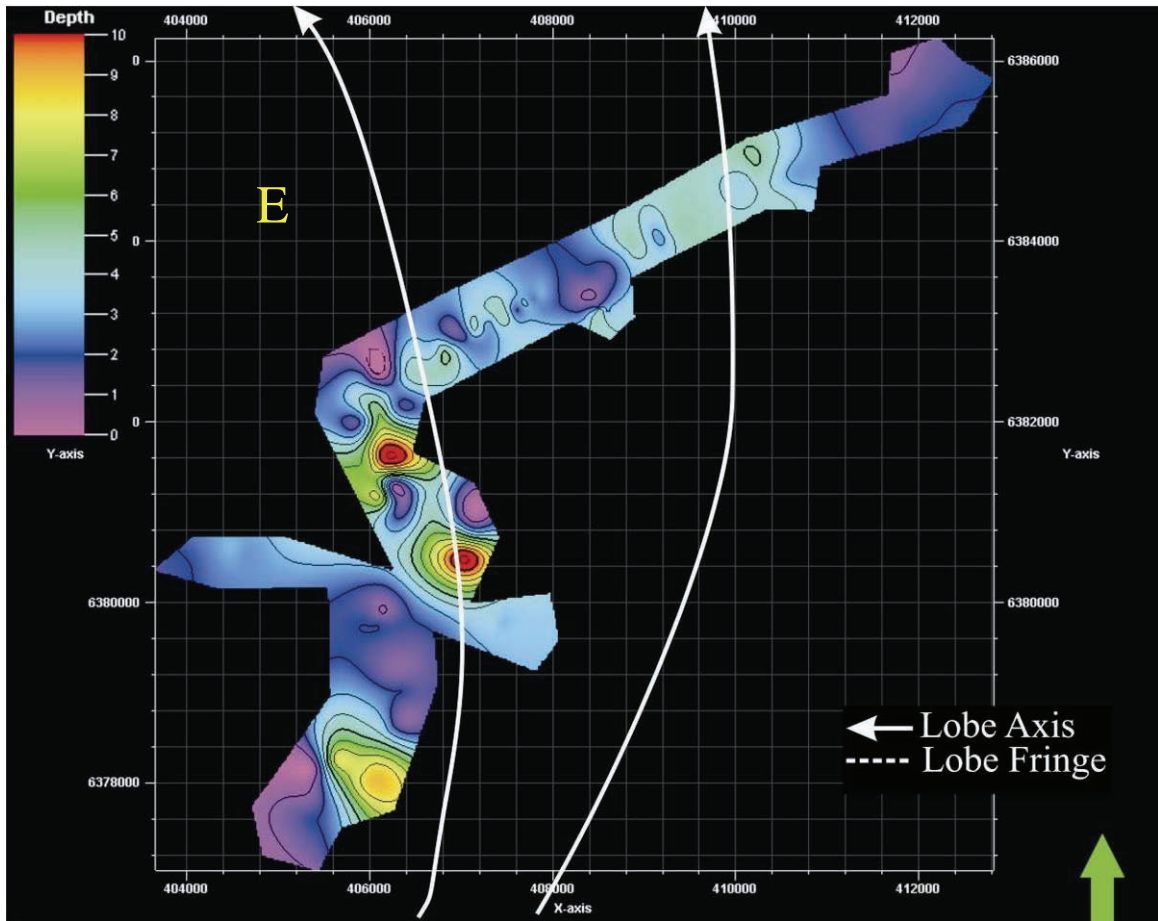
Appendix C Petrel Thickness Maps



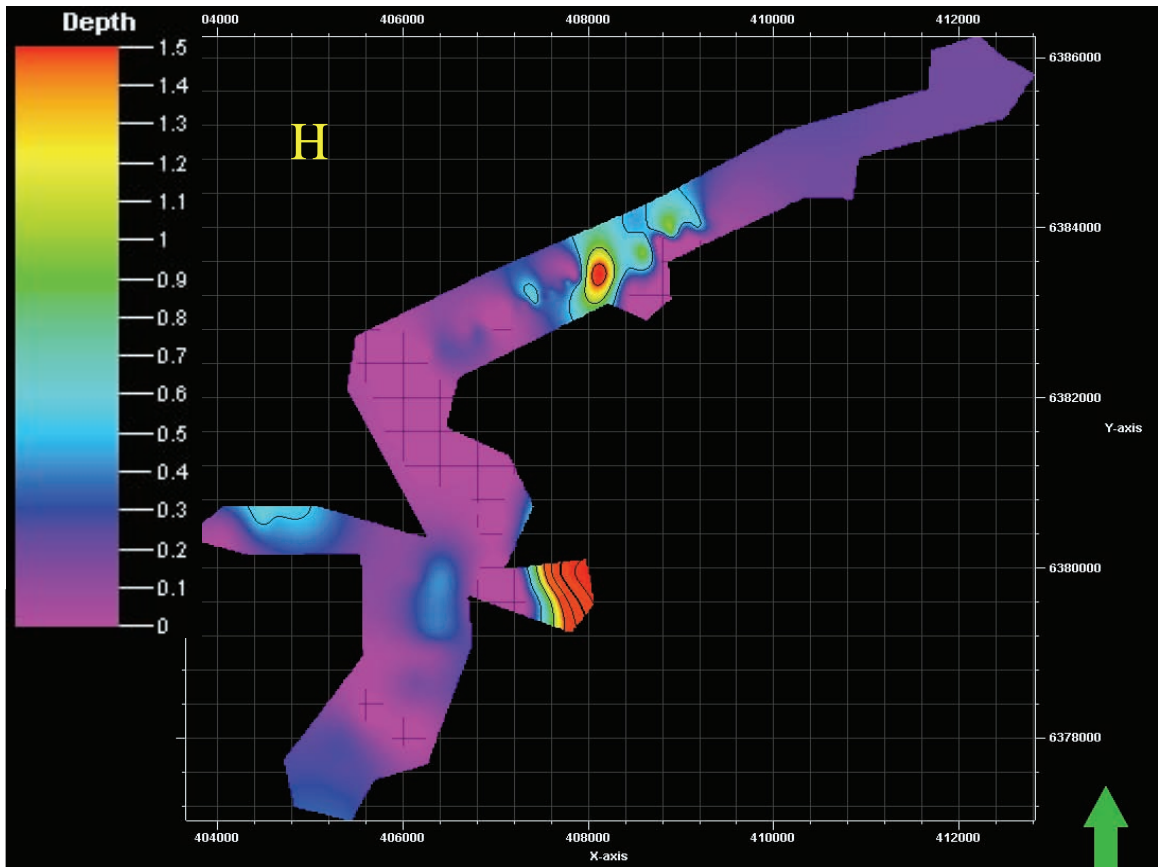
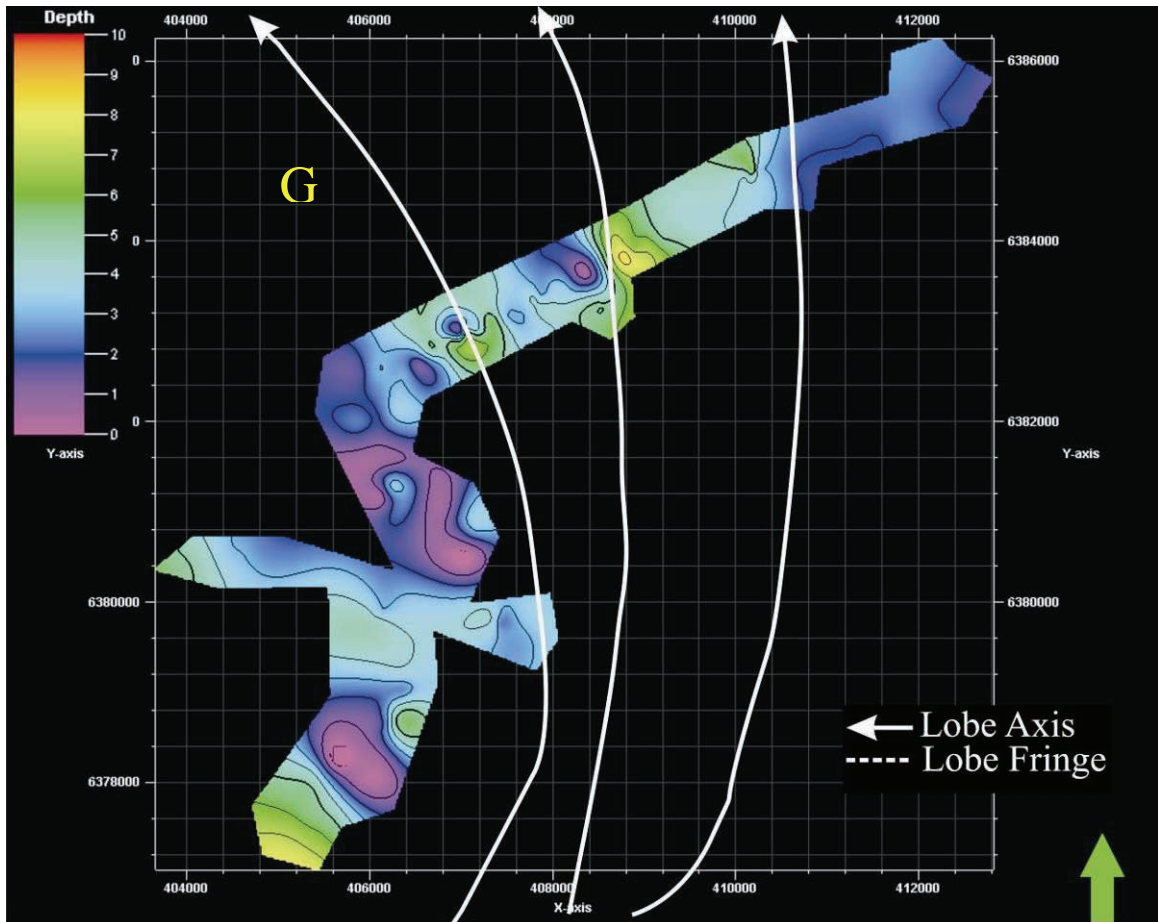
Appendix C Petrel Thickness Maps



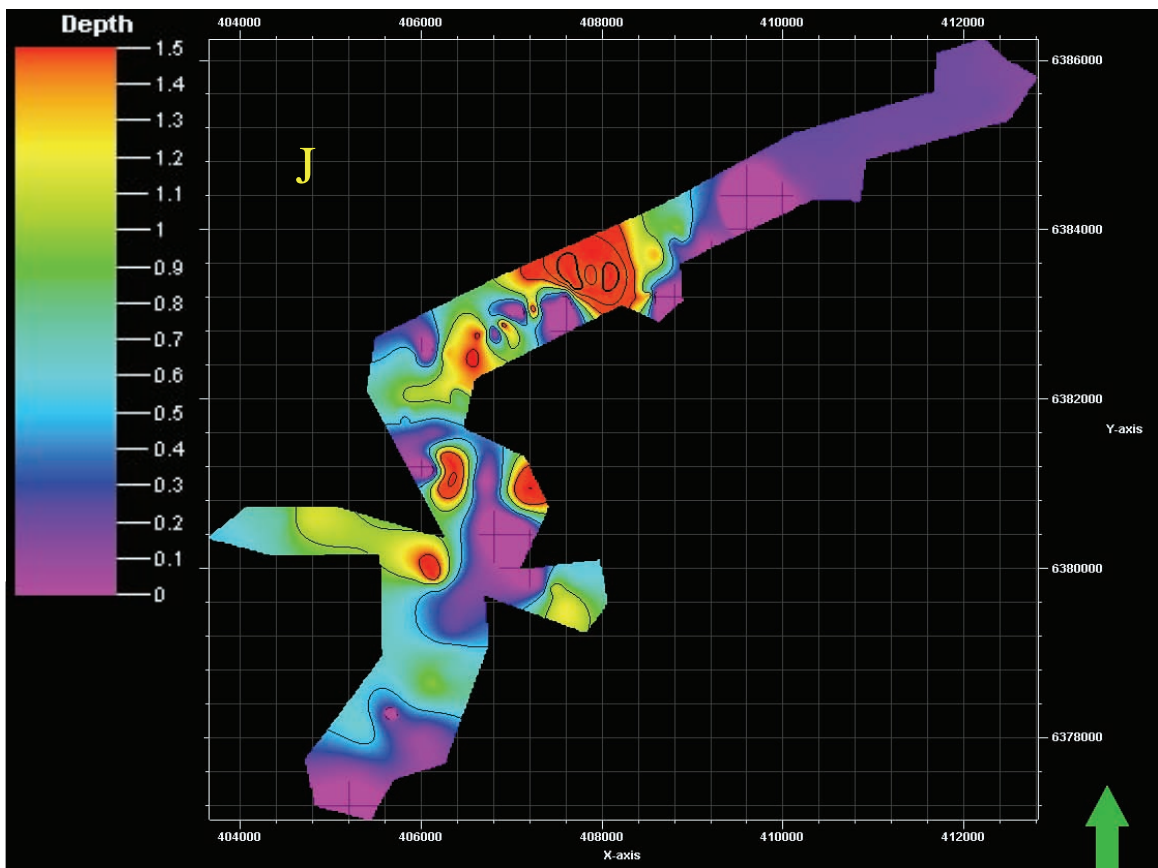
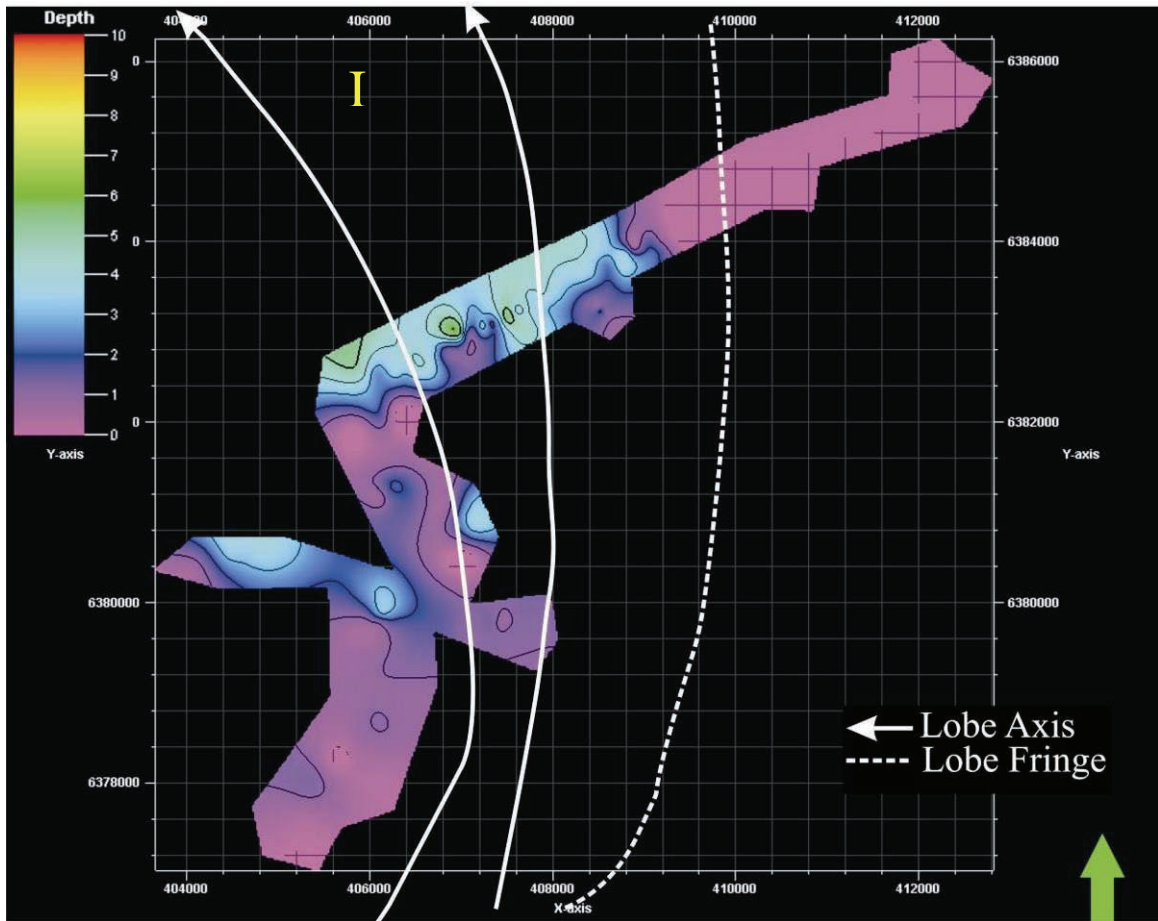
Appendix C Petrel Thickness Maps



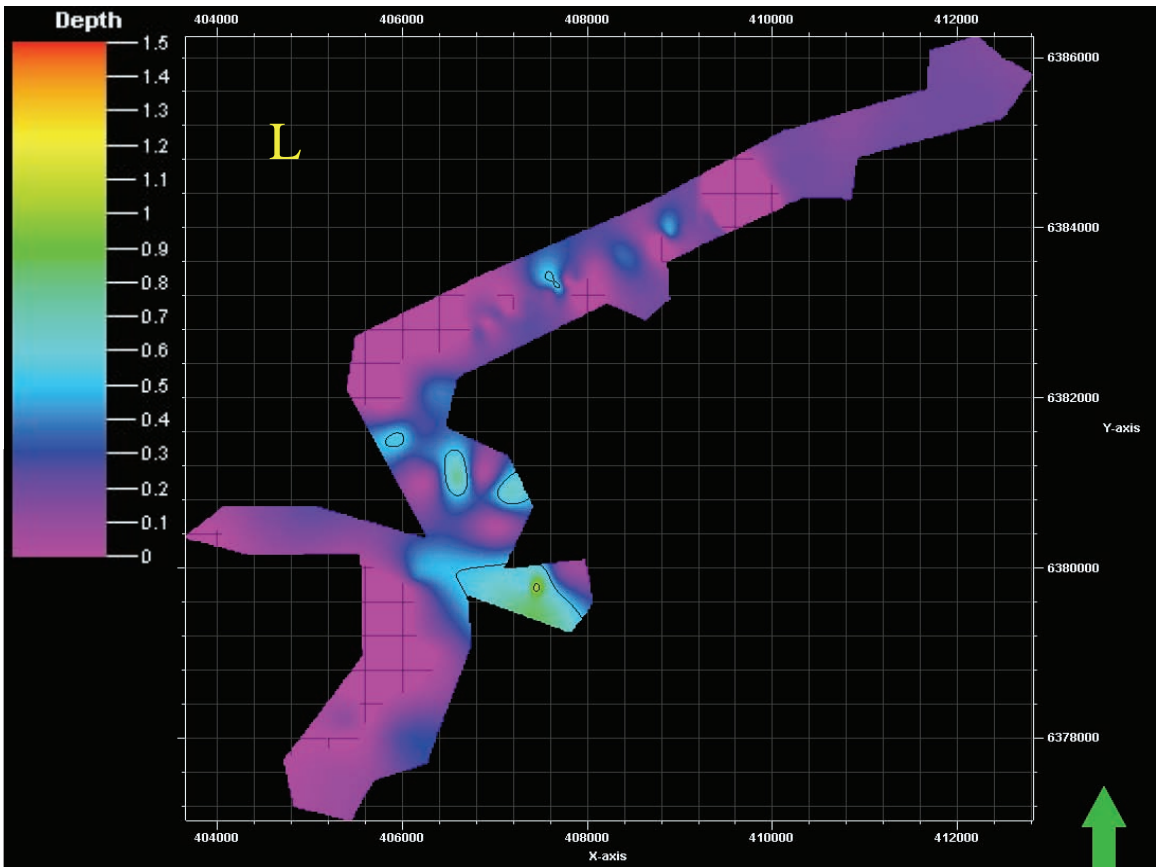
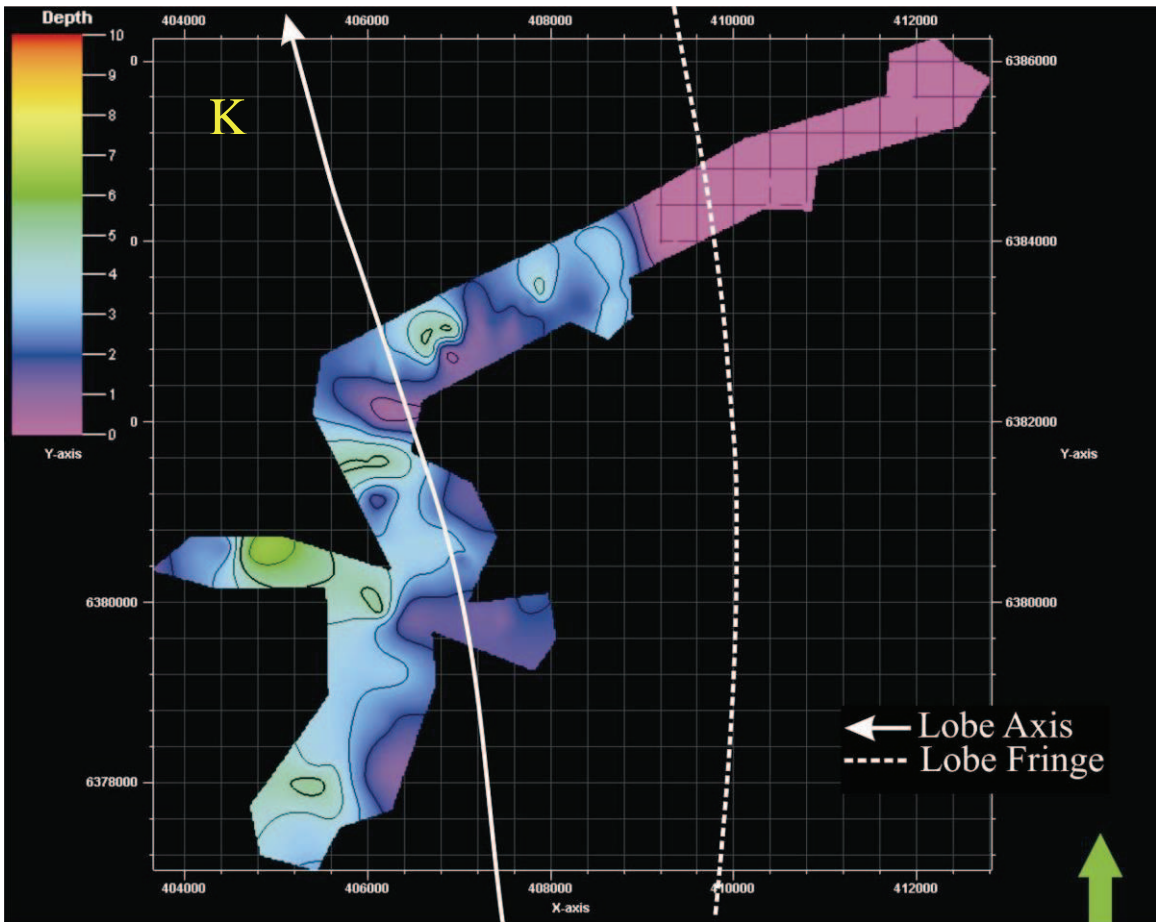
Appendix C Petrel Thickness Maps



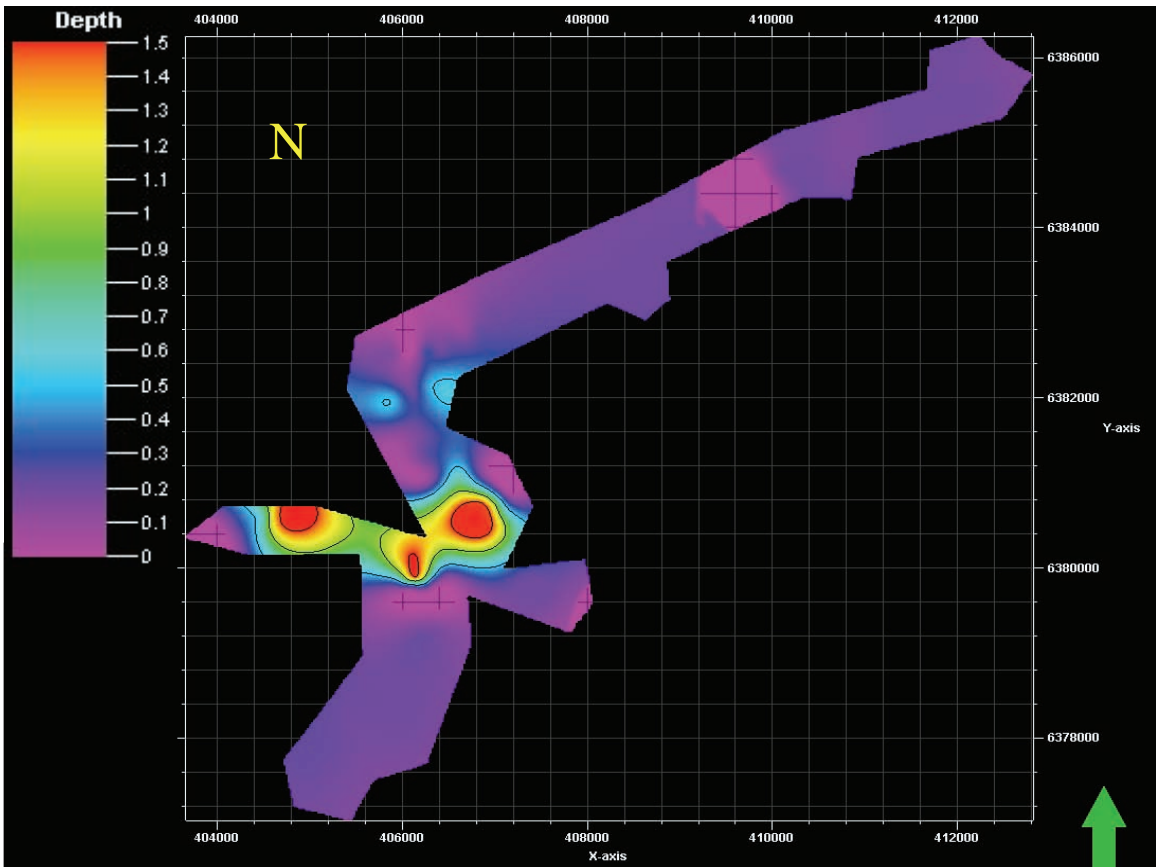
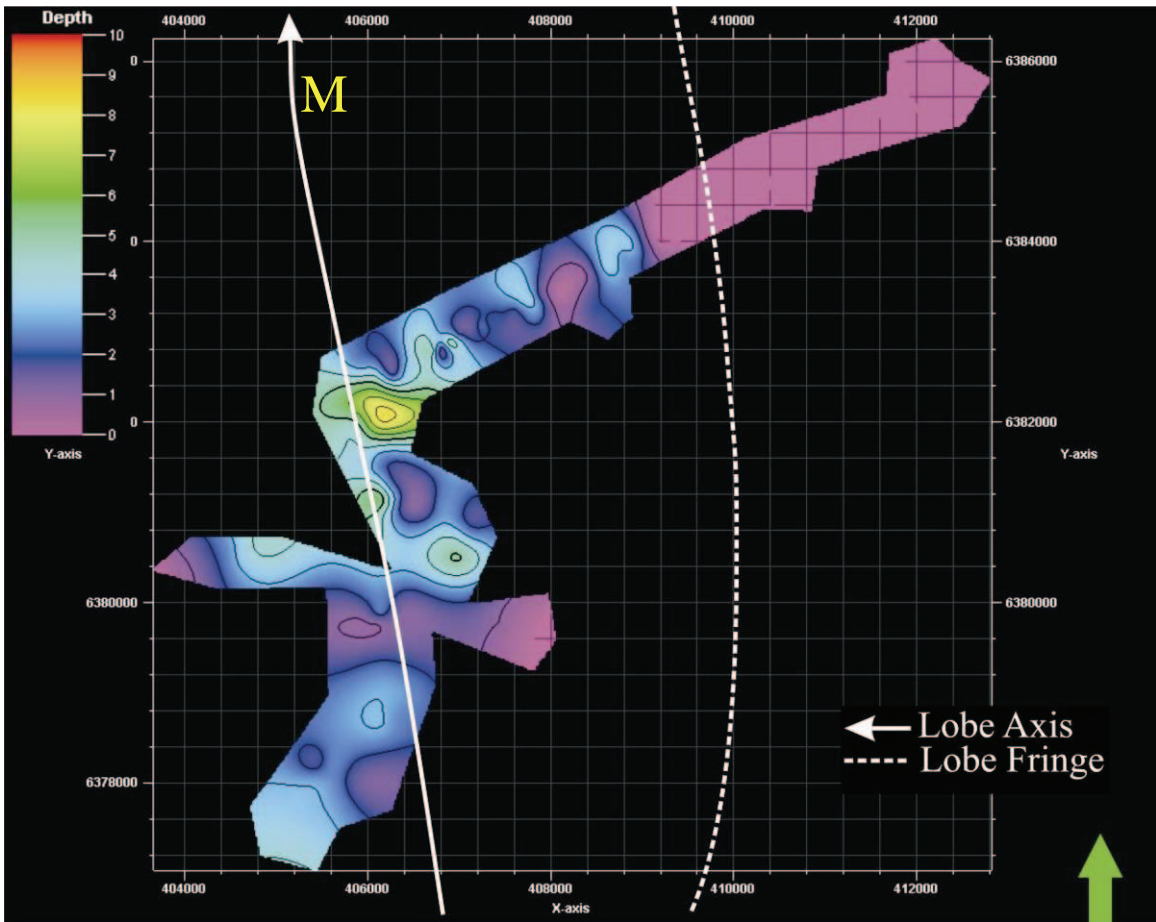
Appendix C Petrel Thickness Maps



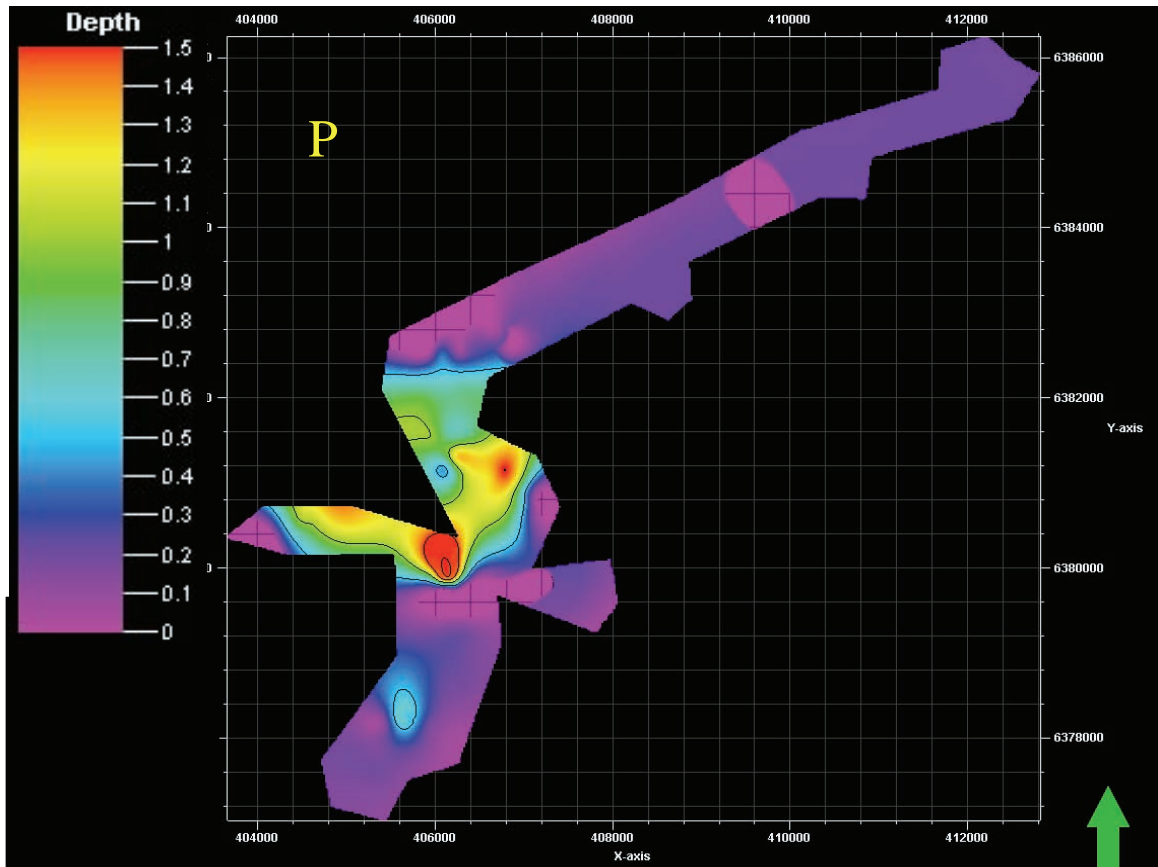
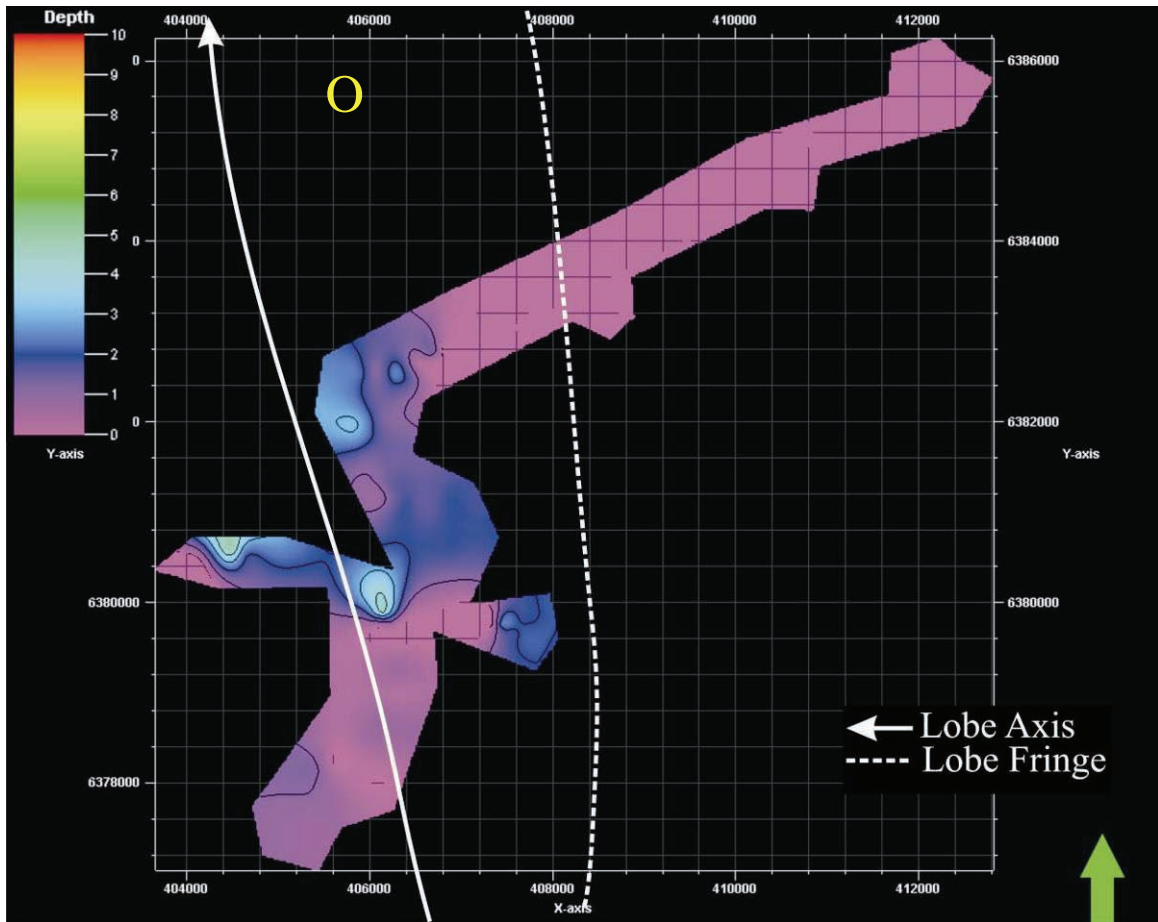
Appendix C Petrel Thickness Maps



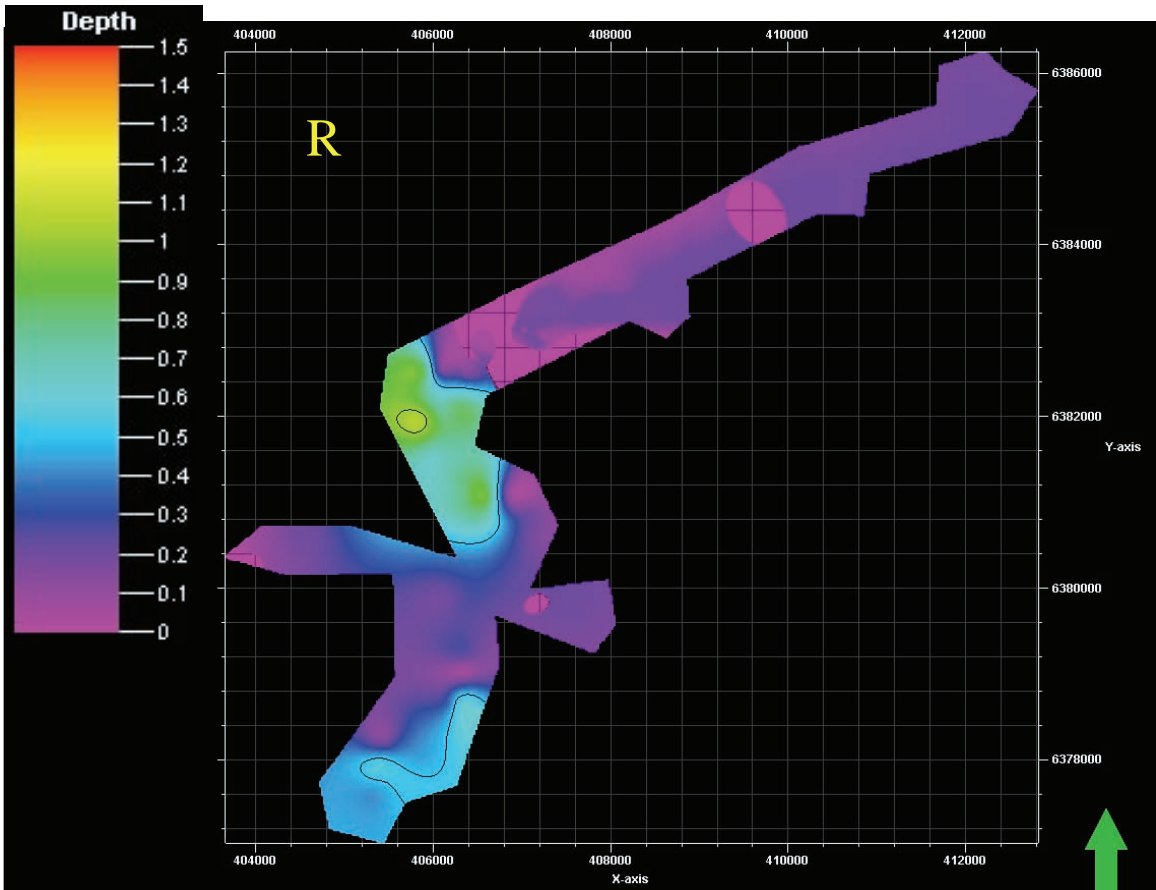
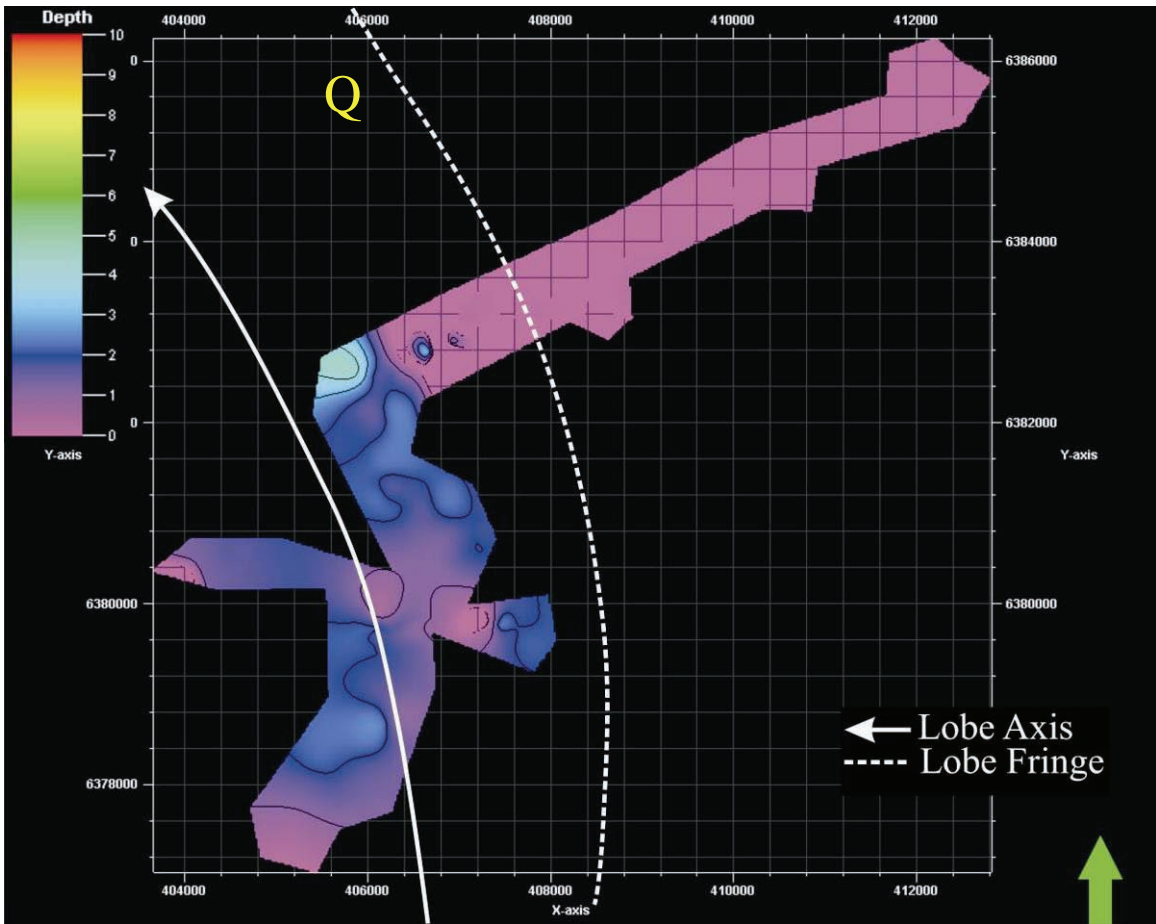
Appendix C Petrel Thickness Maps



Appendix C Petrel Thickness Maps



Appendix C Petrel Thickness Maps



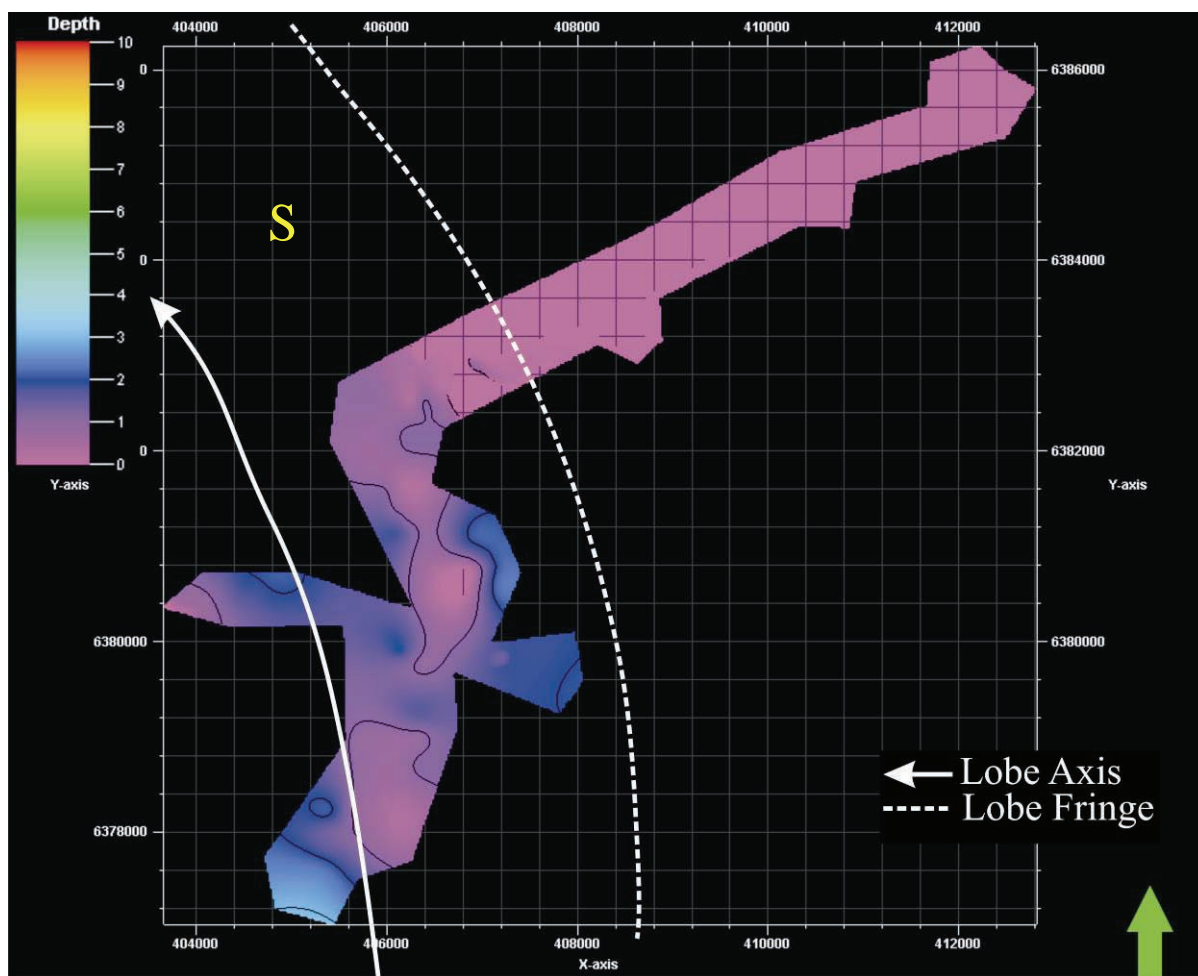


Figure C.2 The final set of Thickness Maps.

**Figure C.2 Legend**

- |                       |                  |
|-----------------------|------------------|
| A - Lobe 6            | K - Upper Lobe 2 |
| B - Interlobe F       | L - Intralobe 2  |
| C - Upper Lobe 5      | M - Lower Lobe 2 |
| D - Intralobe 4       | N - Interlobe B  |
| E - Lower Lobe 5      | O - Lobe 1       |
| F - Interlobe E       | P - Interlobe A  |
| G - Upper Lobe 4      | Q - Sub Lobe 2   |
| H - Intralobe 3       | R - Intralobe 1  |
| I - Lower Lobe 4      | S - Sub Lobe 1   |
| J - Interlobe C and D |                  |